DISENTANGLING THE BRANCHED RESPIRATORY CHAIN OF *SHEWANELLA ONEIDENSIS* MR-1

By

Kody Lee Duhl

DISSERTATION

Submitted to
Michigan State University
in partial fulfillment of the requirements
for the degree of

Biochemistry and Molecular Biology – Doctor of Philosophy

2022

ABSTRACT

DENTANGLING THE BRANCHED RESPIRATORY CHAIN OF SHEWANELLA *ONEIDENSIS* MR-1

By

Kody Lee Duhl

Bacteria possess a wide range of metabolic pathways, allowing them to adapt to an array of environmental changes. Focusing on these different metabolic pathways allows us to observe how bacteria catabolize substrate or use anabolic pathways to generate biomass. A more in-depth look shows that many of these pathways are redundant, meaning a single organism can conduct the same overall reactions differing only by the types of enzymes or intermediates used. Overlapping pathways are common in bacteria and have become a focal point of metabolism research to determine the advantages of conserving redundant pathways throughout evolution.

The metal reducing bacterium *Shewanella oneidensis* MR-1 is a practical model organism for metabolic studies, as it has substantial branching within its respiratory pathways. In this work, we focused on the extensive electron transport chain (ETC) of *S. oneidensis* MR-1 to understand the importance of seemingly redundant respiratory complexes and their functions during aerobic growth. The *S. oneidensis* MR-1 genome encodes four different NADH dehydrogenases (NDHs): a proton-pumping Type I NDH (Nuo), two sodium-pumping NDHs (Nqr1 and Nqr2), and one type II ‘uncoupling NDH (Ndh). NDHs oxidize NADH to move electrons into the ETC and generate ion-motive force that drives ATP synthesis, active transport, and motility. We determined that either Nuo or Nqr1 was required for aerobic growth in minimal medium. The presence of theoretically redundant complexes (Nqr2 and Ndh) did not rescue cell growth. Further, we determined that knocking out NDHs led to the inability to properly oxidize

NADH. NADH build up inhibited the tricarboxylic acid cycle causing an amino acid synthesis defect and inhibiting growth of the *S. oneidensis* strain lacking Nuo and Nqr1.

Recently, bacterial metabolic models have been developed to explain the use of energetically inefficient pathways during fast growth. Two standout models postulate that energetically inefficient pathways are used to reduce a cell's proteome cost by eliminating thermodynamic barriers or to reduce dependence on the ETC as cells grow larger. We sought to uncover if these models applied to the respiratory chain of *S. oneidensis* MR-1 during aerobic growth, as the ETC can vary in energetic efficiency based on the combination of NDH and terminal oxidase used. Our findings indicate that the models apply to *S. oneidensis* MR-1 in the context of overflow metabolism during growth at higher growth rates, while the structuring of the ETC was not in agreement. Most importantly, determined that both carbon metabolism and the ETC were restructured for adaptive growth under differing conditions. As carbon metabolism became less efficient at faster growth rates, the NDH step of the ETC became more efficient, using complexes with higher coupling efficiencies.

This work is dedicated to my wife, Shirrelle Evered, and my family,
especially to my grandfather, Richard Marisnick, who passed away during my first year at Michigan State University in 2017.
I know you would be proud and are always watching over us,
particularly making sure that I keep the lines straight
when mowing the lawn.

ACKNOWLEDGEMENTS

There are many people that I would like to thank for their support as I complete my time at Michigan State University. First, I would like to thank my wife, Shirrelle, for all the love and support that she has given me since we met in 2013. Without her, I would not currently be where I am today. I know that the last six years have been just as tough on her as they have on me, and she has handled it like a champion. Whether it was the midnight runs to the lab that I swore would only take 15 minutes and would turn into a multiple hour trip, helping me get through the frustrations of projects not working, or even the countless hours spent listening to fellow grad students and I ramble on about our projects, she was always there for me. Not to mention the fact that she somehow convinced me to take in our two street cats, Salem and Kylo, who aided in keeping us sane throughout the COVID-19 pandemic. I cannot wait to see what the post-graduate student life holds for us, and I could not ask for a better partner to go on life's next adventure with.

I would like to thank my parents for their immense support. Lucky for them, while growing up I decided that I wanted to play the two most expensive sports in ice hockey and lacrosse. Even while mortgaging their future, their unwavering support allowed me to succeed, and that sentiment remains true to this day. Without those opportunities to be involved in sports, I am not sure that I would have the work ethic and drive that has allowed me to advance through my career. Furthermore, I want to thank the Evered family for taking me in as their son and always giving me the motivation and support to keep pushing forward.

Ultimately, I would like to thank Dr. Michaela TerAvest and all the wonderful members of the TerAvest Lab. Michaela took me in as her first graduate student and was always extremely

supportive and helpful. For all the projects that did work, there were many others that did not, so I would like to thank her for her continued support and help to keep me on the correct track when I needed it most. To my fellow labmates: you all have been awesome and incredibly helpful during my time at MSU. I am grateful for everything, whether it was entertaining my wild ideas, answering questions, or editing my writing/presentations, thank you. My thesis committee, including Dr. Daniel Ducat, Dr. Gemma Reguera, Dr. Denis Proshlyakov, and Dr. Lee Kroos (who joined the committee on such short notice) all deserve a massive thank you for helping me navigate my projects and life as a graduate student. I would also like to thank the Biochemistry and Molecular Biology Department for their support, funding, and for allowing me to be able to conduct research over the last six years and continue my professional development.

TABLE OF CONTENTS

LIST OF TABLES

LIST OF FIGURES

KEY TO ABBREVIATIONS

ATP	Adenosine triphosphate
CCCP	Carbonyl cyanide m-chlorophenylhydrazone
DMSO	Dimethyl sulfoxide
DO	Dissolved oxygen
ETC	Electron transport chain
HPLC	High performance liquid chromatography
IPTG	Isopropylthio-β-galactoside
LB	Lysogeny broth
LC	Liquid chromatography
MS	Mass spectrometry
NAD^+	Nicotinamide adenine dinucleotide (oxidized)
NADH	Nicotinamide adenine dinucleotide (reduced)
NAG	N-acetylglucosamine
NDH	NADH dehydrogenase
PAGE	Polyacrylamide gel electrophoresis
PCR	Polymerase chain reaction
PMF	Proton-motive force
SA/V	Surface area to volume ratio
SDS	Sodium dodecyl sulfate
SMF	Sodium-motive force
TCA	Tricarboxylic acid

TMAO	Trimethylamine N-oxide
WT	Wild-type

Chapter 1: Variability of *Shewanella oneidensis* MR-1 metabolism and respiratory pathways

Authors: Kody Lee Duhl[1] and Michaela A. TerAvest[1]

[1]Department of Biochemistry and Molecular Biology, Michigan State University, East Lansing, MI, USA

1.1. Introduction to *Shewanella oneidensis* MR-1

Diversity among bacteria comes in a variety of forms, whether it is size and shape, or methods of metabolism. Gross structural differences are readily apparent under a microscope, as bacteria can be (relatively) large or small and shaped as rods, spheres, commas, or spirals (1, 2). Bacterial metabolism is equally diverse, although the differences may be harder to observe. Metabolic processes encompass how bacteria break down substrate molecules during catabolism or generate biomass through anabolism (3–7). Many metabolic pathways have common features and conduct similar overall reactions that only differ by using different enzymes or intermediates (8, 9). Often, a single organism will have overlapping or branching pathways with similar functions, but key differences that make them advantageous over other pathways in specific conditions. Investigating the relative advantages of each pathway can help us understand how microbes adapt to their environment and discover new ways to engineer metabolism for biotechnology.

The metal reducing bacterium *Shewanella oneidensis* MR-1 is a γ-proteobacterium isolated from freshwater lake sediment. It maintains versatile metabolic pathways including the ability to respire with many different terminal electron acceptors including oxygen, fumarate, nitrate, nitrite, dimethyl sulfoxide, trimethylamine N-oxide, solid metal oxides, and electrodes (10–15). Respiration with solid metal oxides and electrodes occurs via the metal reduction (Mtr) pathway (16, 17). The Mtr pathway consists of two decaheme cytochromes (MtrA and MtrC) housed in a β-barrel porin in the outer membrane (MtrB) (18). The inner membrane tetraheme cytochrome (CymA) delivers electrons from quinol oxidation into the Mtr pathway for export out of the cell (18). Once electrons pass through the Mtr pathway, they are transferred to solid metal oxides or electrodes via flavin mediated shuttling or direct contact (14, 17, 19, 20). This

ability has yielded many studies within bioelectrochemical systems for electrosynthesis, i.e., generation of products of interest by reversing the Mtr pathway (21).

The ability to use a variety of terminal electron acceptors for respiration is only one aspect of respiratory versatility in *S. oneidensis* MR-1. Redundancies are also present in the aerobic electron transport chain (ETC) (22). Quinone-linked lactate and formate dehydrogenases provide additional entrances for electrons into the ETC (10). For NADH, NADH dehydrogenases (NDHs) are responsible for moving electrons into the respiratory chain. NDHs are inner membrane bound oxidoreductase complexes that oxidize NADH to NAD^+, while transferring electrons to quinones in the inner membrane and contributing to proton-motive force (PMF) generation. The *S. oneidensis* MR-1 genome encodes four NDHs: a Type I proton translocating NDH (Nuo; 540 kDa), two sodium-translocating NDHs (Nqr1; 210 kDa and Nqr2; 212 kDa), and one Type II NDH (Ndh; 4.7 kDa) (10). The genome also encodes three aerobic terminal oxidases that reduce oxygen and contribute to ion gradient generation. The aerobic terminal oxidases are: an aa_3-type cytochrome *c* oxidase (Cox; 147 kDa), a cbb_3-type cytochrome *c* oxidase (Cco; 179 kDa), and a cytochrome *bd* ubiquinol oxidase (Cyd; 100 kDa) (10, 23, 24). The cytochrome *c* oxidases also require the cytochrome bc_1 complex (Pet; 93 kDa) for quinone oxidation and cytochrome *c* reduction (10, 23).

The highly branched ETC of *S. oneidensis* MR-1 raises a question: what is the unique function of each branch? Each of the four NDHs in the *S. oneidensis* MR-1 genome perform the same redox reaction but maintain different coupling efficiencies. The proton-pumping Type I NADH dehydrogenase, Nuo, maintains the highest coupling efficiency, transporting four protons (H^+) to the periplasmic space per NADH oxidation event (10, 25). The two sodium-transporting NDHs, Nqr1 and Nqr2, transport two sodium ions (Na^+) per NADH oxidation (10, 25). The Type

II NDH, Ndh, does not couple the oxidation of NADH with proton or sodium ion pumping (25, 26) (Fig. 1.1). Likewise, the terminal oxidases transfer different numbers of protons per turnover. The cytochrome *c* oxidases use a quinone reduction loop with the Pet complex (93 kDa) ($4H^+/2e^-$) and proton transport coupled with the reduction of oxygen to water to yield high coupling efficiencies ($2H^+/2e^-$ for Cco and $4H^+/2e^-$ for Cox) (23–25, 27–29) (Fig. 1.1). Conversely, the cytochrome *bd* ubiquinol oxidase only uses a quinone reduction loop for proton transport (2 $H^+/2e^-$) and does not pump protons (25, 29, 30) (Fig. 1.1). Overall, depending on the combination of NDH and terminal oxidase used, the coupling efficiency of ions transported to the periplasmic space per NADH oxidation event can vary from $2H^+/2e^-$ to $12H^+/2e^-$ (25).

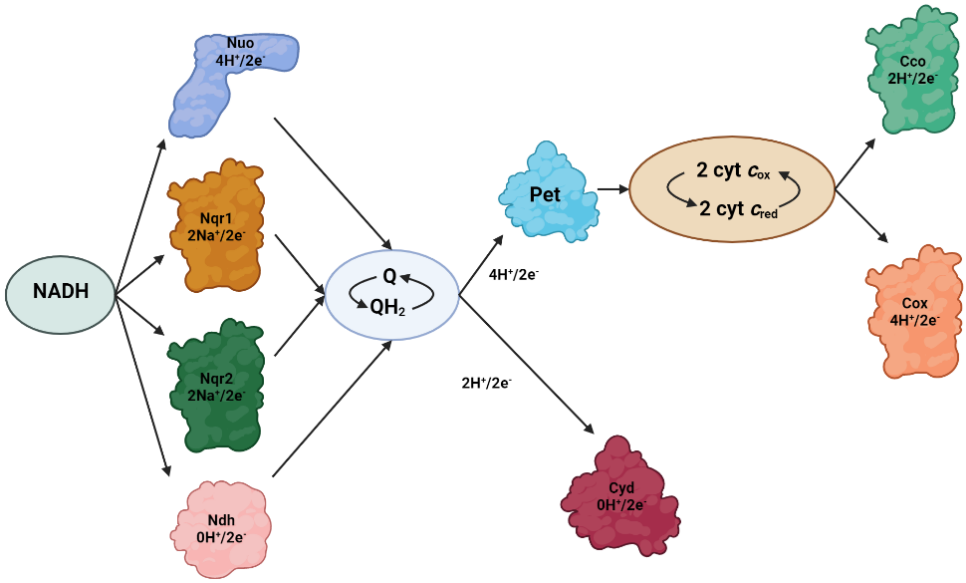

Figure 1.1. Branched respiratory chain of *S. oneidensis MR*-1. Diagram detailing the branching of the *S. oneidensis* MR-1 respiratory chain including: each NDH and their coupling efficiencies for NADH oxidation and proton transport, quinone reduction/oxidation and associated proton transport, and the terminal oxidases and their coupling efficiencies for cytochrome *c* oxidation/oxygen reduction (Cco and Cox) or quinone oxidation and oxygen reduction (Cyd). Image generated using BioRender.com.

1.2. What is the purpose of branched ETCs in bacteria?

Branched electron transport chains are common in bacteria and may provide flexibility to adjust to environmental changes (26, 31–34). Specifically, different ETC components may help cells adapt to varying oxygen concentrations. For example, the terminal oxidases have differing oxygen affinities. The terminal oxidase are classified subgroups based on structure and oxygen affinity: heme-copper A-, B-, and C-type oxidases (HCOs), and *bd*-type ubiquinol oxidases (35, 36). The A-type terminal oxidases have low oxygen affinity, whereas B-type, C-type, and the *bd* ubiquinol oxidases have high oxygen affinity (35). The high oxygen affinity terminal oxidases such as the *bd* ubiquinol oxidase and C-type HCOs may help cells scavenge oxygen during microaerobiosis and their expression is induced in low oxygen condition (29, 31, 35, 37, 38). Further, oxygen concentrations higher than 50 nM inhibit the *bd* ubiquinol oxidase in *E. coli* (39). With atmospheric oxygen concentrations being roughly 9.4 mM, inhibition of the *bd* ubiquinol oxidase may force electron flux through proton-pumping terminal oxidases to aid in PMF generation under oxic conditions (39). In response to sufficient oxygen concentrations, the proton-pumping A-type HCO is the predominant terminal oxidase in *E. coli* (33, 35, 40, 41). In contrast, the A-type HCO (Cox) in *S. oneidensis* MR-1, is rarely expressed and Cox mutants show no growth defect in typical laboratory growth conditions (38). Le Laz *et al.* found that the cbb_3 cytochrome *c* oxidase in the predominant terminal oxidase under oxic conditions (38).

Although they do not react with oxygen directly, expression of NDHs is also affected by oxygen concentration. In *Escherichia coli*, expression of Type I NDH increases with increasing oxygen levels, while the Type II NDH expression was higher under anaerobic and microaerobic conditions (42). In *S. oneidensis* MR-1, there is some evidence that Nqr1 is upregulated under

aerobic conditions, while Nqr2 is not (10). Overall, less is known about the role of oxygen in regulating NDH expression.

Using different branches of the ETC can also be affected by substrate availability. Carbon catabolite repression for optimal growth occurs when bacteria 'select' preferred carbon sources by downregulating genes required for alternative metabolite catabolism (32). The process has been studied in heterotrophic bacteria with highly branched respiratory pathways, namely the *Pseudomonas* spp. (32). This phenomenon has been directly linked to the expression of the A-type Cyo terminal oxidase in *Pseudomonas* spp., as they coordinate their ETC complexes depending on growth conditions (31, 32). Likewise, starvation under oxic conditions has been found to elicit expression of the aa_3-type terminal oxidase, Cox, in *S. oneidensis* MR-1 (24), although its function was previously believed to have been lost (29). More recent work indicates that the aa_3-type terminal oxidase is used alongside the cbb_3-type oxidase when *S. oneidensis* MR-1 is provided with pyruvate or acetate rather than its preferred carbon source, lactate (43).

An additional layer of complexity in branched ETCs is that the branches have different coupling efficiencies. The lack of proton-coupled transport with NADH oxidation for the Type II Ndh raises questions regarding its function, but its use could impart some advantages. Multiple studies have found evidence that Ndh is essential or important for aerobic growth (26, 44). One possibility is that using the Type II NDH could avoid pumping protons under high membrane potential conditions, when flux through the Type I NDH would be slowed due to its proton pumping function (26). Ndh is also involved in feedback loops associated with redox state ($NADH:NAD^+$), where it is expressed under high $NADH:NAD^+$ conditions to thwart toxicity of low NAD^+ levels (45). However, questions remain about how Ndh expression impacts overall

ATP yield and growth, and how the use of an energetically inefficient ETC branch could be beneficial.

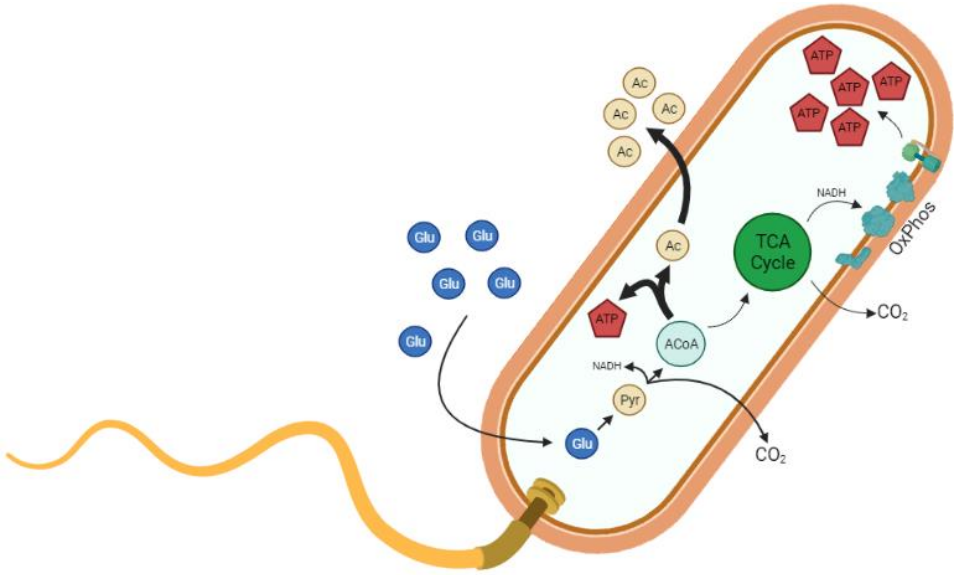

Figure 1.2. Bacterial overflow metabolism. Diagram of the differences between aerobic respiration to overflow metabolism. As growth rates increase, more carbon flux is diverted to acetate secretion and away from the tricarboxylic acid cycle (denoted by arrow thickness).

1.3. Why do energetically inefficient pathways exist?

Energetic inefficiency can become a dominant strategy during bacterial carbon metabolism, although it seems maladaptive. Several models have been proposed to explain why an organism would use pathways that are energetically inefficient. These pathways have mostly been studied in the context of 'overflow metabolism' in *E. coli*, which is the secretion of acetate even when sufficient oxygen is present for complete substrate oxidation to CO_2 (Fig. 1.2). This behavior has puzzled researchers because respiration can theoretically generate 32 ATP per molecule of glucose metabolized, while overflow metabolism generates only 4 ATP (5, 46). Despite the energetic inefficiency, *E. coli* uses overflow metabolism under oxic conditions with an excess of substrate and/or when growing at a high rate (47, 48). Limited respiratory capacity has been presented as an explanation for overflow metabolism, where respiratory complexes become

saturated due to high substrate influx, however, this was determined to not be the root cause of overflow metabolism in *E. coli* (49, 50).

Another possible explanation for energetically inefficient pathways could be that it is more advantageous for the cell to reduce the protein cost of metabolic pathways, rather than to maximize ATP generation. For example, overflow metabolism significantly reduces enzyme cost because the enzymes that catalyze the tricarboxylic acid (TCA) cycle and make up the ETC are not required for acetate secretion (47). The overall proteome fraction for the TCA cycle and oxidative phosphorylation machinery lessens as growth rates increase in *E. coli* due to overflow metabolism generating ATP via substrate-level phosphorylation (47, 51). Altogether, overflow metabolism maintains the ability to generate ATP, but lowers the total proteome cost of metabolic enzymes (47, 52). While overflow metabolism does result in fewer ATP generated per molecule of substrate, the reduction in proteome fraction taken up by TCA cycle enzymes and oxidative phosphorylation machinery may free up more of the cell's translational capacity to contribute to replication processes.

Generating fewer ATP per molecule of substrate during overflow metabolism may also provide a benefit in the form of thermodynamic favorability. Reactions with large, negative ΔG values provide driving force to keep reaction flux moving in the forward direction. Incomplete substrate oxidation during overflow metabolism results in a lower enzyme requirement due to the increased driving force resulting from the reduced ATP generation (53). The same concept is observed in bacterial glycolysis (8, 9). Bacteria capable of conducting both the Embden-Meyerhof-Parnas (EMP; 2 ATP/glucose) and Entner-Doudoroff (ED; 1 ATP/glucose) pathways can take advantage of limiting both proteome cost and removing thermodynamically unfavorable reactions. The enzymatic cost of the ED pathway is significantly less than that of the EMP

pathway, but it produces fewer ATP per molecule of substrate (8). Therefore, it appears that using energetically inefficient pathways to lower proteome cost and utilize more thermodynamically favorable reactions could become more advantageous at higher substrate uptake and growth rates (54).

Another explanation for not using pathways that generate the highest amount of ATP is the membrane real estate hypothesis (55). This hypothesis suggests that bacterial cells are on average larger when growing at a high growth rate, leading to a reduction in the surface area to volume ratio (SA/V) (55). The reduction in SA/V may lead to a mismatch between the ETC and cytosolic metabolism, because space for ETC complexes is inherently limited (55, 56). Szenk *et al*. show that the ability to oxidize NADH in the ETC becomes limited at higher growth rates, and as a result, the cell exhibits increased NADH:NAD^+ (55). Further, the high NADH:NAD^+ leads to TCA cycle repression and results in acetate secretion, as experimentally observed at high growth rates (47, 48, 55–57). Overflow metabolism generates fewer NADH than the TCA cycle, lessening the requirement for NADH recycling by the ETC (55, 56)

Overall, these hypotheses focus on the use of overflow metabolism but could also help explain the use of other energetically inefficient pathways, including ETC components with low coupling efficiencies. Here, we conducted novel studies regarding the function of the branched ETC of *S. oneidensis* MR-1.

1.4. Research overview

This research seeks to determine how *S. oneidensis* MR-1 structures its electron transport chain under differing growth conditions. Chapter Two explores the importance of each of the four NDHs in *S. oneidensis* MR-1 during growth in minimal medium under oxic conditions. Single-mutant strains were generated by knocking out the terminal subunit of each NDH in the genome

with in-frame deletion mutagenesis. Growth of the single-mutant strains was analyzed with two different carbon sources (D,L-lactate and N-acetylglucosamine) under oxic conditions. We determined that the Nqr2 and Ndh knockouts did not exhibit any growth defects, while the Nuo and Nqr1 knockouts exhibited slightly reduced cell densities and growth rates with both carbon sources. Further analysis showed that Nuo and Nqr1 mutant strains also lagged behind the wild-type (WT) *S. oneidensis* MR-1 in consuming the metabolic byproduct acetate. We then generated a double-knockout strain lacking Nuo and Nqr1, which was unable to grow in minimal medium under oxic conditions. Overall, we found that the activity of either Nqr1 or Nuo was required for growth in minimal medium under oxic conditions.

Chapter Three is a more in-depth look at the growth defect caused by deletion of Nuo and Nqr1 in *S. oneidensis* MR-1. We observed that the double knockout strain grew in Lysogeny Broth (LB), but not in minimal medium. To investigate this, we broke LB into its individual components: yeast extract, tryptone (trypsin digested casein), and NaCl, and determined that tryptone rescued the growth of the double-knockout strain. With growth rescued, we were able to assess its ability to metabolize supplemented carbon sources. Compared to the WT strain, the double-knockout could not fully consume all available substrate (D,L-lactate or N-acetylglucosamine) and was unable to metabolize pyruvate and acetate. Using an intracellular redox sensing system to monitor NADH:NAD^+, we observed that the double-knockout strain exhibited higher levels of NADH:NAD^+ compared to the WT strain. These data, combined with the requirement to supplement tryptone suggested that the double-knockout strain exhibited decreased TCA cycle function due to inhibition by high NADH levels. As a result, the lack of amino acid precursors generated from the TCA cycle led to the inability of the double knockout strain to growth without tryptone.

Chapter Four of this dissertation dives into how *S. oneidensis* MR-1 structures metabolic pathways and its ETC under differing growth conditions. Due to the redundancy in ETC complexes in the *S. oneidensis* MR-1 genome, we hypothesized that *S. oneidensis* MR-1 modulates the structure of the ETC under differing growth conditions. We conducted growth, metabolite, and proteome analysis on *S. oneidensis* MR-1 during steady-state growth at low and high growth rate conditions in a fermenter under oxic conditions. Metabolite data suggested that carbon flux through the TCA cycle decreased and shifted towards overflow metabolism in the high growth rate condition. We also observed reduced abundance of the enzymes controlling the first three steps of the TCA cycle and an increase in those required for acetate secretion. Regarding the ETC, Nuo, Nqr1, and Cco exhibited increased abundance at the high growth rate while Ndh, Nqr2 and Cox were more abundant at the low growth rate condition. These results suggest that ETC regulation in *S. oneidensis* is nuanced and there may be different pressures on energetic efficiency at the different steps.

Overall, we obtained a better picture of how metabolism and the ETC of *S. oneidensis* MR-1 operate. We have shown the importance of specific NDHs during aerobic respiration, regulation of the TCA cycle via NADH:NAD^+, and use of energetically efficient pathways at high growth rates. Additionally, even though the studies conducted within this dissertation were focused on aerobic metabolism, the data obtained has implications for biotechnological uses of *S. oneidensis* MR-1. Currently, electrosynthesis to generate products of interest within bioelectrochemical systems is dependent on the function of the *S. oneidensis* MR-1 respiratory chain (21). Understanding how the ETC is structured and recreating conditions where the respiratory chain is optimized for efficiency is paramount in increasing the effectiveness of electrosynthesis for sustainable energy purposes.

Chapter 2: *Shewanella oneidensis* MR-1 utilizes both sodium- and proton-pumping NADH dehydrogenases during aerobic growth

This chapter contains an edited version of a previously published research article in *Applied and environmental microbiology*, Volume 84, Pages: e00415-18.

Authors: Kody Lee Duhl[1], Nicholas M. Tefft[1], and Michaela A. TerAvest[1]

[1]Department of Biochemistry and Molecular Biology, Michigan State University, East Lansing, MI, USA

2.1. Abstract

Shewanella oneidensis MR-1 is a metal reducing bacterium with the ability to utilize many different terminal electron acceptors, including oxygen and solid metal oxides. Both metal oxide reduction and aerobic respiration have been studied extensively in this organism. However, electron transport chain processes upstream of the terminal oxidoreductases have been relatively understudied in this organism, especially electron transfer from NADH to respiratory quinones. Genome annotation indicates that *S. oneidensis* MR-1 encodes four NADH dehydrogenases: a proton-translocating dehydrogenase (Nuo); two sodium ion-translocating dehydrogenases (Nqr1 and Nqr2); and an 'uncoupling' dehydrogenase (Ndh), but none of these complexes has been studied. Therefore, we conducted a study specifically focused on the effects of individual NADH dehydrogenase knockouts in *S. oneidensis* MR-1. We observed that two of the single mutant strains, Δ*nuoN* and Δ*nqrF1*, exhibited significant growth defects compared with wild type. However, the defects were minor and only apparent under certain growth conditions. Further testing of a double mutant strain, Δ*nuoN*Δ*nqrF1*, yielded no growth in minimal media under oxic conditions, indicating that Nuo and Nqr1 have overlapping function, but at least one is necessary for aerobic growth. Co-utilization of proton- and sodium ion-dependent energetics has important implications for growth of this organism in environments with variable pH and salinity, including microbial electrochemical systems.

2.2. Importance

Bacteria utilize a wide variety of metabolic pathways that allow them to take advantage of different energy sources, and to do so with varying efficiency. The efficiency of a metabolic process determines the growth yield of an organism, or the amount of biomass it produces per amount of substrate consumed. This parameter has important implications in biotechnology and

wastewater treatment, where low growth yields are often preferred to minimize production of microbial biomass. In this study, we investigated respiratory pathways containing NADH dehydrogenases with varying efficiency (i.e., the number of ions translocated per NADH oxidized) in the metal-reducing bacterium *Shewanella oneidensis* MR-1. We observed that two different respiratory pathways are used concurrently, and at least one must be functional for growth under oxic conditions.

2.3. Introduction

Shewanella oneidensis MR-1 is a facultative anaerobe with the capability to respire using a wide variety of terminal electron acceptors in the absence of oxygen (11). One of the best-studied aspects of this organism is its use of solid metal oxides and electrodes as terminal electron acceptors (58). *S. oneidensis* MR-1 interacts with solid electron acceptors via the Mtr pathway, which transfers electrons to the acceptor either through direct contact or soluble flavin electron shuttles (59–61). This capability is useful in many different bioelectrochemical technologies (16, 62–64). For example, *S. oneidensis* MR-1 has been engineered to act as a biosensor by linking Mtr expression, and therefore electric current generation, to a chemical signal in the environment (65, 66). 'Unbalanced fermentation' has also been developed in *S. oneidensis* MR-1, allowing it to overcome redox imbalance between substrates and products by releasing excess reducing equivalents to an anode electrode via the Mtr pathway (67).

While the Mtr pathway and other terminal oxidoreductases are well-studied, upstream processes that transfer electrons into the respiratory quinol pool are less understood. *S. oneidensis* MR-1 uses a variety of complexes to transfer electrons into the quinol pool, and these may use one of several different electron donors including primary substrates, such as lactate, or electron carriers, such as NADH (68). In *S. oneidensis* MR-1, there has been significant research

on lactate dehydrogenases (69, 70), hydrogenases (71, 72), and formate dehydrogenases (73). However, to our knowledge, the NADH dehydrogenases have only been studied incidentally in whole-genome expression profiling, without specific gene deletion or biochemical studies. Four NADH dehydrogenases are encoded in the genome of *S. oneidensis* MR-1: one predicted to pump protons (Nuo, SO_1009 to SO_1021), two predicted to pump sodium ions (Nqr1, SO_1103 to SO_1108; Nqr2, SO_0902 to SO_0907), and one predicted to be 'uncoupling' that does not translocate ions across the inner membrane (Ndh, SO_3517) (10). We note that the 'Nqr1' and 'Nqr2' labels are not used consistently across studies and genome databases, but here we refer to them as shown above.

Both sodium-pumping NADH dehydrogenases (Nqr) are found in all sequenced genomes in the *Shewanella* genus, while the proton-pumping NADH dehydrogenase (Nuo) has been found in only a few isolates, including *S. oneidensis* MR-1 (10). The same pattern has been observed with sodium- and proton-dependent flagellar stators, with *S. oneidensis* MR-1 being the only isolate known to contain the proton-dependent MotAB flagellar rotation system, while all sequenced *Shewanella* isolates contain the sodium-dependent PomAB system (74). Although this suggests that the sodium-motive force (SMF) is the major energetic gradient used by *S. oneidensis* MR-1, other studies point to the importance of proton-motive force (PMF). For example, the proton-specific uncoupler carbonyl cyanide m-chlorophenyl hydrazone (CCCP) induces biofilm dissolution in *S. oneidensis* MR-1 (75). Further, PMF generation by a light-driven proton pump improves current production and survival of *S. oneidensis* MR-1 in bioelectrochemical systems (76). Finally, we observed with BLAST (77) that the F_0F_1 ATP synthase of *S. oneidensis* MR-1 appears to be powered by PMF due to the lack of specific residues necessary for sodium ion transport (78). Of course, PMF and SMF cannot be completely

disentangled because both are composed of two components: membrane potential ($\Delta\Psi$) and concentration gradient of the coupling ion (ΔpH or $\Delta[Na^+]$). PMF and SMF are further connected by proton-sodium antiporters. The *S. oneidensis* MR-1 genome encodes several Na^+/H^+ antiporters: NhaA, NhaB, NhaC, NhaD, and two in the cation:proton antiporter-1 family (79). Therefore, it may be possible for *S. oneidensis* MR-1 to use sodium as the primary ion for respiratory coupling but convert SMF to PMF through antiporters for ATP synthesis. While this may appear to be an inefficient strategy, a recent review describes several organisms that utilize this method of oxidative phosphorylation, indicating that it may have advantages in some environments (80).

While NADH dehydrogenase activities have not been directly studied in *S. oneidensis* MR-1, some basic information about their function can be gleaned from the large amount of transcriptomic data collected for this organism. Several studies have detected significant changes in transcriptional regulation of the NADH dehydrogenases depending on the growth condition. Rosenbaum et al. (81) found upregulation of the proton-pumping NADH dehydrogenase (*nuo*) in electrode-grown biofilms compared with aerobically-grown planktonic cells. In contrast, Beliaev et al. (11) found decreased expression of *nuo* and *nqr2* with oxygen and metal oxide electron acceptors compared to fumarate. These studies show that NADH dehydrogenase expression is dependent on electron acceptor type, but do not yet reveal a clear pattern.

Studies on known *S. oneidensis* MR-1 regulons also help predict when each NADH dehydrogenase is expressed. The regulation of Nqr NADH dehydrogenases appears to be based on carbon source type, energy levels within the cell, and the presence of specific electron acceptors. The *nqr2* operon is regulated by the hexose-dependent HexR regulator, suggesting expression of this NADH dehydrogenase depends on the available carbon source (82). In

contrast, *nqr1* is not predicted to be part of the HexR regulon, but rather it is regulated by the cAMP-dependent Crp regulator (83). The Fnr-like regulator EtrA also appears to play a role, leading to increased expression of *nqr2* under anoxic conditions, and increased expression of *nqr1* under oxic conditions (84). Although it is unclear if Nqr1 and Nqr2 differ in function, due to high sequence identity, differential regulation of each dehydrogenase suggests that they serve distinct roles in metabolism.

NADH is one of the most important electron carriers in cellular metabolism and appears to be critical for respiratory activity in *S. oneidensis* MR-1, based on the presence of genes encoding four different NADH dehydrogenases in its genome. However, electron transport from NADH to the quinol pool in *S. oneidensis* MR-1 has been understudied compared with terminal oxidases. To understand how *S. oneidensis* MR-1 couples growth to processes such as electric current production and environmental metal cycling, it is essential to understand how PMF and SMF are generated during respiration. Therefore, we have conducted a directed study on the role of each putative NADH dehydrogenase in the *S. oneidensis* MR-1 genome by generating in-frame deletions to disrupt each complex and studying phenotypes of the mutant strains under oxic conditions. Our strategy was informed by a new analysis of an existing whole-genome fitness profiling dataset.

2.4. Results

2.4.1 Mining a whole-genome fitness dataset for NADH dehydrogenase utilization patterns

We analyzed an existing whole-genome fitness profiling dataset from a study by Deutschbauer et al. (85) to gain initial insights into environmental conditions that influence the function of each NADH dehydrogenase encoded in the *S. oneidensis* MR-1 genome. In the study, a whole-genome transposon mutant library was grown under more than 200 different conditions. Fitness

of the mutants was measured by change in abundance of sequence tags throughout the experiment. To focus on specific carbon sources, we plotted fitness scores of NADH dehydrogenase mutant strains in a subset of 55 conditions where the library was grown in minimal medium under oxic or anoxic conditions with lactate or N-acetylglucosamine (NAG) as the substrate (Figure 2.1). Conditions with differing nitrogen, sulfur, and carbon sources (other than NAG and lactate) were excluded from the subset. Mutants in *nuo* (proton-dependent) and *nqr1* (sodium ion-dependent) genes showed the greatest fitness defects under oxic conditions. This effect was weaker with lactate than with NAG, which is unsurprising considering that lactate oxidation theoretically generates 4 NADH per molecule compared to 13 NADH per molecule for NAG (Figure 2.2). Mutants with insertions in *ndh* (uncoupling) and *nqr2* (sodium ion-dependent) genes showed greater fitness defects in anoxic conditions compared to oxic conditions. In general, all fitness defects were weak under anoxic conditions, which may be due to the lack of significant TCA cycle activity in *S. oneidensis* MR-1 when oxygen is absent (86), resulting in less NADH generation from most substrates. Based on this analysis, we focused on oxic conditions, which showed the largest overall fitness defects for the NADH dehydrogenase mutants in the library. We chose two different carbon sources, sodium D,L-lactate and NAG, to understand the effects of substrates that generate differing amounts of NADH.

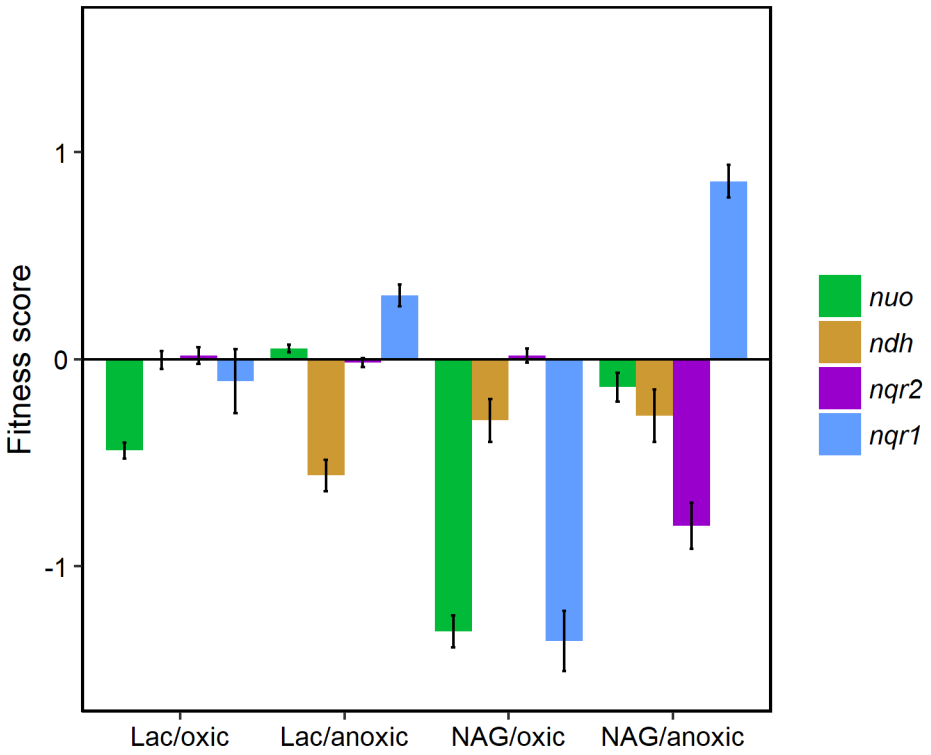

Figure 2.1. Fitness analysis of NADH dehydrogenase mutants. Fitness of NADH dehydrogenase mutants under several growth conditions: D,L-lactate/oxic, D,L-lactate/anoxic, NAG/oxic, and NAG/anoxic. Values are averaged across loci in each operon and across multiple growth conditions that fit the descriptions above. Error bars represent standard deviation. Fitness is relative to aerobic growth in LB. All data were generated by Deutschbauer et al (43).

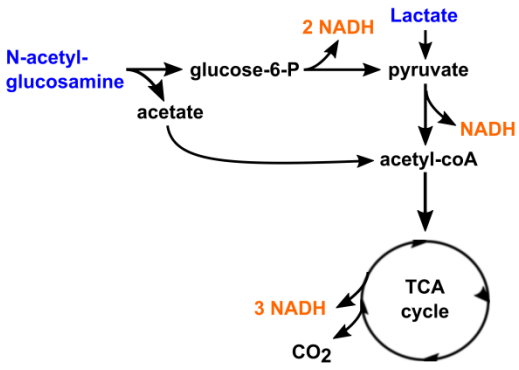

Figure 2.2. Carbon metabolism in *S. oneidensis* MR-1. NAG and lactate metabolism in *Shewanella oneidensis* under aerobic conditions.

2.4.2. Analysis of NADH dehydrogenase mutant growth and metabolism

To study the impact of NADH dehydrogenase activity on growth and metabolism, we created an in-frame deletion in an essential gene in each putative NADH dehydrogenase-encoding operon in *S. oneidensis* MR-1; *nuoN* (SO_1009), *ndh* (SO_3517), *nqrF1* (SO_1108), and *nqrF2* (SO_0907). Deletions were made in the terminal gene in each operon to restrict downstream pleiotropic effects while removing function of each dehydrogenase. We cultured wild type *S. oneidensis* MR-1 (WT) and the NADH dehydrogenase mutants in minimal medium in 24-well plates and measured growth via OD_{600}. Our measurements aligned well with observations from the whole-genome fitness analysis, confirming that culturing the mutants using D,L-lactate or NAG has differential effects on growth. The Δ*ndh* and Δ*nqrF2* mutants did not show growth defects with either NAG or D,L-lactate as carbon sources under oxic conditions and therefore were omitted from further study (Figure S2.1).

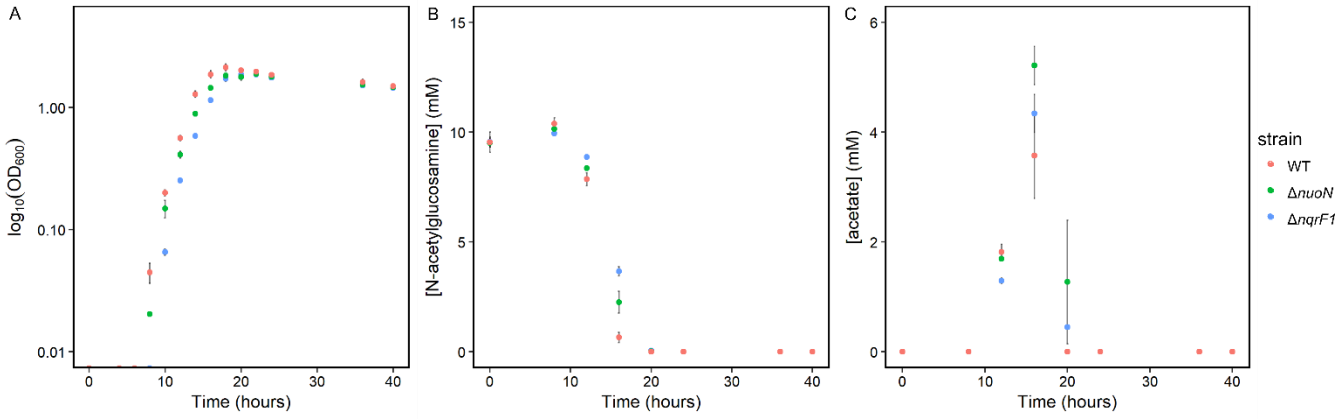

Figure 2.3. WT and NDH mutant growth on NAG. (A) Analysis of WT, Δ*nuoN*, and Δ*nqrF1* grown in 50 mL M5 minimal medium with 10 mM NAG in a 250-mL flask. (B) NAG concentration in culture supernatant, and (C) acetate concentration in culture supernatant.

Growth studies were repeated using a higher volume in flasks. As predicted by fitness data and growth in 24-well plates, both Δ*nuoN* and Δ*nqrF1* showed growth defects in minimal

medium supplemented with 10 mM NAG as the carbon source (Figure 2.3A). Both mutants had significantly decreased growth rates compared with WT: 0.93 ± 0.05 h^{-1} for WT, 0.76 ± 0.06 h^{-1} for Δ*nuoN*, and 0.81 ± 0.04 h^{-1} for Δ*nqrF1* (Table 2.1). To better understand the mechanism of the growth defect, the concentrations of substrates and metabolic byproducts in the culture were monitored by HPLC throughout growth. We observed that both mutants consumed significantly less NAG than WT at the 12- (Δ*nqrF1*, $p \leq 0.01$; Δ*nuoN*, $p \leq 0.05$) and 16-hour (Δ*nqrF1*, $p \leq 0.001$; Δ*nuoN*, $p \leq 0.01$) time points (Figure 2.3B). Acetate accumulation in cultures of both mutant strains was significantly higher than in cultures of WT at 20 hours of growth ($p \leq 0.01$) although all strains had consumed the excreted acetate by 40 hours (Figure 2.3C). No other major products were observed.

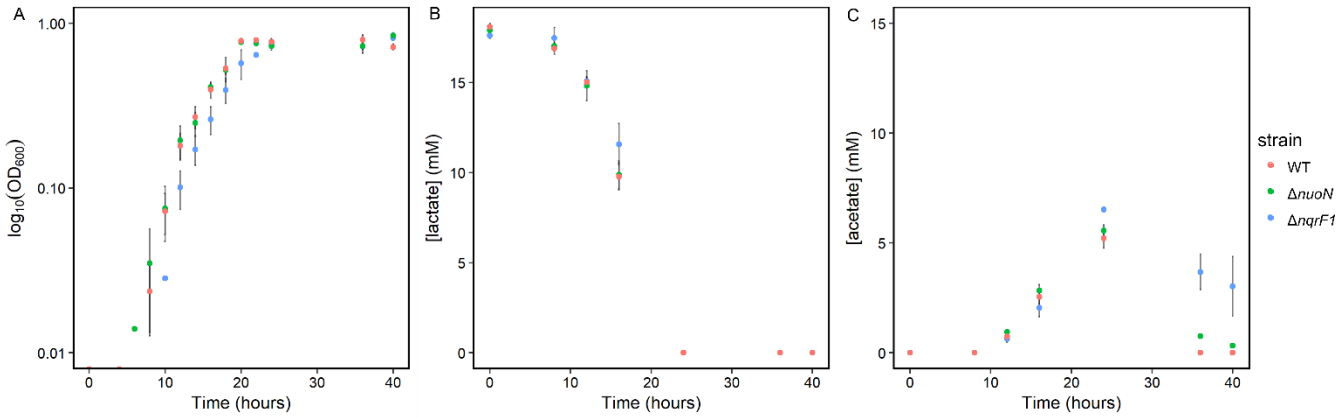

Figure 2.4. WT and NDH mutant growth on D,L-lactate. (A) Analysis of WT, Δ*nuoN*, and Δ*nqrF1* grown in 50 mL M5 minimal medium with 20 mM D,L-lactate in a 250-mL flask. (B) D,L-lactate concentration in culture supernatant, (C) acetate concentration in culture supernatant.

Flask growth experiments were also performed using 20 mM D,L-lactate as the substrate. Growth rates were not significantly different from WT for either Δ*nqrF1* or Δ*nuoN* (Table 2.1). However, Δ*nqrF1* showed a distinct delay in growth although all cultures were inoculated to the same cell density at the same time (i.e., overall OD_{600} is significantly lower than WT from 12 to

16 hours). This effect is less pronounced than the growth rate defect with NAG, but was repeatable (Figure 2.4A, Figure S2.1). Similar to growth, D,L-lactate consumption and acetate accumulation by the Δ*nuoN* mutant were essentially indistinguishable from WT. However, the Δ*nqrF1* mutant displayed subtle differences from WT. Δ*nqrF1* used D,L-lactate more slowly than WT during early logarithmic growth (Figure 2.4B). However, by 24 hours both WT and Δ*nqrF1* both consumed all available lactate (Figure 2.4B). Δ*nqrF1* also accumulated 25% more acetate than WT at 24 hours and had not fully consumed it by 40 hours (Figure 2.4C).

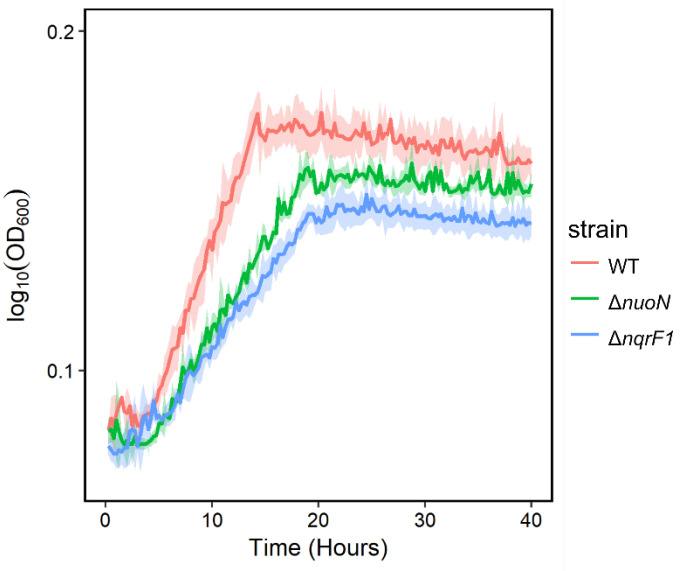

Figure 2.5. WT and NDH mutant growth on acetate. Growth of WT, Δ*nuoN*, and Δ*nqrF1* in 1 mL of M5 medium containing 10 mM sodium acetate in a 24-well plate.

Because we observed increased acetate accumulation by the mutant strains with both substrates, we hypothesized that they had a decreased capacity to consume acetate as a substrate compared to WT. To determine if the mutant strains exhibited a reduced ability to utilize acetate, we conducted a 24-well growth experiment in minimal medium supplemented with 10 mM acetate (Figure 2.5). Both mutant strains Δ*nuoN* and Δ*nqrF1* exhibited growth defects compared to WT in this growth condition (Table 2.1). The WT, Δ*nuoN*, and Δ*nqrF1* grew at rates of 0.55 ±

0.04 h^{-1}, 0.36 ± 0.02 h^{-1} ($p \leq 0.01$), and 0.32 ± 0.01 h^{-1} ($p \leq 0.001$), respectively. The Δ*nuoN* mutant reached a final OD_{600} that was 4% ($p = 0.17$) less than WT and Δ*nqrF1* reached a final OD_{600} that was 12% ($p \leq 0.01$) less than WT, potentially reflecting a reduced efficiency of the overall electron transport chain.

2.4.3. NADH dehydrogenase mutants exhibit reduced acid tolerance

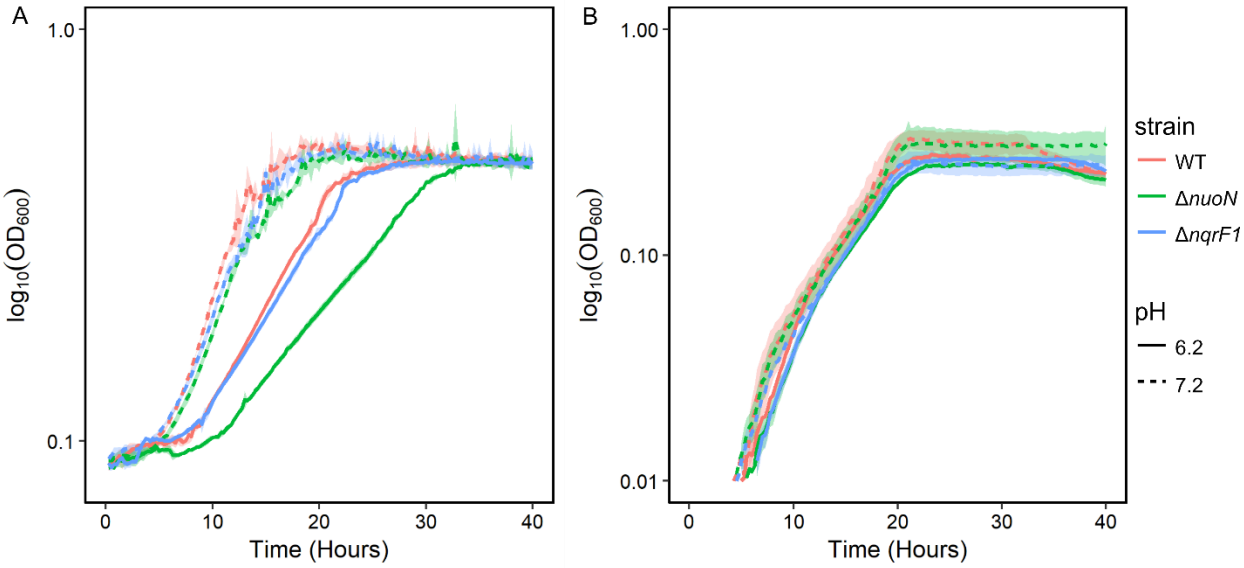

Figure 2.6. Acid tolerance of WT and NDH mutants. Growth of WT, Δ*nuoN*, and Δ*nqrF1* in 1 mL of M5 media containing (A) 10 mM NAG or (B) 20 mM D,L-lactate at a pH of 6.2 or 7.2 in 24-well plates.

To exacerbate the effects of the deletions, we cultured the mutant strains in acidic medium to cause an additional burden on membrane potential. We compared growth in minimal medium at pH 7.2 or 6.2 with 10 mM NAG or 20 mM D,L-lactate as the carbon source (Figure 2.6). Indeed, lower pH increased the defects of both mutant strains when grown with NAG. At lower pH, the Δ*nuoN* strain exhibited a stronger defect than the Δ*nqrF1* strain. When grown with D,L-lactate, mutants grew similarly at pH 7.2 or pH 6.2 indicating that acid stress alone was not a strong enough stressor on membrane potential to cause changes in growth with a substrate producing

minimal NADH and relying on quinone-linked dehydrogenases.

2.4.4. A Δ*nuoN*Δ*nqrF1* double mutant is incapable of aerobic growth in minimal media

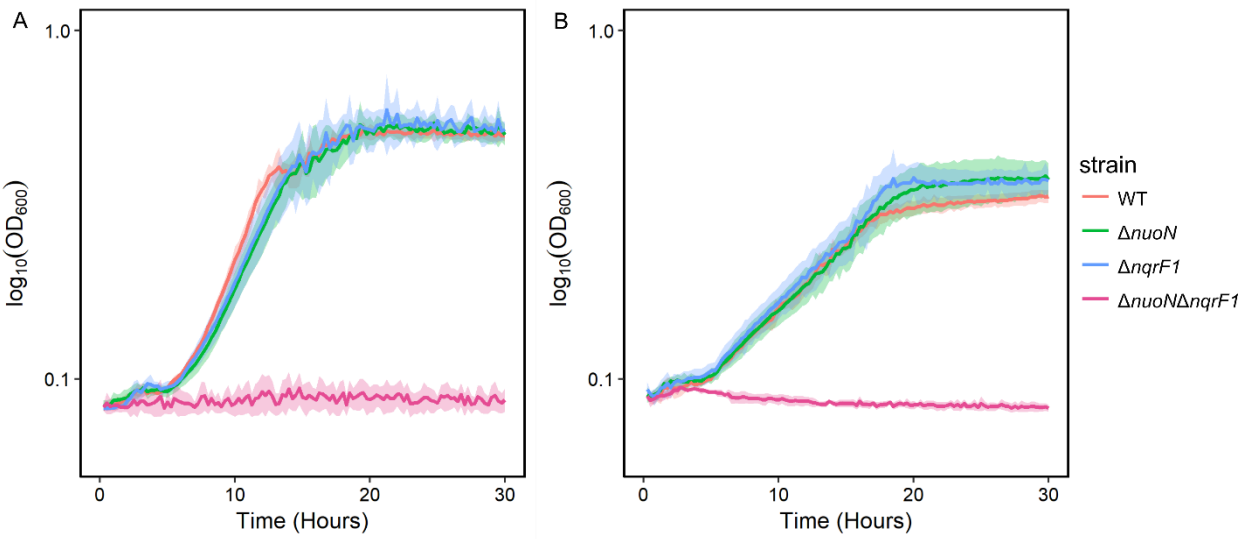

Figure 2.7. Double-knockout is incapable of growth in minimal medium with NAG or D,L-lactate. Growth of WT, Δ*nuoN*, Δ*nqrF1*, and Δ*nuoN*Δ*nqrF1* in 1 mL of M5 medium containing (A) 10 mM NAG or (B) 20 mM D,L-lactate in 24-well plates.

Because both Δ*nuoN* and Δ*nqrF1* strains exhibited only minor differences compared to WT, we created a Δ*nuoN*Δ*nqrF1* double knockout strain to determine whether these complexes have overlapping function. In contrast to the single mutants, this double mutant is incapable of aerobic growth in in minimal media supplemented with either 10 mM NAG or 20 mM D,L-lactate in 24-well plates (Figure 2.7). We also attempted to grow this strain in the same media in flasks and observed no change in OD_{600} over time (data not shown). Even in LB medium, this strain exhibited severely reduced growth compared with WT (Figure S2.2). Because the Δ*nuoN*Δ*nqrF1* strain was unable to grow in minimal media, we did not conduct additional analyses on its phenotype. We complemented the double mutant strain with either *nuoN* or *nqrF1* expressed *in trans* from a multi-copy plasmid. We observed enhanced growth rates in LB for both

complemented strains compared with Δ*nuoN*Δ*nqrF1* carrying a plasmid with GFP (Figure S2.3). This indicates that the growth defect observed for the double mutant was due to the absence of these genes, rather than an off-target effect.

2.5. Discussion

2.5.1. Implications of growth defects in NADH dehydrogenase mutant strains

Growth deficiencies in the single and double knockout strains show that both Nuo and Nqr1 are important for aerobic growth and metabolism in *S. oneidensis* MR-1. The subtle phenotypes of the single mutant strains indicate that the two complexes have significant functional overlap, and that it is not necessary for both to function under the tested conditions. However, the severe defect of the double mutant strain indicates that Nqr2 and Ndh are unable to compensate for the combined loss of Nuo and Nqr1, indicating that at least one is necessary. We hypothesize that Ndh cannot compensate because it does not generate PMF or SMF, and that Nqr2 cannot compensate because it is not significantly expressed under aerobic conditions. Our data suggests that Nqr1 plays a greater role than Nuo under the tested conditions due to the more significant phenotypes of the Δ*nqrF1* strain. This is unsurprising, given the distribution of each of these in the genus, as discussed in the introduction. However, Nuo may play a more important role in managing acid stress, considering that at pH 6.2 a greater growth defect was observed for Δ*nuoN* than for Δ*nqrF1*. These data suggest that although the two NADH dehydrogenases are likely used concurrently during aerobic respiration, they also have distinct roles.

2.5.2. Changes in metabolism suggest inhibition of the TCA cycle by increased intracellular NADH

We observed that carbon sources that must be processed by the TCA cycle (and therefore,

generate NADH) exacerbate the growth defect in the single mutant strains. Metabolism of both NAG and acetate rely primarily on NADH as the electron carrier to feed the electron transport chain, while lactate may be partially oxidized by quinone-linked dehydrogenases that bypass NADH. We observed that growth with lactate was much less sensitive to the NADH dehydrogenase deletions than growth with the other substrates. It is somewhat surprising that growth defects were stronger with acetate than with NAG, although this may be explained by the possibility to generate formate through pyruvate formate lyase during NAG (or lactate) metabolism, but not during acetate metabolism. Acetate metabolism may be further hindered by allosteric reduction of activity of TCA cycle enzymes by high levels of NADH in the mutant strains. Although we have no direct measurements of intracellular NADH levels, accumulation of extracellular acetate during growth on NAG and D,L-lactate suggests that insufficient TCA cycle activity in the mutants forces acetate excretion. In the case of NAG, the acetate may be produced by either initial removal of the acetyl group or by production of acetyl-coA after glycolysis, but either way, the acetate is being excreted rather than being processed.

2.5.3. Roles of sodium ion vs proton energetics in *S. oneidensis* MR-1

We observed that Nuo and Nqr1 have overlapping function but did not elucidate how electron flux is partitioned between them when both are present. Analysis of the *Shewanella* genus provides some evidence that more flux would be directed to Nqr1, which would align well with our growth observations. While most *Shewanella* isolates originate from marine environments, *S. oneidensis* MR-1 was isolated from a freshwater lake. This habitat difference seems to be reflected in *Shewanella* energetics (87). *Shewanella* spp. generally utilize only sodium-ion based energetics, which can be advantageous in a marine environment, but *S. oneidensis* MR-1 has gained complexes for proton-based energetics through horizontal gene transfer. For example, all

sequenced genomes in the *Shewanella* genus encode sodium ion-dependent Nqr NADH dehydrogenases, but *S. oneidensis* MR-1 is one of only a few strains that encode the proton-dependent NADH dehydrogenase, Nuo (10, 88). Similarly, *S. oneidensis* MR-1 is the only strain in the genus with both SMF- and PMF-driven flagellar machinery, while the rest of the genus only has the SMF-driven system (74). Previous studies have not observed strong defects for knocking out PMF-dependent systems (22, 89) and our results reveal slightly stronger defects for Nqr1 mutants than Nuo mutants. This suggests that sodium remains an important coupling ion in *S. oneidensis* MR-1 despite its acquisition of PMF-dependent machinery. The potential benefits of maintaining both systems in the *S. oneidensis* MR-1 genome remain unclear.

The co-utilization of proton- and sodium-dependent energetics in *S. oneidensis* MR-1 raises the question of whether SMF and PMF could be conserved separately for different cellular functions. While the $\Delta\Psi$ component is shared between PMF and SMF, the ΔpH and $\Delta[Na^+]$ components can vary and thereby influence the relative activity of PMF- versus SMF-dependent processes. *S. oneidensis* MR-1 preferentially utilizes its sodium-ion dependent stator, but its ATP synthase does not contain the necessary residues for sodium ion transport, indicating that it is proton-dependent (77, 78). This arrangement could allow *S. oneidensis* MR-1 to favor either motility or ATP synthesis by upregulating Nqr1 or Nuo, respectively. Antiporters may also be utilized to interconvert between ΔpH and $\Delta[Na^+]$ and thereby allow adaptive utilization of ion gradients for different functions (79, 90). Further study is needed to determine whether *S. oneidensis* MR-1 utilizes its coupling ion flexibility to conserve energy for different purposes.

2.5.4. Implications of Na^+ dependent energetics for bioelectrochemical technologies

The ability to use a sodium-based respiratory system may have wide-ranging impacts on the physiology of *S. oneidensis* MR-1 in bioelectrochemical systems, particularly because local pH

extremes near electrodes can be a major limiting factor (91). Previous analysis of biocathode processes has suggested that sodium ion-based respiration may be advantageous for organisms on a biocathode because of high local pH at the electrode (91). The localized alkaline pH at the biocathode can lead to loss of PMF in the biofilm and hinder proton-dependent respiration (92). Therefore, *S. oneidensis* MR-1 may represent a promising chassis for engineering cathodic bioelectrochemical technologies, such as microbial electrosynthesis. Understanding the interactions between pH and the NADH dehydrogenases at the electrode would also allow us to better explore the genetic optimization of organisms in bioelectrochemical systems in general.

2.5.5. Perspectives for future work

To better understand the specific function of each dehydrogenase, it is necessary to generate triple knockout strains, leaving only one functional NADH dehydrogenase in the genome, wherever possible. Membrane preparations from such strains could be used to confirm activity of each of these dehydrogenases through biochemical assays. If these strains are nonviable, a recently developed CRISPR interference system could be utilized to 'knock down' expression of the NADH dehydrogenases (93). This study focused on Nqr1 and Nuo mutants because Nqr2 and Ndh mutants showed no growth defects in oxic conditions, however, we hypothesize that Nqr2 and Ndh mutants will exhibit growth defects under anoxic conditions. Future study of all four mutant strains under anoxic conditions would also provide the opportunity to explore a wider range of thermodynamic constraints on metabolism, which may influence respiratory efficiency.

2.6. Conclusion

Under the laboratory conditions tested, *S. oneidensis* MR-1 utilized both Nqr1 and Nuo to oxidize NADH and conserve energy during aerobic growth. While single mutants lacking the

activity of either complex grew only slightly slower than WT, a double-knockout lacking both was completely incapable of growth in minimal media. Although two additional NADH dehydrogenases are encoded in the genome, either Nuo or Nqr1 was required for aerobic growth in minimal media. Changes in accumulation of acetate suggest that when either of these complexes is absent, intracellular NADH levels increase, and potentially inhibit TCA cycle activity. We suggest that co-utilization of Nuo and Nqr results in adaptive metabolic redundancy and may represent a mechanism by which *S. oneidensis* MR-1 could conserve energy for different purposes, such as motility (preferentially sodium ion-dependent) and ATP generation (likely proton-dependent).

2.7. Materials and Methods

2.7.1. Analysis of a whole-genome fitness profiling dataset

Fitness data for *S. oneidensis* MR-1 transposon mutants was downloaded as a supplementary information file for the whole-genome fitness profiling study by Deutschbauer et al. (85). Fitness values were averaged across each NADH dehydrogenase operon and across groups of conditions. Values for libraries grown in minimal medium were plotted.

2.7.2. In-frame deletion of loci from the *S. oneidensis* MR-1 genome

Deletions of target genes were made using the pDS3.0 non-replicative vector as previously described and confirmed by PCR (40). Fusion products were made via PCR, generating tagged complementary sequence fragments that were subsequently linked following the cross-over PCR protocol. Six primers were designed and used for each strain, with the unique tag sequences added to the 5i and 3i primers (Table 2.2). Fusion products were inserted into the pDS3.0 vector with T4 ligase and transformed into chemically competent *E. coli* WM3064 cells via heat shock.

The plasmids were transferred to *S. oneidensis* MR-1 via a conjugation protocol similar to Webster et al. (66). Primary conjugants were screened for gentamycin resistance and insertion into the genome was confirmed via two PCR reactions: one reaction with FO and 3o primers; and another with 5o and RO primers. Primary integrants were grown for 8 hours in LB without NaCl, then plated on LB without NaCl and with 10% sucrose. Individual colonies were screened via PCR using FO and RO flanking primers (Table 2.2) to identify deletion mutants. To acquire the double mutant strain, it was necessary for the resolution step of the protocol to be extended from 18 hours to 22 hours. At 18 hours, the cells still maintained antibiotic resistance indicating that the plasmid had not yet resolved out of the genome of most cells.

2.7.3. Growth conditions

All strains were pre-cultured in LB medium (Miller, Accumedia) for 16 hours. Pre-cultures were washed with M5 medium and standardized to OD_{600}=1.0 prior to use. All growth experiments utilized the following M5 minimal medium recipe: 1.29 mM K_2HPO_4, 1.65 mM KH_2PO_4, 7.87 mM NaCl, 1.70 mM NH_4SO_4, 475 μM $MgSO_4 \cdot 7H_2O$, 10 mM HEPES, 0.01% (w/v) casamino acids, 1X Wolfe's mineral solution (Al was not included), and 1X Wolfe's vitamin solution (riboflavin was not included), pH adjusted to 7.2 with 1 M NaOH. Either NAG or sodium D,L-lactate was added to a final concentration of 10 mM or 20 mM, respectively, unless noted otherwise. We conducted an additional experiment to ensure that differences in sodium concentration between NAG and D,L-lactate did not cause significant changes in growth (Figure S2.4). We did not observe any significant difference, therefore extra sodium was not routinely added to medium with NAG.

High-throughput growth experiments were performed in clear 24-well culture plates (Sigma, SIAL0526) using 1 mL M5 medium, with four replicates per strain. Wells were

inoculated with 10 µL of standardized pre-culture (washed in M5 and diluted to OD_{600}=1) and incubated in a Synergy HTX plate reader (BioTek Instruments, Winooski, VT) at 30°C with maximal shaking amplitude and minimal shaking speed. OD_{600} was recorded by the instrument at 15-minute intervals. High-throughput growth pH experiments were performed in 24-well plates as described above with the following modifications: M5 was prepared with the pH adjusted to 6.2 with 1 M HCl prior to autoclaving, 24-well plates were prepared with triplicates for each strain in each condition: M5 pH 7.2 and M5 pH 6.2.

Flask growth experiments were performed in 250-mL Erlenmeyer flasks using 50 mL of M5 media supplemented with either 20 mM D,L-lactate or 10 mM NAG. Flasks were inoculated with 50 µL of standardized pre-culture and incubated in a floor shaker (New Brunswick Scientific, 12500) at 30°C and shaking at 275 rpm. Cultures were grown in triplicate for 40 hours. Growth was monitored by removing 1 mL every two hours starting four hours post inoculation and measuring the OD_{600}. Samples were stored at -20°C prior to preparation for HPLC analysis.

2.7.4. HPLC analysis

HPLC analysis was performed on a Shimadzu 20A HPLC, using an Aminex HPX-87H column with a Micro-guard Cation H^+ guard column (BioRad, Hercules, CA) at 55°C. Samples were analyzed with a 0.6 mL/min flow rate, in 5 mM sulfuric acid with a 30-minute run time. Eluent was prepared by diluting a 50% HPLC-grade sulfuric acid solution (Fluka) in Milli-Q water and then degassing the solution at 37°C for 3-5 days before use. Compounds of interest were detected by refractive index (RID-20A). Samples were prepared by centrifuging 1 mL samples taken from flask growth for 10 minutes at 13,000 x g in a microcentrifuge (Minispin Plus, Eppendorf) to remove cells. The supernatant was removed and transferred to a 2.0-mL glass

HPLC vial. Standards were prepared at concentrations of 1, 2, 5, 10, and 20 mM for D,L-lactate, NAG, and sodium acetate. Samples were maintained at 10°C by an auto-sampler throughout analysis.

2.7.5. Complementation

The double mutant strain was complemented using an IPTG-inducible plasmid, pRL814 (a generous gift from Dr. Robert Landick, University of Wisconsin, Madison). pRL814 was isolated from *E. coli* using an E.Z.N.A plasmid DNA kit (Omega Bio-Tek). Prepared plasmid DNA was linearized using NdeI and HindIII (New England Biolabs). *S. oneidensis* MR-1 Genomic DNA was isolated using the UltraClean Microbial DNA isolation kit (MO Bio, Carlsbad, CA). Primers used to amplify *nuoN* or *nqrF1* from *S. oneidensis* MR-1 genomic DNA were generated using the NEBuilder tool (New England Biolabs, Ipswich, MA). Linearized pRL814 and *nuoN* or *nqrF1* were assembled using NEBuilder High Fidelity DNA assembly kit (New England Biolabs, Ipswich, MA) using the standard protocol (94). Following assembly *E. coli* WM3064 chemically competent cells were transformed with either pRL814_*nuoN* or pRL814_*nqrF1*. WM3064 strains were then used in conjugation with *S. oneidensis* MR-1 into the Δ*nuoN*Δ*nqrF1* strain. In parallel, WM3064 strains bearing unmodified pRL814 (which expresses GFP), were used in conjugation with wild type MR-1 and Δ*nuoN*Δ*nqrF1*. The control and complemented strains were grown in LB medium containing 100 μM IPTG and 50 μg/mL spectinomycin. Growth experiments were conducted in 24-well plates, with a 1 mL culture volume, in LB medium containing 100 μM IPTG and 50 μg/mL spectinomycin. Wells were inoculated with 10 μL of standardized pre-culture (washed in LB + 100 μM IPTG + 50 μg/mL spectinomycin and diluted to OD_{600}=1) and incubated in a Synergy HTX plate reader (BioTek

Instruments, Winooski, VT) at 30°C with maximal shaking amplitude and minimal shaking speed. OD_{600} was recorded by the instrument at 15-minute intervals.

2.7.6. Data analysis

Analysis of growth and HPLC data was performed using Rstudio (95) using the following packages: ggplot2 (96), reshape2 (97), dplyr (98), and TTR (99). Analysis of growth rates from flask growth experiments were performed using R package ‘growthcurver’ using default values with background correction set to “min” (100).

2.8. Acknowledgements

This research was partially supported by a fellowship from Michigan State University under the Training Program in Plant Biotechnology for Health and Sustainability (T32-GM110523). The authors thank Dr. Robert Landick for the pRL814 plasmid and information regarding its use. The authors also thank Dr. N. Cecilia Martinez-Gomez for helpful comments on the experiments and manuscript.

Chapter 3: *Shewanella oneidensis* NADH dehydrogenase mutants exhibit an amino acid synthesis defect

This chapter contains an edited version of a previously published research article in *Frontiers in Energy Research*, Volume 7.

Authors: Kody Lee Duhl[1] and Michaela A. TerAvest[1]

[1]Department of Biochemistry and Molecular Biology, Michigan State University, East Lansing, MI, USA

3.1. Abstract

Shewanella oneidensis MR-1 is a dissimilatory metal reducing bacterium with a highly branched respiratory electron transport chain. The *S. oneidensis* MR-1 genome encodes four NADH dehydrogenases, any of which may be used during respiration. We previously determined that a double-knockout of two NADH dehydrogenases, Nuo and Nqr1, eliminated aerobic growth in minimal medium. However, the double-knockout strain was able to grow aerobically in rich medium. Here, we determined that amino acid supplementation rescued growth of the mutant strain in oxic minimal medium. To determine the mechanism of the growth defect, we monitored growth, metabolism, and total NAD(H) pools in *S. oneidensis* MR-1 and the NADH dehydrogenase knockout strain. We also used a genetically encoded redox sensing system and determined that NADH/NAD^+ was higher in the mutant strain than in the wild-type. We observed that the double-knockout strain was able to metabolize D,L-lactate and N-acetylglucosamine when supplemented with tryptone, but excreted high concentrations of pyruvate and acetate. The requirement for amino acid supplementation, combined with an apparent inability of the mutant strain to oxidize pyruvate or acetate suggests that TCA cycle activity was inhibited in the mutant strain by a high NADH/NAD^+.

3.2. Introduction

Shewanella oneidensis MR-1 is a model organism studied for its ability to respire with a variety of terminal electron acceptors, including oxygen, nitrate, TMAO, metal oxides, and electrodes (11, 12, 69, 101–104). Underlying the respiratory versatility of *S. oneidensis* MR-1 is a highly branched electron transport chain, including four NADH dehydrogenases and 3 aerobic terminal oxidases, along with specialized terminal oxidases for a variety of electron acceptors (10, 85, 105). Even within use of a single electron acceptor, *S. oneidensis* MR-1 can remodel its electron

transport chain depending on environmental conditions. For example, the *cbb*$_3$ cytochrome oxidase and the *bd* quinol oxidase are regulated in response to oxygen concentration, with the *bd* oxidase being upregulated under microaerobic conditions (29). A third aerobic terminal oxidase, the *caa*$_3$ cytochrome oxidase, is rarely expressed in *S. oneidensis* MR-1 and has only been observed under high oxygen, low organic carbon conditions (24). The variety of respiratory complexes and their differential regulation may allow *S. oneidensis* MR-1 to optimize metabolic flux and energy conservation under the wide range of redox conditions it experiences in the environment.

Differential expression of respiratory complexes has wide-ranging effects on physiology because the electron transport chain is essential to maintaining redox balance and generating ion-motive forces by translocating H^+ or Na^+ across the inner cell membrane. The ion-motive forces generated by the electron transport chain power ATP synthesis, transport, and flagellar rotation, making them essential to the growth and maintenance of the cell (74, 89, 106). Differential regulation of electron transport chain complexes will affect cellular energetics because the complexes vary kinetically and in their efficiencies of energy conservation. For example, the NADH dehydrogenases range from pumping $4H^+$ per electron pair (Nuo), to $2Na^+$ per electron pair (Nqr1 and Nqr2, $2Na^+/2e^-$), to 0 ions per electron pair (Ndh) (10). By upregulating Nuo, *S. oneidensis* can gain the maximum ion-motive force for each NADH oxidized, whereas by upregulating Ndh, it can maintain a homeostatic redox state ($NADH/NAD^+$) even when the demand for ion-motive forces is low.

Evidence of electron transport chain remodeling at the NADH dehydrogenase step has previously been found in *Bacillus subtilis*. The type II NADH dehydrogenase, Ndh, is directly linked to a regulatory loop driven by $NADH/NAD^+$ within the cell. As NADH levels increase,

Ndh is upregulated to ensure large fluctuations in NADH/NAD^+ do not occur (45). *Escherichia coli* has also alters the ratio of its type I and type II NADH dehydrogenases depending on growth conditions (107–109). With four NADH dehydrogenases encoded in the genome, it appears likely that remodeling of the electron transport chain for energy conservation and redox maintenance also occurs in *S. oneidensis* MR-1. To better understand the *S. oneidensis* MR-1 electron transport chain, we have begun to characterize the roles of NADH dehydrogenases in physiological processes such as redox homeostasis and energy conservation.

We previously found that the presence of either Nuo or Nqr1 is required for growth under oxic conditions in minimal medium with D,L-lactate or N-acetylglucosamine (NAG) as the substrate (101). However, we did not determine whether the growth defect was caused by an inability to maintain sufficient ion-motive force across the membrane or lack of capacity to re-oxidize NADH. We hypothesized that the growth defect in a Nuo/Nqr1 double knockout strain was due to an inability to re-oxidize NADH, rather than lack of ion-motive forces, because *S. oneidensis* is capable of aerobic growth without ATP synthesis via the F_0F_1-ATP synthase (110). To test this hypothesis, we monitored growth, substrate utilization, product formation, redox state, and NAD(H) pools in the mutant strain. We analyzed redox state in real-time using a genetically encoded redox sensing system based on a transcriptional regulator, Rex, from *Bacillus subtilis* (111). We observed broad metabolic disruption in the double mutant strain. Growth was rescued by amino acid supplementation, suggesting that the growth defect was caused by an inability to synthesize amino acids because of TCA cycle inhibition.

3.3. Results

3.3.1. *S. oneidensis* NADH dehydrogenase mutant requires amino acid supplementation

We previously developed NADH dehydrogenase knockout strains of *S. oneidensis* MR-1 and found a severe growth defect for a strain lacking Nuo and Nqr1 (Δ*nuoN*Δ*nqrF1*). The Δ*nuoN*Δ*nqrF1* strain was able to grow in lysogeny broth (LB) but not in M5 minimal medium under oxic conditions (101). To determine which components of LB enabled growth, we grew the double-knockout strain in M5 minimal medium supplemented with the major components of LB; 0.5% and 1.0% (w/v) tryptone, or 0.25% and 0.5% (w/v) yeast extract. Both tryptone and yeast extract stimulated growth of Δ*nuoN*Δ*nqrF1*, but tryptone had a much greater effect than yeast extract. Addition of 1% tryptone enabled growth rates and final densities similar to the double-knockout in LB medium albeit with a prolonged lag phase (Figure 3.1).

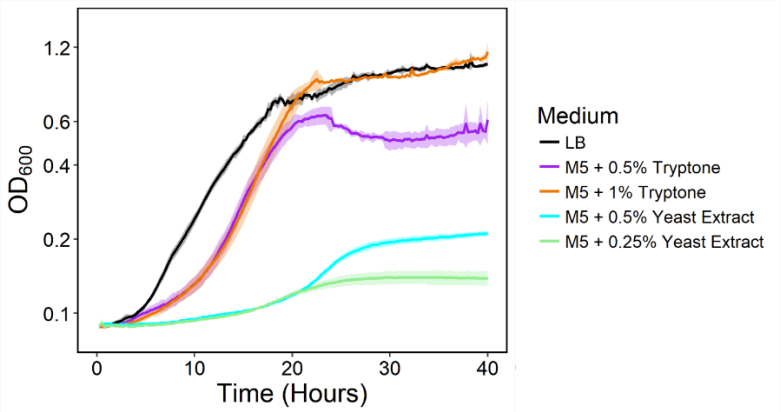

Figure 3.1. LB components rescue double mutant growth. Growth of the Δ*nuoN*Δ*nqrF1* strain in LB (black) or M5 medium supplemented with 0.5% (w/v) (purple) and 1.0% (w/v) (orange) tryptone, and 0.25% (w/v) (light green) and 0.5% (w/v) (cyan) yeast extract in 1-mL volumes in 24-well plates at 30°C with shaking.

To investigate why tryptone addition rescued growth of Δ*nuoN*Δ*nqrF1*, we grew the strain in M5 supplemented with 0.1% tryptone and 20 mM D,L-lactate or 10 mM NAG. To minimize the influence of tryptone as a carbon and energy source, 0.1% (w/v) tryptone was used instead of 0.5% or 1.0%. WT and Δ*nuoN*Δ*nqrF1* were grown for 48 hours in 24-well plates in

the semi-minimal medium with or without an additional carbon source to determine if Δ*nuoN*Δ*nqrF1* used either D,L-lactate or NAG in the presence of tryptone. The presence of 20 mM D,L-lactate increased growth of WT and Δ*nuoN*Δ*nqrF1* compared with 0.1% tryptone alone, suggesting that the mutant strain was capable of metabolizing D,L-lactate in the presence of tryptone (Figure 3.2A). HPLC analysis confirmed that after the 48-hour incubation period, WT used 100% and Δ*nuoN*Δ*nqrF1* used ~75% of the D,L-lactate (Table 3.1). The same results were observed with NAG as the substrate. Both WT and Δ*nuoN*Δ*nqrF1* grew to a higher OD_{600} with NAG and used 100% and ~70% of the NAG, respectively (Figure 3.2B and Table 3.1). The growth rate of Δ*nuoN*Δ*nqrF1* was decreased compared to WT with both D,L-lactate and NAG, indicating a growth defect even in the presence of 0.1% tryptone ($p \leq 0.001$). To determine whether the effect of the tryptone was due to amino acid supplementation, we also compared growth of the wild-type and mutant supplemented with 0.5% casamino acids or a defined mixture of amino acids and 20 mM D,L-lactate or 10 mM NAG. WT grew with the casamino acids and the defined amino acid mixture, but Δ*nuoN*Δ*nqrF1* was unable to grow, suggesting that peptides may be a better amino acid source for *S. oneidensis* than free amino acids, as observed previously (112).

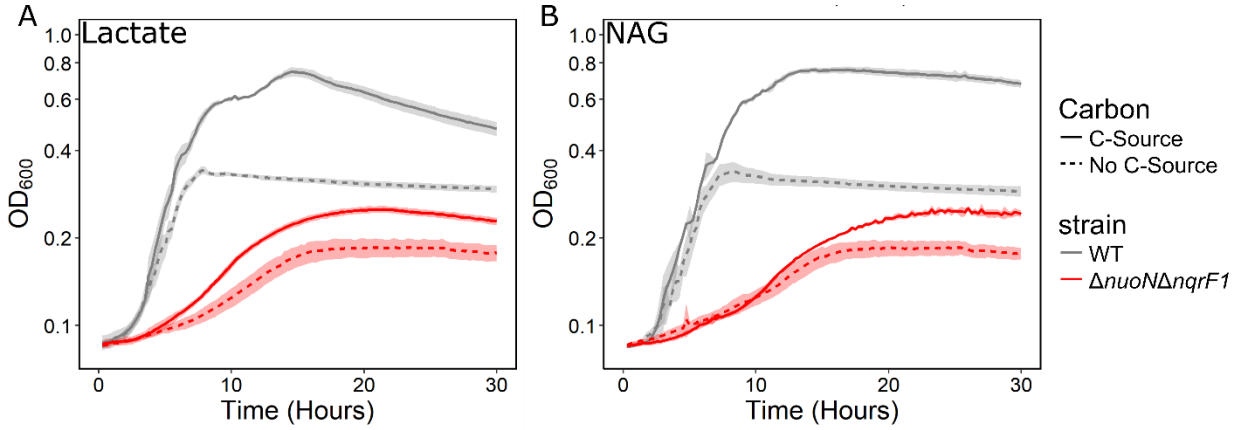

Figure 3.2. Tryptone addition to minimal medium rescues carbon utilization. Growth of WT (grey) and Δ*nuoN*Δ*nqrF1* (red) in M5 minimal medium supplemented with 0.1% tryptone, with (solid line) or without (dashed line) (A) 20 mM DL-lactate or (B) 10 mM NAG as a carbon source. Growth in 1 mL medium in 24-well plates at 30°C with shaking.

3.3.2. Analysis of growth, metabolism, and NAD(H) in Δ*nuoN*Δ*nqrF1*

To clarify the effects of knocking out both Nqr1 and Nuo from *S. oneidensis* MR-1, growth experiments were repeated in 250-mL Erlenmeyer flasks in 50-mL culture volumes. Prior to these experiments, growth was only monitored in 24-well plates in 1-mL culture volumes. Scaling up to 50 mL culture volumes allowed us to sample multiple times throughout growth to monitor metabolic products, and internal redox state ($NADH/NAD^+$). When grown in this culture format in M5 supplemented with 0.1% tryptone and 20 mM D,L-lactate as a carbon source, Δ*nuoN*Δ*nqrF1* again exhibited a severe growth defect compared to WT (Figure 3.3A). The doubling times for WT and Δ*nuoN*Δ*nqrF1* were 0.524 ± 0.053 h and 1.300 ± 0.083 h, respectively ($p \leq 0.001$). Further, Δ*nuoN*Δ*nqrF1* did not fully deplete the D,L-lactate, while WT consumed all available D,L-lactate by 12 hours (Figure 3.3B). WT cultures briefly accumulated small amounts of pyruvate and acetate between hours 6 and 14 of growth, but both were completely consumed by 14 hours. In contrast, Δ*nuoN*Δ*nqrF1* cultures accumulated large amounts of pyruvate and acetate, i.e., >50% of lactate was converted to these products and

excreted (Figures 3.3C and 3.3D). Pyruvate and acetate accumulation in the Δ*nuoN*Δ*nqrF1* cultures remained high through the end of the experiment and it appeared that the mutant strain could not utilize these excreted products. To determine if knocking out Nqr1 and Nuo affected redox state in Δ*nuoN*Δ*nqrF1*, we conducted a colorimetric NADH and NAD^+ assay. We investigated NADH/NAD^+ and total NAD(H) pools. Overall, we did not find consistent differences in NADH/NAD^+ between WT and the mutant, which was unexpected, considering that two NADH dehydrogenases were deleted. However, the total NAD(H) pool of Δ*nuoN*Δ*nqrF1* was 1.75-fold higher than that of WT (Table 3.2).

In 50-mL cultures of M5 supplemented with 0.1% (w/v) tryptone and NAG, Δ*nuoN*Δ*nqrF1* also exhibited a growth defect compared to WT (Figure 3.4A). The doubling times for WT and Δ*nuoN*Δ*nqrF1* were 0.838 ± 0.065 h and 1.823 ± 0.118 h, respectively ($p \leq 0.001$). The ability to utilize NAG as a carbon source was also hindered compared to WT (Figure 3.4B). Similar to what we observed in D,L-lactate, WT cultures accumulated little pyruvate and acetate, while the mutant cultures accumulated high concentrations of these products (>50% of NAG was converted to these products) (Figures 3.4C and 3.4D). In this condition, the redox quantification assay data showed inconsistent NADH/NAD^+ ratios at the time points sampled. Again, the total NAD(H) pool of Δ*nuoN*Δ*nqrF1* was two-fold larger than that of WT at OD_{600}=0.2 (Table 3.2).

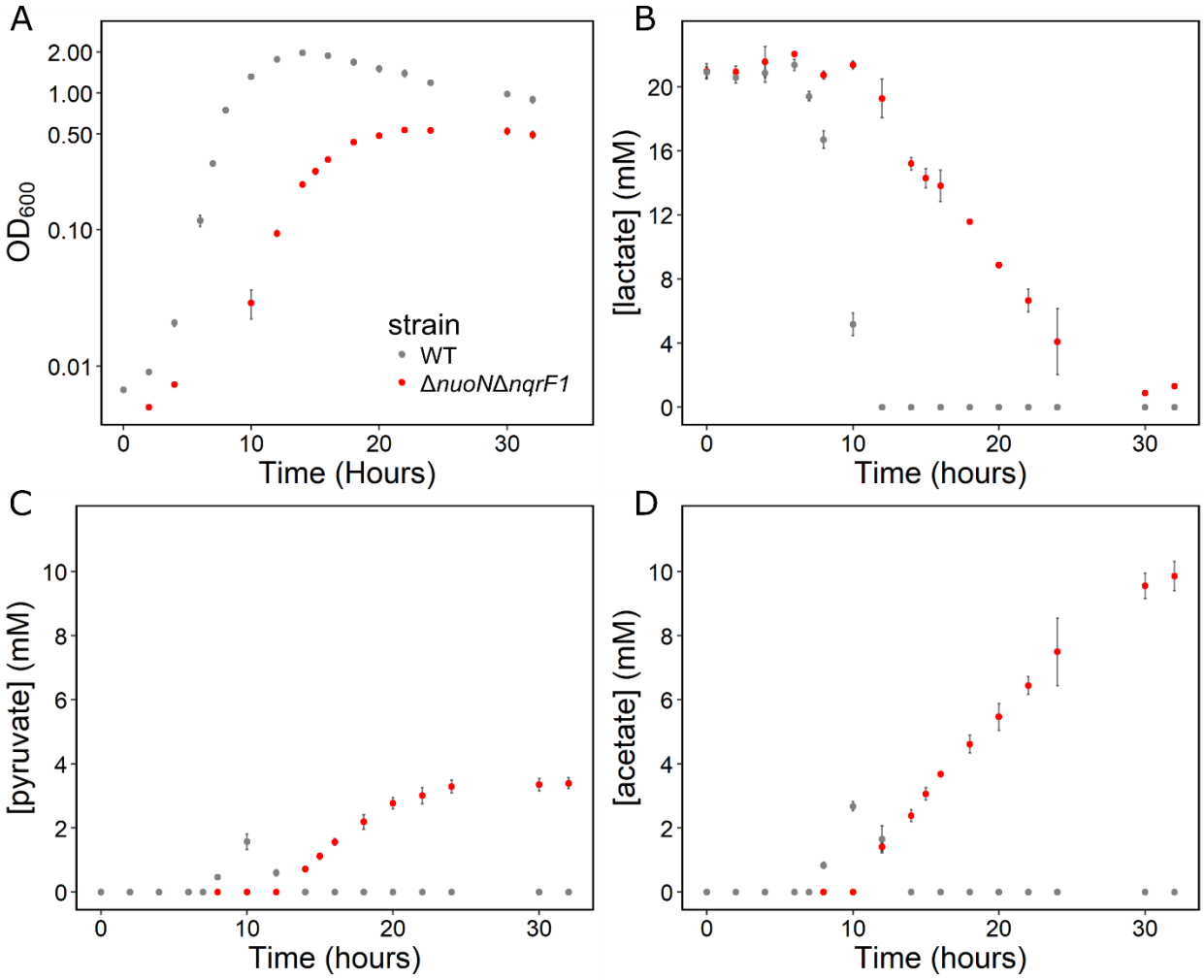

Figure 3.3. The double mutant secretes higher amounts of fermentative metabolites with D,L-lactate as carbon source. (A) Growth of WT (grey) and Δ*nuoN*Δ*nqrF1* (red) in 50-mL culture volumes of M5 minimal medium supplemented with 0.1% tryptone and 20 mM D,L-lactate. (B) D,L-lactate utilization by WT and Δ*nuoN*Δ*nqrF1*. (C) Pyruvate and (D) acetate concentrations in culture supernatants.

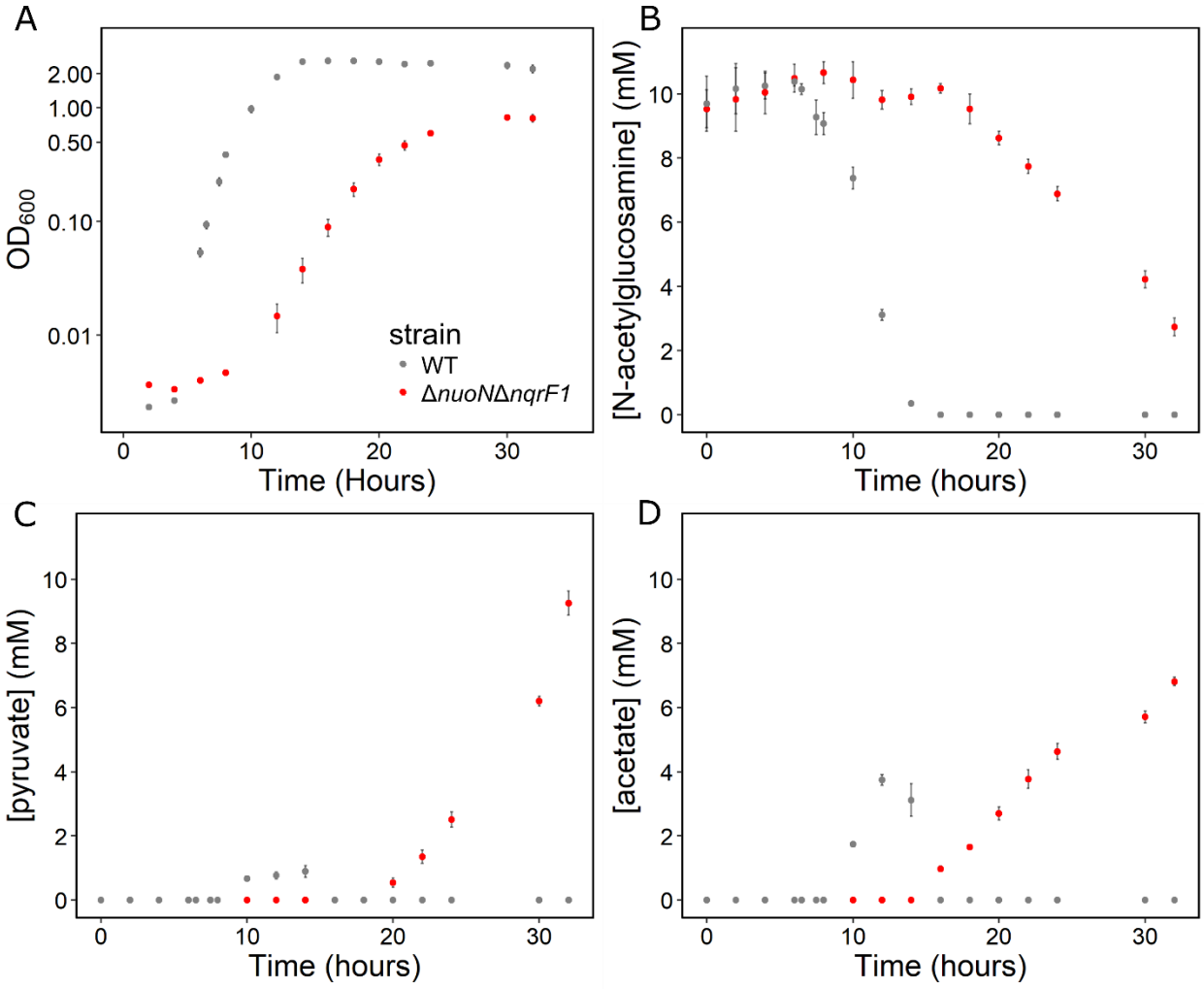

Figure 3.4. The double mutant secretes higher amounts of fermentative metabolites with NAG as carbon source. (A) Growth of WT (grey) and Δ*nuoN*Δ*nqrF1* (red) in 50-mL culture volumes of M5 minimal medium supplemented with 0.1% tryptone and 10 mM N-acetylglucosamine (NAG). (B) NAG utilization by WT and Δ*nuoN*Δ*nqrF1*. (C) Pyruvate and (D) acetate concentrations in culture supernatants.

Altogether, our measurements of NADH/NAD^+ ratios were not consistently different between the two strains. This was unexpected, because the deletion of NADH dehydrogenases, combined with the accumulation of pyruvate and acetate suggest an accumulation of NADH in the mutant strain. We hypothesized that the sampling procedure for the redox assay may have biased the results because it included a 10-minute centrifugation step during which the redox state of the cells could change. To determine whether oxygen levels may have influenced redox

state during the centrifugation step, we measured oxygen consumption in centrifuge tubes. We transferred 25 mL of shaking cultures to a 50 mL conical tube and measured dissolved oxygen concentrations over time. We found that WT and Δ*nuoN*Δ*nqrF1* consumed oxygen at rates of 0.068±0.004 mg/L s^{-1} and 0.058±0.008 mg/L s^{-1} (normalized to OD_{600}), respectively. At these rates, both strains depleted all dissolved oxygen in the culture samples in five minutes or less (Figure S3.1).

We also measured the oxygen consumption rates of both strains in a custom device and found that it was 2.273±0.152 μM/s for WT and 0.936±0.134 μM/s for Δ*nuoN*Δ*nqrF1* at OD_{600}=0.2. During the NADH/NAD^+ extraction process, assuming the initial oxygen concentration in the medium is saturated at 8 mg/L (250 μM) and that no additional oxygen dissolves into the liquid during the centrifugation step, all oxygen in the samples would be consumed within the first two to four minutes of the centrifugation. These calculations are complicated by the possibilities that oxygen in the headspace (10 mL) could dissolve into the sample and that as the cells pellet in the centrifuge, they could create a local environment with even less dissolved oxygen. However, these calculations do suggest that oxygen limitation occurs for both strains during the centrifugation step, thereby causing equalization of the NADH/NAD^+ ratios of the two strains. This helps to explain why we did not observe consistent differences between redox state and only observed differences in the total NAD(H) pool sizes.

3.3.3. Analyzing NADH dehydrogenase knockouts using a genetically-encoded sensor

Because sampling cells for the enzymatic NADH/NAD^+ assay likely biased our results, we monitored redox state in real-time with a transcriptionally regulated redox sensor (111). The sensor is based on the transcriptional repressor Rex from *B. subtilis* (111). This redox sensor results in increased green fluorescent protein (GFP) production when NADH/NAD^+ increases.

We introduced the sensor into *S. oneidensis* MR-1 and the NADH dehydrogenase knockout strain, Δ*nuoN*Δ*nqrF1*. To determine whether the redox sensor was functional in *S. oneidensis* MR-1, we monitored reporter fluorescence during an aerobic to anaerobic transition. Two sets of triplicate 50-mL WT (with redox sensor) cultures were grown aerobically for 6 hours. After incubating under oxic conditions, one of the triplicate sets was incubated on the benchtop without shaking for 2 hours, then transferred to an anoxic environment and given 50 mM fumarate as a terminal electron acceptor. We expected the reporter output to increase in cultures that were moved to an anaerobic environment because limitation of available terminal electron acceptor will increase intracellular NADH/NAD^+. Increased NADH accumulation has previously been observed in *E. coli* cultures in anaerobic conditions versus aerobic conditions (113). As predicted, fluorescence output from *S. oneidensis* with the Rex-based sensor increased in cultures that were transitioned from an aerobic to an anaerobic environment compared to the cultures that remained aerobic (Figure 3.5). These results suggest that the sensor functions as expected in *S. oneidensis* MR-1 and responds to increased NADH/NAD^+.

We conducted growth experiments and monitored OD_{600} and reporter fluorescence in *S. oneidensis* MR-1 and Δ*nuoN*Δ*nqrF1* in 24-well plates. Fluorescence per OD_{600} was higher in Δ*nuoN*Δ*nqrF1* than WT during log-phase and early stationary phase for both carbon sources, suggesting that the mutant strain exhibits increased NADH/NAD^+ during growth (Figure 3.6). However, it is important to note that the redox sensor altered growth of the strains. Therefore, we conducted a side-by-side comparison between strains with and without the sensor. We observed that the presence of the Rex-based redox sensor delayed growth of WT by about 14 hours with D,L-lactate and 18 hours with NAG (Figure 3.7). Lag times varied somewhat between experiments (Figures 3.6 and 3.7), possibly due to small differences in the growth phase of the

overnight cultures used for inoculum. However, we consistently observed an extended lag phase in WT containing the Rex sensor. The sensor also affected the growth rates of both strains with either D,L-lactate or NAG as the substrate, although the growth rate of the mutant was still lower than WT in all cases (Table 3.3). We conducted HPLC analysis of metabolites generated by the strains containing the Rex sensor. Similar to strains without the sensor, WT was able to deplete all initial carbon source, while the mutant was not (Table 3.4). Also in line with results without the sensor, the mutant strain produced significant amounts of acetate and pyruvate, while WT did not.

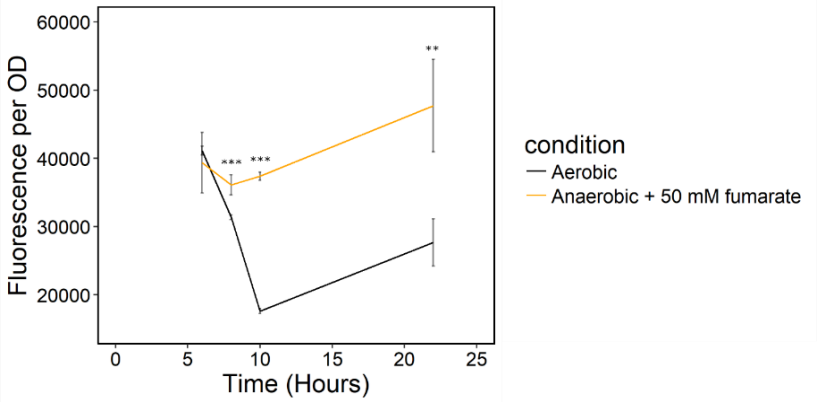

Figure 3.5. Testing the Rex redox sensing system functionality. Transition of *S. oneidensis* MR-1 with the Rex redox sensor growing in triplicate 50-mL cultures of LB from an oxic to an anoxic environment. The aerobic set (black) remained oxic and shaking and the anaerobic set of triplicates was given 50 mM fumarate as a terminal electron acceptor when moved to an anoxic environment (**) ($p \leq 0.01$) and (***) ($p \leq 0.001$) denote significance of difference from the aerobic culture.

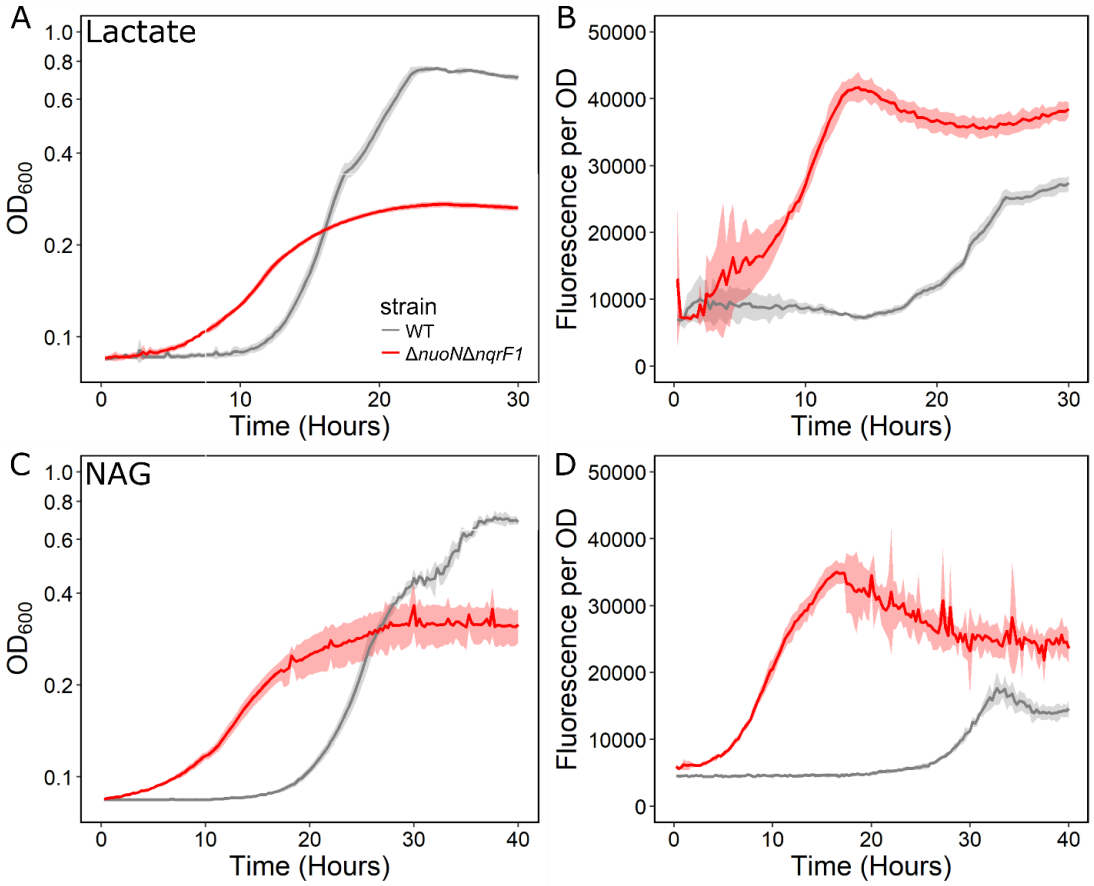

Figure 3.6. The double mutant strain exhibits increased NADH/NAD$^+$. (A) Analysis of growth of the WT and Δ*nuoN*Δ*nqrF1* strains that contain the Rex sensor in 1-mL culture volumes of M5 supplemented with 0.1% tryptone and 20 mM D,L-lactate while at 30°C with shaking. (B) Fluorescence output normalized to OD_{600} with D,L-lactate as the substrate. (C) Analysis of growth of the WT and Δ*nuoN*Δ*nqrF1* strains that contain the Rex sensor in 1-mL culture volumes of M5 supplemented with 0.1% tryptone and 10 mM NAG. (D) Fluorescence output normalized to OD_{600} with NAG as the substrate.

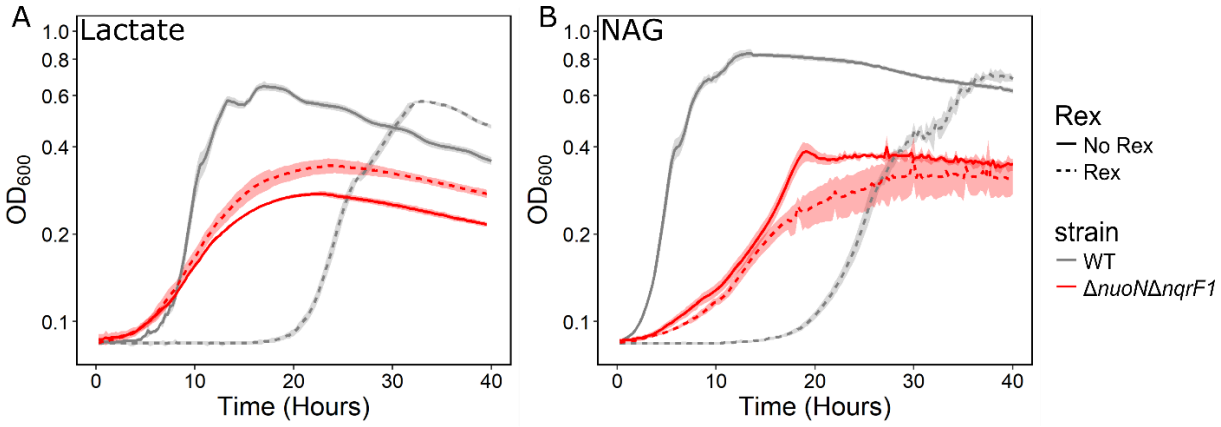

Figure 3.7. Rex redox sensor affects the growth of WT. Comparison of growth of WT (grey), Δ*nuoN* (green), Δ*nqrF1* (blue), and Δ*nuoN*Δ*nqrF1* (red) strains with (solid line) and without (dashed line) the Rex redox sensor in M5 supplemented with 0.1% tryptone and (A) 20 mM D,L-lactate or (B) 10 mM NAG. Growth conditions were done in 1-mL culture volumes in 24-well plates at 30°C with shaking.

3.4. Discussion

As observed in our previous work, Δ*nuoN*Δ*nqrF1* was unable to grow under oxic conditions in M5 minimal medium with either D,L-lactate or NAG as the substrate (101). However, we have now observed that addition of 0.1% (w/v) tryptone to the medium allowed Δ*nuoN*Δ*nqrF1* to grow. The major component of tryptone is free amino acids and peptides, suggesting that the mutant strain requires amino acid supplementation and cannot make sufficient amino acids *de novo* to support growth. Together with accumulation of acetate and pyruvate the requirement for tryptone suggests reduced TCA cycle activity because some TCA reactions are required for *de novo* amino acid synthesis (114). However, there are caveats to using tryptone because it is an undefined tryptic digest of casein and could contain other nutrients. We observed that other sources of amino acids, including casamino acids (acid-hydrolyzed casein) or defined amino acids did not rescue growth of the mutant. However, we propose that the rescue was caused by peptides in the tryptone, not by other nutrients. While there are minor differences in carbohydrate and mineral content between tryptone and casamino acids, these differences are small in

comparison to the total mineral and carbohydrate content of the overall medium recipe (115). Further, previous work indicated that *S. oneidensis* MR-1 is incapable of using individual amino acids as carbon sources but is capable a wide variety of defined dipeptides (112). This suggests that *S. oneidensis* MR-1 is much more efficient in peptide uptake than free amino acid uptake, which would explain why tryptone rescues growth of the mutant, while casamino acids do not.

Along with the growth defect observed in the NADH dehydrogenase knockout strain, another finding of this study was that total NAD(H) pool sizes differed significantly between WT and Δ*nuoN*Δ*nqrF1*. With either D,L-lactate or NAG as carbon sources, we observed roughly two-fold increases in the total NAD(H) pools. We hypothesize that the increased NAD(H) pool size is caused by NAD^+ synthesis to counteract the increase in [NADH] within the cell caused by the limitation of NADH dehydrogenase activity. In *S. oneidensis* MR-1, NAD^+ synthesis is regulated by the repressor NrtR. When [NAD^+] decreases, NrtR is released from promotors to allow expression of NAD^+ synthesis related genes (116). Because we observed increased NAD(H) pool sizes in the Δ*nuoN*Δ*nqrF1* mutant strain, we propose that excess [NADH] and limited [NAD^+] led to overexpression of genes involved in NAD^+ synthesis.

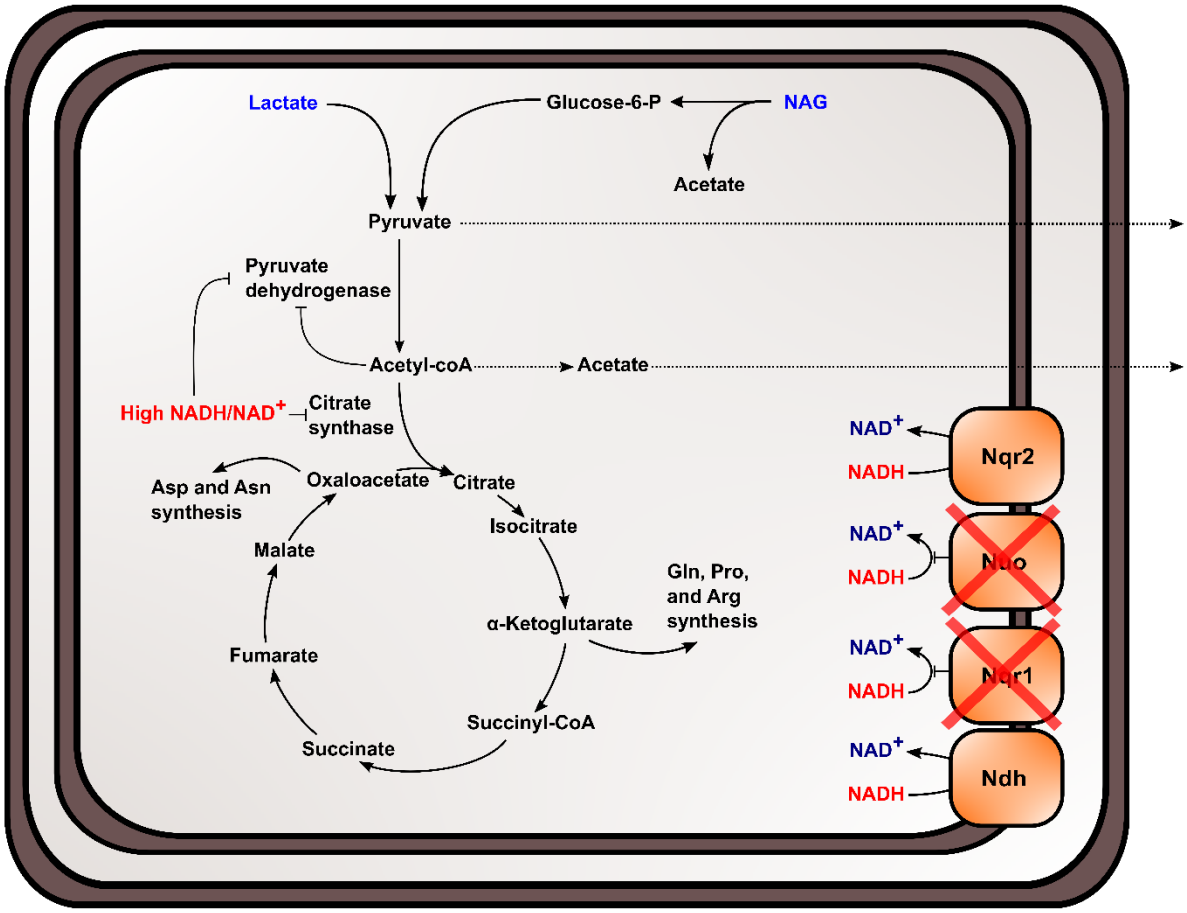

Figure 3.8. Modeling the double mutant strain. Proposed effect of knocking out NADH dehydrogenases in *S. oneidensis* MR-1 and the subsequent effects on NADH oxidation, redox state, and TCA cycle inhibition within the cell.

The TCA cycle and upstream reactions are also affected by changes in internal redox state and NAD(H) pool size. NADH is an inhibitor of citrate synthase, which converts acetyl-CoA and oxaloacetate to citrate to bring carbon into the TCA cycle (Stokell et al., 2003; Weitzman and Jones, 1968). This suggests that increased NADH/NAD^+ may inhibit TCA cycle function by affecting citrate synthase activity. Furthermore, reactions upstream of the TCA cycle maybe affected, because pyruvate dehydrogenase (Pdh) activity is also regulated by NADH/NAD^+ and acetyl-CoA concentrations in *S. oneidensis* MR-1 (69, 83). Reduced citrate synthase activity would increase acetyl-CoA concentrations, which may inhibit Pdh function,

together with increased NADH/NAD^+. It also has been previously shown that Pdh activity can be affected by both NADH/NAD^+ and NAD(H) pool size (119), meaning activity is slowed when NADH/NAD^+ ratios within the cell increase. Metabolic analysis of the mutant strain supports the hypothesis that pyruvate oxidation and TCA cycle activity were inhibited in Δ*nuoN*Δ*nqrF1* and further explains previous data observed in single-knockouts of Nqr1 and Nuo (101). We observed excretion of high levels of pyruvate and acetate by Δ*nuoN*Δ*nqrF1*, which would be expected if flux through the TCA cycle is blocked (Figure 3.8). It is also important to note that all four of the NADH dehydrogenases have not been knocked out of *S. oneidensis* MR-1 in this study. This study sought to understand the roles of the two aerobically expressed NADH dehydrogenases (10, 101), even though the other NADH dehydrogenases may play a role in redox state regulation in the Δ*nuoN*Δ*nqrF1* mutant strain.

To better understand the effects of NADH dehydrogenase knockouts on the physiological redox state in *S. oneidensis* MR-1 throughout growth, we used the Rex-based redox sensing system developed by Liu et al. (2019). One of the major limitations to standard NADH and NAD^+ quantification assays is the need to remove the bacteria from their growth environment to conduct extractions. We found that the cell harvest and extraction procedure may cause shifts in the cells' redox state. Prior to quenching with acid or base solution in the protocol, shaking of the cultures is ceased and samples are transferred to 15 mL conical tubes (120), likely leading to oxygen limitation. We have shown that the cells likely deplete all oxygen within the medium during the centrifugation step, creating an oxygen limited environment that can influence and equalize redox state in both *S. oneidensis* strains. Conversely, the Rex-based redox sensor directly interacts with intracellular NADH and NAD^+ and allows real-time, qualitative measurements of NADH/NAD^+ via fluorescent reporter output (111). This allowed us to assess

NADH/NAD^+ without processing the cells in a way that would influence redox state. Our data show that the sensor works as expected in *S. oneidensis* and that Δ*nuoN*Δ*nqrF1* exhibits increased fluorescence output compared to WT.

While the sensor did influence growth of the strains, we were still able to gain qualitative measurements of the internal redox state. It is not clear why the addition of the Rex sensor influenced growth in *S. oneidensis* MR-1. In *E. coli*, the Rex sensor did not appear to influence growth (111). It is possible that the metabolic burden generated from carrying the redox sensing system caused the changes, and that use of different plasmid backbones or promoters would reduce the effects of the sensor. However, we believe that the output of the sensor is still a valuable source of information for this study for multiple reasons; the sensor generated the expected output for an aerobic to anaerobic transition and the overall phenotypes and differences between WT and the mutant remained similar with the sensor. I.e., the mutant strain still grew to a lower final OD_{600} and at a slower rate than the WT when the sensor was present (Figure 3.6 and Table 3.3). Further, differences in substrate consumption and acetate and pyruvate accumulation remained similar when the sensor was present, with the mutant strain failing to utilize all available carbon source and accumulating acetate and pyruvate. WT with the sensor was able to consume all available substrate and did not accumulate acetate or pyruvate. Although the sensor appeared to affect WT more than the mutant, the general effect on both strains appears similar, and the essential phenotypes remain the same; therefore, we believe that the sensor output reflects real differences in intracellular NADH/NAD^+ between the strains.

Altogether, our data indicate that deletion of NADH dehydrogenases affected NAD(H) pool sizes, NADH/NAD^+, and upstream metabolic activities, specifically by inhibiting the TCA cycle and blocking amino acid synthesis. Because we have shown that deleting NADH

dehydrogenases from *S. oneidensis* MR-1 led to increased NADH/NAD^+ levels, larger NAD(H) pool sizes, and metabolic shifts within the cell, NADH dehydrogenase knockouts may provide an avenue for metabolic engineering. When engineering pathways in bacteria to generate products that are redox cofactor-dependent, it is advantageous to make modifications to that organism to generate higher levels of NADH (121). If enzyme concentrations no longer limit the rate of product formation, then the availability of redox cofactors may become limiting (121, 122). For example, it was necessary to eliminate pathways that compete for NADH in *E. coli* to improve 1-butanol production (123). Increasing NADH generation has also been used to enhance electric current production by *S. oneidensis* MR-1 (124). These studies show the importance of NADH availability when engineering redox cofactor-dependent pathways. We have shown that knocking out NADH dehydrogenases and eliminating a competing pathway for NADH in *S. oneidensis* MR-1 increases the availability of NADH, which provides a possible background strain for metabolic engineering in *S. oneidensis* MR-1. With additional NADH available in these NADH dehydrogenase mutant strains, we could direct NADH into synthetic pathways for product formation, even when oxygen is present, as indicated by the high levels of pyruvate and acetate accumulation by the mutant strain.

3.5. Methods and Materials

3.5.1. Generating NADH dehydrogenase knockout strains containing the Rex redox sensor

Each single NADH dehydrogenase knockout and the Δ*nuoN*Δ*nqrF1* double-knockout strain were generated in a previous study and confirmed by complementation (101). The Rex redox sensor plasmids were received from Dr. Vatsan Raman and Yang Liu at the University of Wisconsin—Madison) and were described in their recent publication (111). The two-plasmid system has one plasmid that constitutively expresses Rex and another that contains a fluorescent

reporter under Rex regulation. The Rex-containing plasmid was transformed into chemically competent *E. coli* WM3064 cells. The plasmid was then transferred to *S. oneidensis* MR-1 and NADH dehydrogenase knockout strains via a conjugation protocol similar to Webster et al. (2014). The plasmid containing the fluorescent reporter was transformed into chemically competent *E. coli* Mach 1 cells via heat shock. The Mach 1 cells were grown at 37°C while shaking for 18 hours in 5 mL cultures. The cultures were used to extract the reporter plasmid via the E.Z.N.A Plasmid DNA Mini Kit I (Omega Bio-tek, D6943-02). Extracted plasmid was then used to transform electrocompetent *S. oneidensis* MR-1 and NADH dehydrogenase strains containing the Rex plasmid via electroporation (125). The presence of both plasmids in each strain were confirmed with antibiotic resistance and PCR.

3.5.2. Growth conditions

Strains were pre-cultured in LB medium for 18 hours. Each pre-culture was normalized to OD_{600} = 1.0 and washed in M5 minimal medium three times by centrifugation and resuspension. Each growth experiment used the following M5 minimal medium recipe: 1.29 mM K_2HPO_4, 1.65 mM KH_2PO_4, 7.87 mM NaCl, 1.70 mM NH_4SO_4, 475 μM $MgSO_4 \cdot 7H_2O$, 10 mM HEPES, 0.01% (w/v) casamino acids, 0.1% tryptone (w/v), 1X Wolfe's mineral solution (aluminum was not included), and 1X Wolfe's vitamin solution (riboflavin was not included), pH adjusted to 7.2 with 1 M NaOH. Carbon donors, either NAG or D,L-lactate, were added to the M5 medium to final concentrations of 10 mM or 20 mM, respectively. The addition of 0.1% tryptone to the M5 minimal medium recipe was the only adjustment from our previous work (101). To determine if amino acids were the key components required to rescue the growth of the double NADH dehydrogenase knockout, two different modifications to the M5 recipe were made: the addition of 0.5% (w/v) casamino acids, or the addition of a defined amino acid mixture containing 20 mM

L-arginine (Alfa Aesar, A15738), 20 mM D,L-aspartic acid (TCI, A0544), 20 mM L-glutamic acid (TCI, G0059), 20 mM L-leucine (VWR, 5811), 20 mM L-lysine monochloride (Acros Organics, 123221000), 20 mM L-proline (TCI P0481), D,L-serine (TCI, S0034), and 20 mM L-valine (V0014). After the amino acids were added to the M5 minimal medium, the pH was readjusted to 7.2 with 5M NaOH and the medium was filter sterilized.

High-throughput growth experiments containing multiple strains were conducted in clear 24-well culture plates (Greiner Bio-One, 662165) in 1 mL culture volumes of M5 medium, with four replicates per strain. Each well was inoculated with 10 μL of normalized pre-culture (OD_{600}= 1.0) and monitored in a Synergy H1 plate reader (BioTek Instruments, Winooski, VT) with orbital shaking at 30°C for 48 hours. For growth and fluorescence experiments involving the Rex redox sensor, growth was monitored at 600 nm and fluorescence output was monitored at an excitation wavelength of 475 nm, and emission wavelength of 509 nm.

Flask growth experiments were conducted in 50 mL culture volumes in 250-mL Erlenmeyer flasks. Experiments were performed in M5 medium supplemented with 0.1% tryptone and 10 mM NAG or 20 mM D,L-lactate. Flasks were inoculated with 50 μL of standardized pre-cultures and incubated in a floor shaker (New Brunswick Scientific, 12500) at 30°C while shaking at 275 rpm. Cultures were grown in triplicate and sampled by removing 1 mL and reading OD_{600} on a spectrophotometer (Eppendorf BioPhotometer, D30).

3.5.3. HPLC analysis

HPLC analysis was conducted as previously described (101).

3.5.4. NADH/NAD^+ quantification assay

The protocol for the NADH/NAD^+ quantification assay was adapted from a previously published method (120). Samples (5 mL) for both NADH and NAD^+ extractions were taken during early logarithmic growth from 50-mL cultures growing in M5 medium containing 20 mM D,L-lactate or 10 mM NAG. Each 5-mL sample was transferred to a sterile 15-mL conical tube (VWR, 89039-664) and centrifuged at 5000 x g at 4°C in a Sorvall ST 8R centrifuge (Thermo Scientific) HIGHConic rotor (Thermo Scientific, 75005709) for 10 minutes. The supernatant was removed from each tube and the pellets were resuspended in 500 µL of 0.1 M HCl containing 500 mM NaCl or 0.1 M NaOH containing 500 mM NaCl for NAD^+ or NADH extractions, respectively. Each sample was transferred to a 1.5-mL microcentrifuge tube and incubated for 5 minutes at 95°C. After incubation, the samples were placed on ice to cool for 10 minutes and then were centrifuged for 5 minutes at 5000 x g at 4°C in the Sorvall ST 8R centrifuge with the microcentrifuge rotor (Thermo Scientific, 75005715). After centrifugation, 300 µL of supernatant were transferred from each sample into new 1.5-mL microcentrifuge tubes and stored at -80°C until the colorimetric assay was conducted.

Each assay was conducted in clear 96-well microplates (Greiner Bio-One, 655101). Standards were prepared from 0.1 mM NAD^+ (NAD trihydrate, Amresco, 0455) and 0.1 mM NADH (NADH disodium trihydrate, Amresco, 0384) stocks. Each standard and sample were aliquoted into duplicate sets of wells in 20 µL volumes. To initiate the assay, 180 µL of master mix was added to each well and the plate is placed in the plate reader to orbitally shake and incubate at 30°C. The wells were monitored at 1-minute intervals with the Synergy H1 plate reader measuring absorbance at 550 nm. The in-well master mix component concentrations are as follows: 0.1 M bicine (VWR, 0149) buffer pH 8.0, 4 mM EDTA disodium salt

(Invitrogen,15576), 1.66 mM phenazine ethosulfate (Sigma-Aldrich, P4544), 0.42 mM thiazolyl blue tetrazolium bromide (Beantown Chemical, 142015), 10% (v/v) ethanol, and 3.2 units/mL alcohol dehydrogenase (Sigma, A3262). NAD^+ and NADH concentrations are determined following the data analysis protocol set out by Kern *et al.* (2014). Because the extraction efficiencies of 0.1 M HCl and NaOH differed, [NAD^+] and [NADH] were normalized to total protein from each extraction determined by conducting the Pierce™ BCA Protein Assay Kit (Thermo Scientific, 23225).

3.5.5. Aerobic to anaerobic transition

Pre-cultures of *S. oneidensis* MR-1 normalized to and OD_{600} of 1.0 were used to inoculate two sets of triplicate 50-mL cultures of LB to an OD_{600} of 0.01. Each set was grown for 6 hours under oxic conditions at 30°C while shaking at 275 rpm. After the 6-hour incubation period each culture was sampled and the one set that would be transitioned to an anoxic environment was placed at room temperature without shaking for 2 hours. After 2 hours, each culture was sampled and the anaerobic cultures were moved to an anaerobic chamber and given 50 mM fumarate as a terminal electron acceptor. Each culture set was incubated for another 12 hours and samples were taken from each culture 2- and 12-hours post-transition.

3.5.6. Oxygen consumption measurements

Oxygen consumption of WT and Δ*nuoN*Δ*nqrF1* was measured within a microfluidic system designed by Dr. Denis Proshlyakov and Nathan Franz (Michigan State University). Samples were added to the microfluidic system and spectroscopically monitored in a custom device. Each run was conducted in triplicate with cultures normalized to and OD_{600} of 0.2 that were shaken at 275 rpm for 10 minutes prior to testing to ensure total oxygen saturation of the medium. Further testing of oxygen consumption was tested in large batch cultures grown in 50 mL of M5 medium

supplemented with 0.1% tryptone and 20 mM D,L-lactate. 25 mL of culture that had been continuously shaking at 30°C at 275 rpm were transferred quickly into a 50 mL conical tube. Oxygen consumption was measured by submerging an oxygen probe (Mettler Toledo InLab® OptiOx, 51344621) in the 25 mL of culture and monitoring [O_2] over time.

3.5.7. Data analysis

Analysis of growth, fluorescence, and HPLC data was performed using Rstudio (95) with following packages: ggplot2 (96), reshape2 (97), dplyr (98), and TTR (99). Growth rates were calculated using R package 'growthcurver' using default values with background correction set to "min" (100). NADH/NAD^+ quantification, BCA assay data, and oxygen consumption data were analyzed in Microsoft Excel (2016).

3.6. Acknowledgements

The authors thank Dr. Cecilia Martinez-Gomez (Michigan State University) for sharing the adapted redox assay protocol, Nicholas Tefft (Michigan State University) for reviewing the manuscript, and Dr. Vatsan Raman and Yang Liu (University of Wisconsin—Madison) for sharing the Rex-based redox sensor and for helpful comments on the manuscript. The authors would also like to thank Dr. Denis Proshlyakov and Nathan Frantz (Michigan State University) for allowing us to use their microfluidic system to measure oxygen consumption. This research was partially supported by a fellowship from Michigan State University under the Training Program in Plant Biotechnology for Health and Sustainability (T32-GM110523). This work was also supported by the USDA National Institute of Food and Agriculture, Hatch project 1009805.

3.7. Conflicts of Interest

The authors report no conflicts of interest.

Chapter 4: *Shewanella oneidensis* MR-1 exhibits overflow metabolism and electron transport chain restructuring at high growth rates

This chapter contains a version of the manuscript that will be submitted to Frontiers in Microbiology.

Authors: Kody Lee Duhl[1] and Michaela A. TerAvest[1]

[1]Department of Biochemistry and Molecular Biology, Michigan State University, East Lansing, MI, USA

4.1. Abstract

Energetically inefficient metabolic pathways are prevalent among bacteria, although it is not clear when or how they are more advantageous than their energetically efficient counterparts. Several competing theories have been proposed to explain the benefit of energetically inefficient pathways, including that the inefficient pathways require less protein synthesis or less space in the membrane. These theories have been applied to glycolytic pathways and overflow metabolism but have not yet been applied to respiratory electron transport chains. The γ-proteobacterium *Shewanella oneidensis* MR-1 has a versatile electron transport chain that can vary in energetic efficiency depending on which complexes are used. To explore the utility of energetically inefficient respiratory pathways, we compared fast- and slow-growing populations of *S. oneidensis* MR-1 in a fermenter, because fast growth induces other energetically inefficient pathways. Daily samples were taken to monitor OD_{600}, D,L-lactate utilization, and acetate production. Upon reaching steady-state growth under each dilution rate, samples were taken for proteomic analysis. We determined that *S. oneidensis* MR-1 exhibited overflow metabolism at high growth rates and observed proteome changes consistent with the changes in carbon flux. *S. oneidensis* MR-1 also restructured its electron transport chain during faster growth, but the changes were not uniformly toward inefficient pathways.

4.2. Importance

Redundancies in bacterial electron transport chains provide multiple possible pathways for electrons to travel during respiration. Redundant respiratory complexes retain differing coupling efficiencies that can lead to differences in the amount of energy conserved per reducing equivalent oxidized. While *Shewanella oneidensis* MR-1 is studied as a model for bioelectrochemical systems, it retains a highly branched electron transport chain that is modified

dependent on growth condition. Recent hypotheses regarding how bacteria regulate metabolic pathway direction do not address the electron transport chain structure, mainly overflow metabolism and respiration. Respiratory chain reorganization has implications for growth and metabolic flux optimization, making it integral for the study and understanding of bacterial physiology and metabolism.

4.3. Introduction

Bacteria use a variety of metabolic strategies to metabolize substrate and generate ATP resulting in different yields of ATP generated per substrate molecule consumed (5, 6). For example, complete oxidation of glucose to CO_2 via respiration yields much more ATP than conversion of glucose to lactic acid or other products via fermentation (5). Therefore, it could be expected that respiration would always be the primary mode of metabolism in the presence of oxygen (49). However, many research groups have shown that fermentation occurs in many circumstances even when oxygen is plentiful. In these instances respiration and fermentation are used simultaneously, leading to a respiro-fermentative metabolic strategy (47, 48, 55, 56, 126). For example, fast growing bacteria sometimes excrete significant amounts of acetate, rather than fully oxidizing glucose to CO_2 even when sufficient oxygen is present (47, 48, 55, 56, 126, 127). This phenomenon is called ‘overflow metabolism’ and has been observed in *Escherichia coli*, *Bacillus subtilis*, and *Shewanella oneidensis* (57, 128, 129). It appears that overflow metabolism occurs at high growth rates when there is an excess of carbon substrate available (47, 55, 56, 127, 130). Overflow metabolism is an energetically inefficient use of the substrate because it generates ATP mainly via substrate-level phosphorylation (4 ATP per glucose) (131). In contrast, during aerobic respiration (32 ATP per glucose) the substrate is completely oxidized to CO_2 and more ATP is generated via oxidative phosphorylation (5).

The use of energetically inefficient pathways is puzzling, but these pathways may be advantageous under certain conditions. One possible explanation is in the tradeoff between proteome and energetic efficiency. Energetically inefficient pathways are more thermodynamically favorable because more energy is lost as heat and not conserved through the production of reducing equivalents and ATP (8). Because of this, the flux-force efficacy of energetically inefficient pathways is higher. Flux-force efficacy details enzymatic reaction flux with respect to the thermodynamic favorability and proteome cost incurred to keep the reaction moving in the forward direction (54). A proteome efficient pathway is defined as requiring less enzymatic protein or utilizing enzymatic complexes that incur a smaller burden for the cell to synthesize (8, 9). By reducing energy efficiency, cells may limit proteome cost in two ways; i) a more negative ΔG for the energetically inefficient pathways to increase the flux-force efficacy of enzymes in the pathway, leading to a lower protein synthesis requirement to maintain the same substrate consumption rate, and ii) by partially oxidizing substrate and avoiding the tricarboxylic acid (TCA) cycle and electron transport chain (ETC) (6, 47, 50, 55, 126). Indeed, Basan *et al.* have shown that the proteome fraction of enzymes in the TCA cycle and oxidative phosphorylation is reduced during overflow metabolism, resulting in higher proteome efficiency (47). The reduction in proteome cost during overflow metabolism may free up transcription and translation machinery for the synthesis of proteins involved in growth and cell division. Directing more resources toward growth at the cost of energy efficiency may be an adaptive strategy when resources are plentiful but competition is high (132). In contrast, cells experiencing carbon limitation are more likely fully oxidize substrate to CO_2, pointing to the importance of maximizing energy yield when resources are limited (47, 127).

Another possible explanation for overflow metabolism is the membrane real estate hypothesis. Szenk *et al.* found that spatial limitation for respiratory complexes in the inner membrane could also explain acetate excretion at high growth rates (55). In *E. coli*, the growth rate is directly correlated with cell size, meaning that at higher growth rates, the surface area to volume ratio (SA/V) of the cell decreases. This leads to a mismatch in the rate of NADH generation by cytosolic processes and the rate of NADH oxidation by the membrane-integrated ETC (55, 56). This mismatch can ultimately lead to high NADH:NAD^+, causing suppression of the TCA cycle and a shift to overflow pathways (55). In conjunction, macromolecular crowding postulates that the ETC requires nearly double the amount of proteome allocation to generate ATP at the same rate as substrate-level phosphorylation (52). Overflow metabolism is mainly ETC-independent, as only a small amount of NADH generated through the conversion of pyruvate to acetyl-CoA must be recycled by the ETC. Therefore, it is less dependent on the use of ETC complexes and reduces the effect of the spatial availability constraint within the inner membrane. By shifting to overflow metabolism, fast growing cells avoid the effects of limited membrane real estate and can continue to generate ATP via substrate-level phosphorylation (55, 56).

Respiratory ETCs also have energetically efficient and inefficient versions. Similar to overflow metabolism (8, 9, 47, 55, 56, 126), a reduction in energetic efficiency of the ETC could be beneficial to reduce proteome cost or save space in the inner membrane. The metal reducing bacterium S. *oneidensis* MR-1 is a useful model for studying respiratory efficiency because it has a highly branched aerobic ETC containing four NADH dehydrogenases (NDHs), a bc_1 (Pet) complex, and three terminal oxidases (22). The four NDHs are: two sodium-pumping NDHs (Nqr1 and Nqr2, $2Na^+/2e^-$), a Type I proton-pumping NDH (Nuo, $4H^+/2e^-$), and a Type II

uncoupling NDH (Ndh, $0H^+/2e^-$). The three terminal oxidases are: an aa_3-type cytochrome *c* oxidase (Cox, $4H^+/2e^-$), a cbb_3-type cytochrome *c* oxidase (Cco, $1H^+/2e^-$), and a cytochrome *bd* ubiquinol oxidase (Cyd, $0H^+/2e^-$) (22, 25, 29). The Pet complex is associated with the two cytochrome *c* oxidases oxidizes quinones to reduce cytochrome *c* and moves $4H^+/2e^-$ to the periplasmic space (22, 25). The Cyd complex oxidizes quinones itself, taking advantage of quinone loops to transport $2H^+/2e^-$ into the periplasm (22, 25). The variety of respiratory complexes encoded in its genome enables *S. oneidensis* MR-1 to modulate a range of different respiratory pathways with varying ATP yields (Table 4.1). Here, we investigated how *S. oneidensis* MR-1 adjusts catabolic pathways between respiration and overflow metabolism and restructures its electron transport chain depending on growth rate. To explore this, we monitored growth and the analyzed the proteome of *S. oneidensis* MR-1 at low and high dilution rates in a continuous flow fermenter.

4.4. Results

We conducted duplicate steady-state growth experiments with *S. oneidensis* MR-1 using a fermenter. The fermenter was fed with M5 minimal medium supplemented with 20 mM D,L-lactate at 0.487 ml/min for the low growth rate condition (34-hour hydraulic retention time) and 3.46 ml/min for the high growth rate condition (4.8-hour hydraulic retention time). Dissolved oxygen was maintained at >80% saturation to ensure oxic conditions throughout experiments. We sampled the fermenter daily to monitor OD_{600} and D,L-lactate and acetate concentrations. During the low dilution rate condition, the OD_{600} values remained below 0.5 and the growth rate was 0.029 h^{-1} (Fig. 4.1A). D,L-lactate limitation occurred around 72 hours of growth during the low dilution rate condition, followed by a reduction in acetate concentration (Fig. 4.1B-C). When the dilution rate was increased, we observed an increase in OD_{600} values to ~0.75 and an increase

in growth rate to 0.207 h^{-1} (Fig. 4.1A). After increasing the dilution rate, the D,L-lactate concentration stabilized at 4-6 mM (Fig. 4.1B), and acetate concentration stabilized at 2-3 mM (Fig. 4.1C).

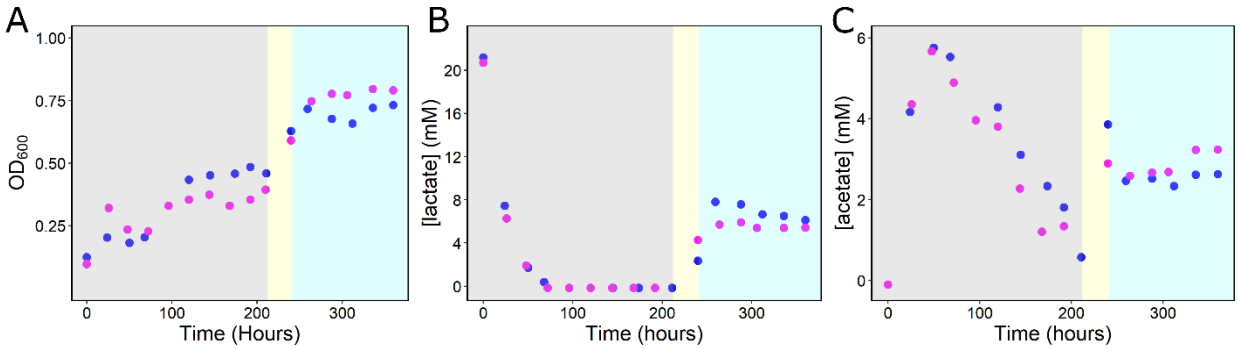

Figure 4.1. Growth of WT in a continuous flow fermenter. (A) Growth of *S. oneidensis* MR-1 in a fermenter in M5 minimal medium supplemented with 20 mM D,L-lactate at low and high dilution rates. Concentrations of (B) D,L-lactate (C) acetate were monitored by HPLC. The blue and pink points indicate duplicate fermenter experiments. The grey, yellow, and light blue backgrounds denote the low (0-212 hours), ramping (212-240 hours), and high dilution rates (240-360 hours), respectively.

Upon reaching steady-state growth in the fermenter, (determined by three turnovers of the 1-L volume) we took daily 13.5-ml samples at each flow rate for proteomic analysis. Of the 20 samples that were taken during the duplicate fermenter experiments, 10 samples (5 low dilution rate and 5 high dilution rate; split between both experiments) were submitted for untargeted proteome analysis by the Michigan State University Mass Spectrometry Core. Samples were analyzed by LC/MS/MS using isobaric labeling with tandem mass tags. All Log_2 fold change data is reported on a 0-centered scale, with positive values indicating greater abundance and negative values indicating decreased abundance in the high growth rate condition. The proteomic analysis confidently identified 2022 proteins of the 4071 annotated in UniProt (23) for *S. oneidensis* MR-1 (23) yielding 49.7% coverage. Of those identified, 789 (38.5%) showed a significant ($p < 0.0001$) change in abundance between the two conditions

(Table S1). Comparative analysis was conducted using the average fold-change from the high dilution rate condition in reference to the low dilution rate condition. Significance was determined using a Permutation Test with the Bonferroni correction in Scaffold proteome analysis software (Proteome Software, Inc., Portland, OR; version 5.1.2). Throughout the results section, we refer to differences with $p < 0.0001$ as significant. We also subdivided the detected proteins into general classifications using annotations developed from the J. Craig Venter Institute database (Table 4.2).

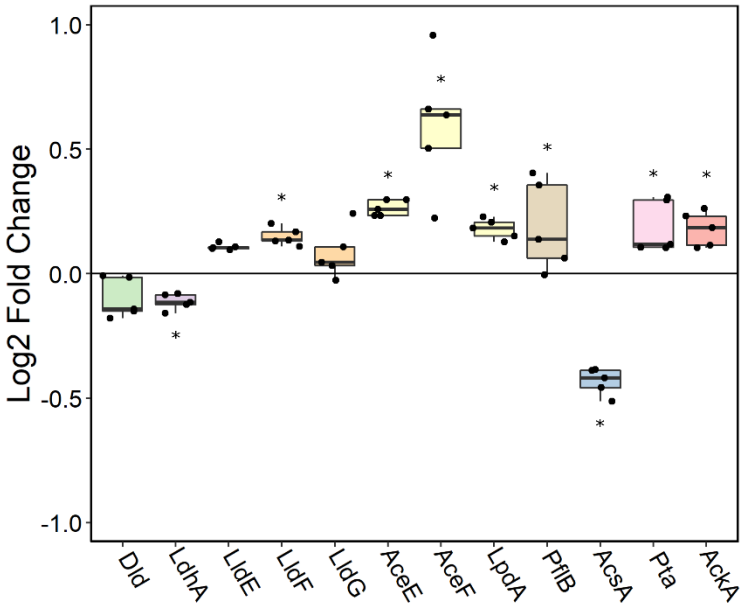

Figure 4.2. Abundance changes of enzymes involved in D,L-lactate metabolism. Relative abundance changes of lactate metabolism, pyruvate decarboxylation, and acetate secretion proteins from steady-state fermenter growth experiments. Values are shown as Log_2 fold change of peptide counts in the high dilution rate relative to the low dilution rate. If subunits of a multimeric complex were identified, they are shown as the same color. Statistical significance is denoted by: (*) $p < 0.0001$.

Comparative proteome analysis showed an increase in abundance of both transcription and translation machinery in *S. oneidensis* MR-1 growing under the high dilution rate condition (Table S4.1). Four subunits of the RNA polymerase (RpoA-D) increased significantly in

abundance, ranging from 0.13- to 0.29-fold. In the faster growing cells, 81.6% of the detected 30S/50S ribosomal proteins increased significantly in abundance from 0.07- to 1.05-fold.

All three annotated lactate dehydrogenases were identified in the proteomic analysis: the two quinone-linked D-lactate dehydrogenase (Dld) and L-lactate dehydrogenase (Lld), and the NADH-dependent fermentative lactate dehydrogenase (LdhA). Both Dld and LdhA decreased in abundance, by -0.099- and -0.113-fold, respectively (Fig. 4.2). In contrast, all three components of the quinone-linked L-lactate dehydrogenase (LldEFG) increased in abundance although the difference was significant only for LldF (Fig. 4.2). Enzymes required for pyruvate oxidation were more abundant at the high dilution rate conditions. Both pyruvate dehydrogenase (AceEF, LpdA) and pyruvate-formate lyase (PflB) exhibited significant increases in abundance compared to the low dilution rate condition (Fig. 4.2). The abundance of acetyl-CoA synthetase, AcsA, significantly decreased at the high dilution rate. Both phosphate acyltransferase (Pta, 0.186-fold, $p < 0.0001$) and acetate kinase (AckA, 0.179-fold, $p < 0.0001$), which convert acetyl-CoA to acetyl phosphate and dephosphorylate acetyl phosphate/generate ATP, respectively, were more abundant in the faster growing cells (Fig. 4.2).

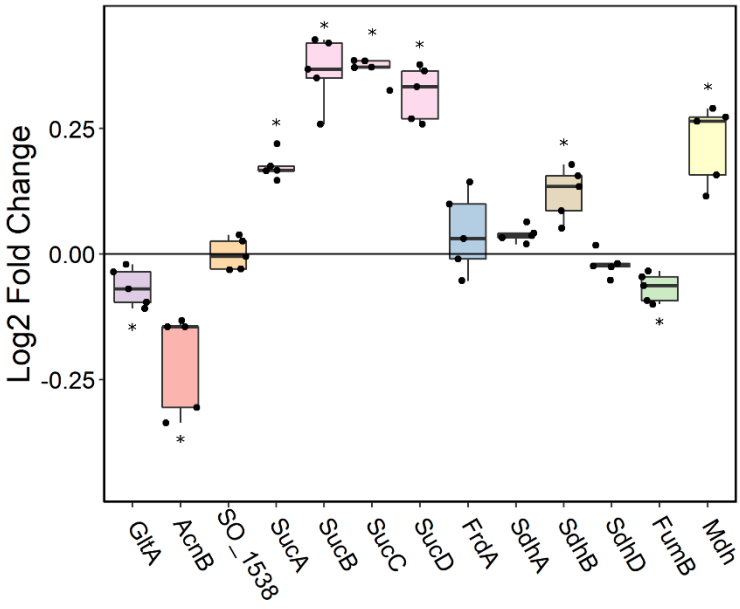

Figure 4.3. Abundance changes of TCA cycle enzymes. Relative abundance of TCA cycle proteins from steady-state fermenter growth experiments, shown as Log_2 fold change of peptide counts in the high dilution rate relative to the low dilution rate. If subunits of a multimeric complex were identified, they are shown as the same color. Statistical significance is denoted by:

(*) $p < 0.0001$.

We observed that the abundance of citrate synthase (GltA; the enzyme that brings acetyl-CoA into the TCA cycle) decreased by 0.066-fold ($p < 0.0001$) (Fig. 4.3 and 4.4). Aconitase (AcnB; responsible for catalyzing the subsequent two reactions in the TCA cycle), also showed a 0.213-fold ($p < 0.0001$) decrease in abundance under the high growth rate condition (Fig. 4.3 and 4.4). Some TCA cycle enzymes exhibited significant abundance increases in the high dilution rate condition, including α-ketoglutarate dehydrogenase (SucA, 0.174-fold; and SucB, 0.365-fold), succinyl-CoA synthetase (SucC, 0.368-fold; and SucD, 0.320-fold), and malate dehydrogenase (Mdh, 0.220-fold). Fumarase (FumB, -0.067-fold, $p < 0.0001$) showed a small reduction (Fig. 4.3 and 4.4). Regarding the glyoxylate shunt, both isocitrase (AceA, -0.758-fold, $p < 0.0001$) and malate synthase (AceB, -0.692-fold, $p < 0.0001$) showed reductions in

abundance (Fig. 4.4). The $NADP^+$-dependent malate dehydrogenase, MaeB (0.499-fold, p <0.0001), which converts malate to pyruvate exhibited an increase in relative abundance during the high growth rate condition (Fig. 4.4). Further, the enzymes that convert oxaloacetate (phosphoenolpyruvate carboxykinase, PckA) and pyruvate (phosphoenolpyruvate synthase, PpsA) to phosphoenolpyruvate, a gluconeogenic precursor, also showed significant increases of 0.470-fold and 0.337-fold (Fig. 4.4), respectively.

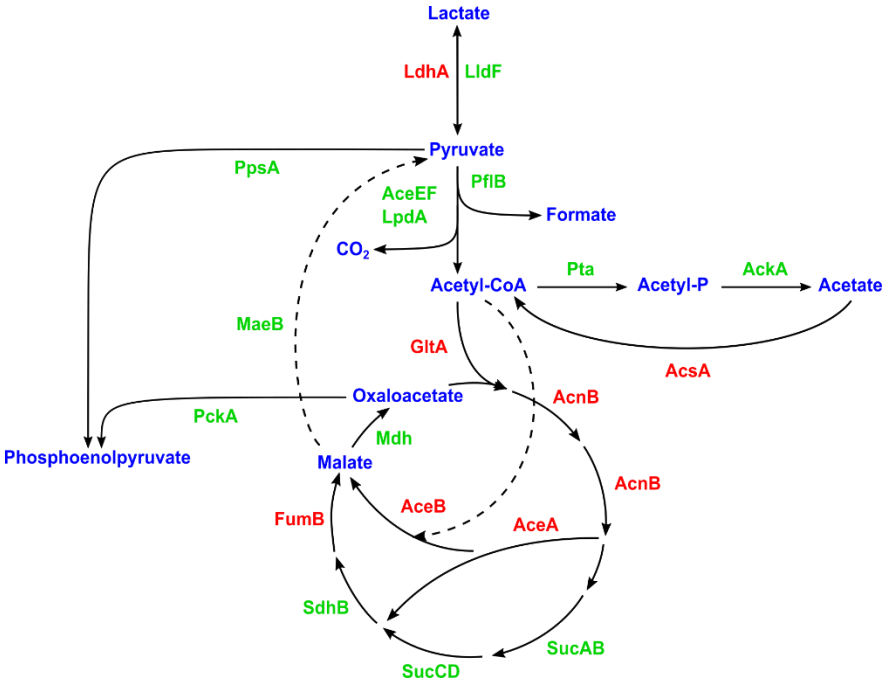

Figure 4.4. D,L-lactate metabolism map. Metabolic map of D,L-lactate metabolism in fast-growing *S. oneidensis* MR-1. Shown are the increases (green) and decreases (red) in relative abundance of enzymes in these pathways when shifted from a low dilution rate to a high dilution rate condition. All enzymes shown exhibit a significance value of $p < 0.0001$. Carbon sources and important intermediates are shown in blue.

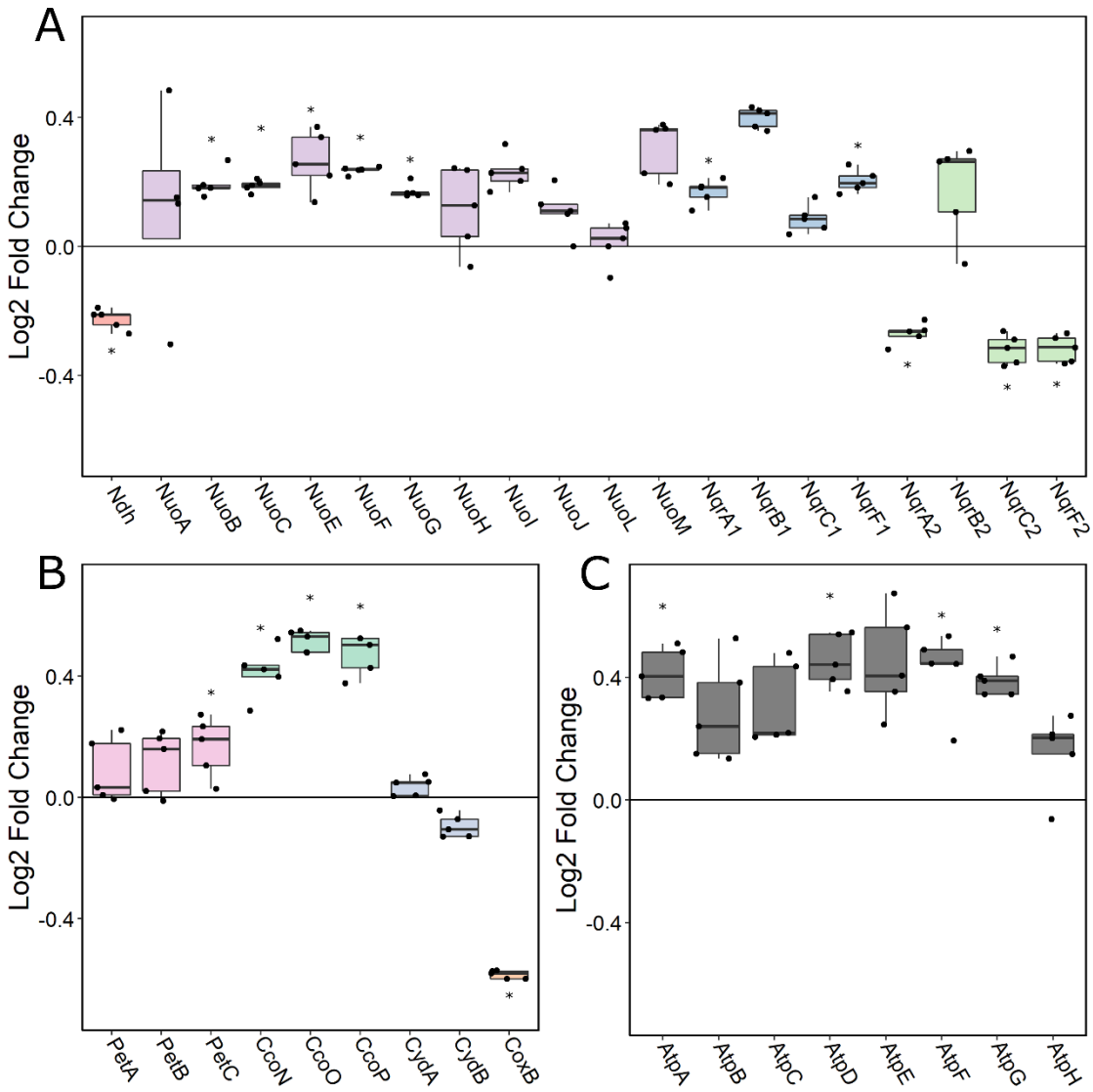

Figure 4.5. Abundance changes of ETC complexes. Relative abundance (A) NADH dehydrogenase complexes, (B) terminal oxidases, and ATP synthase from steady-state fermenter growth experiments, shown as Log2 fold change of peptide counts in the high dilution rate relative to the low dilution rate. If subunits of a multimeric complex were identified, they are shown as the same color. Statistical significance is denoted by: (*) $p < 0.0001$.

We detected peptides from each of the respiratory complexes of interest in *S. oneidensis* MR-1. Overall, Ndh abundance decreased under the high growth rate condition (Fig. 4.5A and Table 4.3). For Nuo, the individual subunits were more abundant in cells growing at a higher growth rate (Fig. 4.5A and Table 4.3). When the dilution rate shifted from low to high,

abundance for identified Nqr1 subunits increased (Fig. 4.5A and Table 4.3). Three of the four Nqr2 subunits showed reduced abundances: NqrA2, NqrC2, and NqrF2 (Fig. 4.5A and Table 4.3). The NqrB2 subunit, on the other hand, did show an abundance increase (Fig. 4.5A and Table 4.3). We also observed changes in both Crp (-0.037-fold, $p = 0.2$) and HexR (0.161-fold, $p < 0.0001$) regulators, which are predicted to be involved in controlling the expression of Nqr1 and Nqr2, respectively (83).

Under the high dilution rate condition, the Subunits of the cbb_3-type oxidase (Cco) that were identified showed increased abundances: CcoN, CcoO, and CcoP (Fig. 4.5B and Table 4.3). The cytochrome *bd* ubiquinol oxidase (Cyd) did not change significantly between the two growth conditions (Fig. 4.5B and Table 4.3). We also observed a significant decrease in the abundance of the aa_3-type oxidase (CoxB) (Fig. 4.5B and Table 4.3). We also observed changes in the oxygen sensing Fnr-like regulator EtrA (-0.129-fold, $p = 0.001$), which is also predicted to regulate all three terminal oxidases, exhibited an abundance decrease (83). For ATP synthase, we see an overall increase in abundance for each of the identified subunits at the higher growth rate (Fig. 4.5C and Table 4.3).

4.5. Discussion

Throughout the fermenter growth experiments, the growth rate of *S. oneidensis* MR-1 was directly correlated with the dilution rate of the fermenter (Fig. 4.1A). Accompanying the high dilution rate is an increase in abundance of transcription and translation machinery in the proteome. *E. coli* studies have shown that faster growing cells finely tune the increase in abundance of transcription/translation machinery for optimal growth (51, 133, 134). *S. oneidensis* MR-1 was consistent with these studies and exhibited abundance increases for both the RNA polymerase subunits and 30S/50S ribosomal proteins (Table S4.1). Although the fold

change increases for RNA polymerase were smaller than the ribosomal proteins, the requirement for more RNA polymerase to generate transcripts may be less important to protein production than ribosome availability. Overall, the increased abundances of RNA polymerase and ribosomal proteins at the higher dilution rate are consistent with observations made in *E. coli* and is a quintessential occurrence in fast growing cells (Table S4.1) (133). These results provide confidence that the methods we used resulted in a true comparison of low and high growth rate proteomes.

We observed that fast growing *S. oneidensis* MR-1 directed metabolic flux through overflow metabolism, as evidenced by acetate accumulation (Fig. 4.1). Conversely, the consistent decline in acetate availability under the low dilution rate condition showed the slower growing cells fully oxidized or assimilated essentially all the available substrate (Fig. 4.1). Comparative proteome analysis also showed that enzymes involved in the conversion of pyruvate to acetate were more abundant in the high growth rate condition (Fig. 4.2). Further, acetyl-CoA synthetase, the enzyme responsible for converting acetate to acetyl-CoA, was more abundant in the low dilution rate condition (Fig. 4.2). This confirms the importance of fully metabolizing all available substrate during D,L-lactate limitation. In *E. coli*, as growth rate increases, cells exhibit a reduction in Acs abundance (48, 135). Here, we show that the same occurs in *S. oneidensis* MR-1, where the reduction in AcsA abundance is directly linked to the secretion of acetate (Fig. 4.1 and 4.2). Lactate is a preferred carbon source for *S. oneidensis* MR-1 and acetate utilization occurs only after D,L-lactate has been nearly or completely diminished (101, 136). With excess lactate available, the cost (1 ATP) of converting acetate to acetyl-P and then to acetyl-CoA does not benefit the cell more than continuing to partially oxidize the excess D,L-lactate via overflow metabolism (32, 136).

In *E. coli*, shifting to overflow metabolism directs carbon flux away from the TCA cycle, with a concomitant reduction in proteome allocation to TCA cycle enzymes (47, 55). Similarly, we observed a decrease in abundance of both citrate synthase and aconitase, which act as the entrance to the TCA cycle (Fig. 4.3). Some enzymes in the second half of the TCA cycle showed significant increases in abundance suggests some continued TCA cycle function, but likely at a reduced capacity. The abundance increases MaeB, PckA, and PpsA (Fig. 4.4) suggest assimilation of TCA cycle intermediates and pyruvate to phosphoenolpyruvate, a gluconeogenic precursor (Fig. 4.4). These enzymes would direct residual TCA cycle flux into anabolic pathways for biomass generation rather than energy conservation.

As for the ETC, we observed that under the high growth rate condition, Nuo, Nqr1, Cco, and ATP synthase increased in abundance (Fig. 4.5). Conversely, Ndh, Nqr2, and Cox were less abundant in faster growing cells (Fig. 4.5). We previously reported the importance of Nuo and Nqr1 for aerobic growth in *S. oneidensis* MR-1 batch cultures, while Ndh and Nqr2 knockouts did not exhibit growth defects under oxic conditions (101). Increased abundance of Cox at the low growth rate condition is interesting, as it has only been identified in *S. oneidensis* MR-1 growing under starvation conditions in the presence of oxygen (24). Our results support the hypothesis that Cox is specifically upregulated during substrate limitation. The lack of abundance changes for Cyd subunits (Fig. 4.5) is unsurprising because it is typically used in microoxic conditions in *S. oneidensis* MR-1 (35, 38, 43). These experiments were conducted in an aerobic environment, therefore Cyd likely was not a dominant terminal oxidase in either growth condition.

The proteome/energetic efficiency tradeoff suggests that cells use less energetically efficient pathways to lower proteome cost during fast growth. Conversely, pathways that

increase energy conservation at a higher proteome cost are used at low growth rates (47, 51, 126). The observed shift from Ndh to Nuo during the high growth rate allows the cells to transport $4H^+$ more per NADH oxidation, leading to a higher efficiency ETC and shows the opposite of the proteome/energetic efficiency tradeoff (25). Nuo also carries a higher proteome cost because the complex is 540 kDa compared to the 4.7 kDa of Ndh (23). Further, because of the lower driving force, the flux force efficacy of Nuo is lower than Ndh, suggesting that a greater number of complexes would be required to maintain equal flux (54). This would incur a higher proteome cost to the cell for not only having to synthesize a larger complex but also a higher quantity of these complexes. For the terminal oxidases, shifting from Cox to Cco is not as severe, as the overall coupling efficiency loss is $2H^+/2e^-$ (25). The proteome cost incurred is also smaller, as the Cox complex size is 147 kDa and the Cco complex is 179 kDa. These findings show that the ETC during fast growth could be functioning at both a higher energetic efficiency ($10\ H^+/2e^-$) and a lower proteome efficiency than the low growth rate ($8\ H^+/2e^-$), which was unexpected considering the simultaneous switch to overflow metabolism.

If membrane real estate was the driving factor controlling expression of the various ETC components, we would expect to see abundance increases in complexes with higher flux force efficacy at the high growth rate condition (55, 56). Increased acetate accumulation and reduced abundance of enzymes that bring carbon into the TCA cycle are consistent with the membrane real estate hypothesis (47, 55–57, 126). One informative aspect of the membrane real estate hypothesis is that the $NADH:NAD^+$ drives suppression of TCA cycle activity, leading to overflow metabolism (55). Previously, we reported that increased $NADH:NAD^+$ in NDH knockout strains led to a reduction in TCA cycle activity, which remains consistent with this model (137). Despite the increase in overflow metabolism, *S. oneidensis* MR-1 also shows

increased abundance of respiratory complexes and oxidative phosphorylation machinery under the high growth rate condition (Fig. 4.5). In this regard, the data obtained in this study does not completely comply with the membrane real estate hypothesis model.

Despite not fully conforming to the membrane real estate hypothesis, one important aspect of the model may help explain *S. oneidensis* MR-1's use of the NDHs under the growth conditions tested in this study. The *E. coli* model generated by Szenk *et al* suggested that redox state was directly linked to cell growth rate (55). They showed that NADH:NAD^+ increases with increasing growth rate and remains low at lower growth rates associated with carbon limitation (55). Therefore, under the lactate limited low flow rate condition, we hypothesize that the cell maintains a low NADH:NAD^+ ratio. The Nuo reaction has an estimated ΔG of 1.1 ± 5.8 kJ/mol NADH kJ/mol compared to -70.9 ± 5.8 kJ/mol NADH for Ndh with an NADH:NAD^+ of 0.01 (55, 138, 139). The low NADH:NAD^+ ratio under starvation conditions may result in an inability to drive the Nuo reaction forward because the ΔG is close to equilibrium compared to the Ndh reaction. In addition, the regulatory mechanisms in *S. oneidensis* MR-1 for Nuo and Ndh are unknown. Predictive genomic analysis in *E. coli* suggests Crp and Fnr (EtrA in *S. oneidensis* MR-1) control Nuo and Ndh expression (83), pointing to a terminal oxidase-like type of regulation.

S. oneidensis MR-1 fits in the models of the proteome/energetic efficiency tradeoff and membrane real estate hypotheses regarding overflow metabolism. On the contrary, regulation of ETC efficiency seems to be more nuanced. NDH use may be driven by NADH:NAD^+ and the thermodynamics of NADH oxidation/proton gradient generation. The terminal oxidases may be more strongly regulated by substrate and oxygen availability than growth rate (24, 25, 35, 38,

43). Overall, we have shown that *S. oneidensis* MR-1 does restructure its carbon metabolism as well as its branched respiratory chain for adaptive growth.

4.6. Materials and Methods

4.6.1. Preculture conditions for fermenter experiments

Wild-type *S. oneidensis* MR-1 cultures were precultured in LB medium (Miller, Neogen) for 18 h at 30°C shaking at 275 rpm. Precultures were washed with M5 medium and standardized to an OD_{600} of 1.0 prior to subculturing in cultures of M5 minimal medium. 100 µL of standardized preculture were used to inoculate 100 mL cultures of M5 minimal medium in 250 mL Erlenmeyer flasks to obtain an initial OD_{600} of 0.001. All subcultures were grown using the following M5 minimal medium: 1.29 mM K_2HPO_4, 1.65 mM KH_2PO_4, 7.87 mM NaCl, 1.70 mM NH_4SO_4, 475 M $MgSO_4 \cdot 7H_2O$, 10 mM HEPES, 0.01% (w/v) Casamino Acids, 1X Wolfe's mineral solution (Al was not included), 1X Wolfe's vitamin solution (riboflavin was not included), and 20 mM sodium D,L-lactate, with the pH adjusted to 7.2 with 5 M NaOH. Cultures were grown at 30°C shaking at 275 rpm in a floor shaker (New Brunswick Scientific, 12500) until they reached an OD_{600} of 1.0. Subcultures were split into two 50 ml aliquots in 50 ml conical tubes (VWR, 89039) centrifuged for 10 minutes at 10,000 x g at 21°C in Sorvall ST 8R centrifuge (Thermo Scientific) HIGHConic rotor (Thermo Scientific, 75005709). Cell pellets were resuspended in 5 mL M5 minimal medium supplemented with 20 mM D,L-lactate and combined to obtain an OD_{600} of 10 in 10 mL of medium.

4.6.2. Fermenter growth conditions

Steady-state growth experiments were conducted in a BiostatA fermenter (Sartorius) at 1 L volume of M5 minimal medium supplemented with 20 mM D,L-lactate. Preparation for experiments included 24-hour equilibration period to allow dissolved oxygen (DO) to reach

100% saturation and ensure no bacterial contaminants were present after setup. DO was controlled with compressed air passed through a 0.2 µm filter and maintained between 80% and 90% saturation throughout the duration of the experiment, while being monitored with a VisiFerm oxygen probe (Hamilton; 243666-211) and Hamilton's ArcAir program. Stirring rate, air bubbling rate, pH, and temperature were maintained by the fermenter's controller unit (Sartorius) and chiller (Sartorius). An EasyFerm Plus (Hamilton; 238633) was used to monitor pH and temperature with the pH value set at 7.5 controlled with 500 mM HCl and temperature set at 30°C.

After the 24-hour equilibration period: the 10 ml of culture at OD_{600} = 10 was used to inoculate the fermenter to a starting OD_{600} value 0.1. Inflow medium containing M5 minimal medium supplemented with 20 mM D,L-lactate was connected as well as an outflow pump to maintain the volume at 1 L. For the low dilution rate condition, the dilution rate from the inflow medium was set at 0.487 ml/min, stirring set at 400 rpm, and bubbling rate set at 1500 ccm. To ramp the fermenter to the high dilution rate condition, an intermediate dilution rate of 2.56 ml/min, stirring at 500 rpm, and bubbling rate of 2500 ccm was used for a 28-hour period. The high dilution rate condition was conducted at 3.46 ml/min, stirring at 600 rpm, and bubbling at a rate of 3000 ccm. Bacterial growth rates in the fermenter are equal to the dilution rate at steady-state growth. Therefore, growth rates were calculated by determining the amount of volume added to the fermenter per hour divided by the total volume of the fermenter. For example, the low flow rate condition maintained a dilution rate of 0.487 ml/min resulting in 29.22 ml of media added per hour, which is then divided by the reaction volume of 1000 ml. This results in the growth rate of 0.029 h^{-1} at that specific dilution rate.

4.6.3. Fermenter sampling

After inoculation, the fermenter was sampled daily for OD_{600} and HPLC measurements. 2-ml samples were removed from the fermenter, 1-ml was used for OD_{600} quantification on a spectrophotometer (Eppendorf BioPhotometer, D30), and 1-ml was stored at -20°C for HPLC analysis. The presence of D,L-lactate was monitored in daily samples with a lactate meter and test strips (Nova Biomedical, 40813). When lactate was not detectable with the lactate meter during the low dilution rate condition and cells reached steady-state growth, 13.5-ml samples were taken daily over a five-day period and stored at -80°C in 15-ml conical tubes (VWR, 89039) for total protein extraction and proteome analysis. Upon ramping to the high dilution rate condition and cells reaching steady-state growth, another set of 13.5-ml samples were taken over a five-day period for protein extraction and proteome analysis. Steady-state growth was determined when three hydraulic turnovers of 1 L volume occurred in the fermenter.

4.6.4. HPLC analysis

D,L-lactate and acetate concentrations were measured via HPLC and analysis was conducted as previously described (101).

4.6.5. Total protein extraction

The 13.5-ml samples from the fermenter experiments were removed from storage at -80°C and thawed at room temperature. Samples were centrifuged at 8,500 x g for 5 minutes to obtain a cell pellet and the supernatant was discarded. Pellets were resuspended in 2 mL of resuspension buffer containing 100% (v/v) B-PER bacterial protein extraction reagent (Thermo, 89822), 50 mM dithiothreitol (Goldbio, DTT10), and one tablet of complete protease inhibitor cocktail (Roche, 1169749801). Samples were vortexed vigorously for 30 seconds and frozen at -80°C for 15 minutes. The samples were then thawed at room temperature and the freeze/thaw cycle was

repeated two more times. After three freeze/thaw cycles, the samples were centrifuged at 12,000 x g for 20 minutes. The supernatant was transferred to a fresh 15-ml conical tube. Protein precipitation was conducted with the addition of 2 ml of precipitation buffer consisting of 100% (w/v) tricholoracetic acid (Fisher, A322-100) and 9.65 mM sodium deoxycholate (Sigma-Aldrich, D6750). Tubes were capped, inverted to mix, and incubated for 24 hours at 4°C. The precipitate was pelleted by centrifugation at 12,000 x g for 20 minutes, washed with 5 ml of ice-cold acetone, and centrifuged again for 20 minutes at 12,000 x g. The supernatant from the wash was discarded and the pellet was centrifuged for 1 minute at 12,000 x g and remaining supernatant was aspirated. Pellets were resuspended in 0.5 ml or 1 ml of resuspension buffer for 5 minutes at 60°C for the low dilution rate and high dilution rate conditions, respectively. The resuspension buffer consisted of 4% (w/v) sodium dodecyl sulfate and 25 mM Tris (VWR, 0497) at pH 8.3. Samples were shaken at 275 rpm at 30°C for 24 hours to fully resuspend the pellet. Quantification of total protein concentration was determined with the Pierce^{TM} BCA Protein Assay Kit (Thermo Scientific, 23225).

4.6.6. SDS-PAGE confirmation of protein quality

Prior to submission for proteome analysis, SDS-PAGE gels were conducted to confirm the protein extractions could be submitted to the Mass Spectrometry Core facility. 20 µl of each bulk protein sample were combined with 20 µl of 2X Laemmli Sample Buffer (Bio-Rad, 161-0737) containing 5% (v/v) 2-mercaptoethanol (Sigma, M3148). Samples were incubated at 95°C, cooled, centrifuged at 16,000 x g for 1 minute, and 20 µl were loaded onto a precast Mini-Protean TGX stain-free gel (Bio-Rad, 4568095). Gels were run at 150 V for 1 hour in 1X TGS buffer (Bio-Rad, 1610732), stained for 30 minutes in 0.1% (w/v)/40% (v/v)/50% (v/v)/10% (v/v) coomassie blue (VWR, 0472)/H_2O/methanol (Sigma-Aldrich, 34860)/glacial acetic acid (EMD,

AX0073-75) stain, and destained overnight in 80% (v/v)/10% (v/v)/10% (v/v) H_2O/methanol/glacial acetic acid solution.

4.6.7. Proteome analysis

Proteome sample aliquots ranging from concentrations of 500 mg/ml to 1200 mg/ml in 100 µl aliquots were submitted to Douglas Whitten of the Michigan State University Mass Spectrometry Core. The following protocol has been developed by the Michigan State University Mass Spectrometry Core:

Aliquots were taken from each sample equal to 80ug and proteins precipitated using chloroform:methanol (1:4). Protein pellets were re-suspended in 270 µL of 4% (w/v) sodium deoxycholate (SDC) in 100 mM tris, pH 8.5, reduced and alkylated by adding TCEP and Iodoacetamide at 10 mM and 40 mM, respectively, and incubated for 5 minutes at 45C with shaking at 2000 rpm in an Eppendorf ThermoMixer R. Trypsin/LysC enzyme mixture, in 50mM ammonium bicarbonate, was added at a 1:100 ratio (w/w) and the mixture was incubated at 37°C overnight with shaking at 1500 rpm in the ThermoMixer. Final volume of each digest was ~300 µL. After digestion, SDC is removed by adding an equal volume of ethyl acetate and trifluoracetic acid (TFA) to 1% (v/v). Samples were then centrifuged at 15,700 x g for 3 minutes to pellet SDC and the supernatant removed to a new tube. Peptides were then subjected to C18 solid phase clean up using StageTips (140) to remove salts and eluates dried by vacuum centrifugation.

Peptide samples were then re-suspended in 100uL of 100mM triethylammonium bicarbonate (TEAB) and labeled with TMT reagents from Thermo Scientific (www.thermo.com) according to manufacturers' instructions. Aliquots of 2uL were taken from each labeled sample and reserved for testing labeling/mixing efficiency by MS. Labeling efficiency was calculated at

> 99% for all labels. Remaining labeled peptides were normalized and mixed 1:1 according to Erdjument-Bromage, et.al (140) and purified by solid phase extraction using C18 SepPaks (www.waters.com). Eluted peptides were dried by vacuum centrifugation to ~2 µl and stored at -20°C. Prior to injection the purified peptides were re-suspended in 2% acetonitrile/0.1%TFA to 20 µl.

The sample was diluted 1:10 on plate in 2% acetonitrile/0.1% TFA and an injection of 5 µl (~2 µg) was automatically made using a Thermo (www.thermo.com) EASYnLC 1200 onto a Thermo Acclaim PepMap RSLC 0.1 mm x 20 mm C18 trapping column and washed for ~5 minutes with buffer A. Bound peptides were then eluted over 245 minutes onto a Thermo Acclaim PepMap RSLC 0.075 mm x 250 mm resolving column with a gradient of 5%B to 38%B in 234 minutes, ramping to 90%B at 235 minutes and held at 90%B for the duration of the run (Buffer A = 99.9% Water/0.1% Formic Acid, Buffer B = 80% Acetonitrile/0.1% Formic Acid/19.9% Water) at a constant flow rate of 300 nl/min. Column temperature was maintained at a constant temperature of 50°C using and integrated column oven (PRSO-V2, Sonation GmbH, Biberach, Germany).

Eluted peptides were sprayed into a ThermoScientific Q-Exactive HF-X mass spectrometer (www.thermo.com) using a FlexSpray spray ion source. Survey scans were taken in the Orbi trap (120,000 resolution, determined at m/z 200) and the top 15 ions in each survey scan are then subjected to automatic higher energy collision induced dissociation (HCD) with fragment spectra acquired at 45,000 resolution. The resulting MS/MS spectra are converted to peak lists using MaxQuant (141), v1.6.3.4 (www.maxquant.org) and searched against a protein sequence database containing all entries for *S. oneidensis* MR-1 (downloaded from www.uniprot.org on 2019-10-15) and common laboratory contaminants (downloaded from

www.thegpm.org, cRAP project) using the Andromeda (142) search algorithm, a part of the MaxQuant environment. The Mascot output was then analyzed using Scaffold, v5.0.1 (www.proteomesoftware.com), to probabilistically validate protein identifications. Assignments validated using the Scaffold 1% FDR confidence filter are considered true. Mascot parameters for all databases were as follows: allow up to 2 missed tryptic sites, fixed modification of Carbamidomethyl Cysteine, variable modification of Oxidation of Methionine, Acetylation of N-term, peptide tolerance of +/- 10ppm, MS/MS tolerance of 0.02 Da, and FDR calculated using randomized database search.

Peptide counts from each proteome sample were normalized to total protein concentrations and converted to Log_2 fold change between the low dilution rate and high dilution rate conditions in the program Scaffold 5 (Proteome Software, version 5.1.1).

4.6.8. Gibbs free energy calculations

Total Gibbs free energy was calculated using ΔG values provided from BioCyc for each ETC complex's reaction (139). Further, we calculated the ΔG for H^+ transport to the periplasm from the ΔG of ATP hydrolysis in exponentially growing *E. coli* cells (-54 kJ/mol) (138), which allowed us to calculate the overall ΔG for each ETC combination. It is important to note that these calculations assume the same membrane potential and NADH:NAD^+ for both ETC configurations.

4.6.9. Data analysis

Analysis of growth and HPLC data was performed using Microsoft Excel (2016) and Rstudio (143) with the following packages: ggplot2 (96), reshape2 (97), dplyr (98), and TTR (99). Proteome analysis was conducted using Scaffold 5 (Proteome Software) and the BioCyc (139) and MetaCyc (144) databases. Statistical analysis was conducted in Scaffold 5. The low growth

rate condition was set as the reference and compared with the high growth rate condition using a permutation test with a Bonferroni correction.

Chapter 5: Conclusions and Future Directions

5.1. Overall goal and primary findings

As a bacterial isolate from a freshwater lake in New York state, *Shewanella oneidensis* MR-1 evolved in an ever-changing environment. This organism adapted to survive rapid changes in substrate availability, the presence of oxygen, or redox stratification while colonizing inthe soil of the lakebed. As a result, *S. oneidensis* MR-1 has a variety of metabolic strategies to adjust to environmental changes, including a highly branched electron transport chain (ETC) (22). The primary goal of this dissertation was to better understand the physiology of the ETC and how it contributes to the metabolic versatility of *S. oneidensis* MR-1. What began as an introductory look into the differing metabolic functions of the four NADH dehydrogenases (NDHs) encoded in the MR-1 genome, gave rise to a larger project aiming to disentangle the functions of different complexes and electron paths in the electron transport chain. While the studies conducted within this dissertation were focused on aerobic growth, understanding the function and optimization of the ETC in *S. oneidensis* MR-1 has implications for its biotechnological uses, such as electrosynthesis. Inward electron transfer in *S. oneidensis* MR-1 for electrosynthesis is dependent on reversing the Mtr pathway and NDH function (21) to reduce NAD^+ to NADH. The reducing equivalents generated from this process can then be used for the synthesis of products of interest through non-native pathways. Therefore, these studies have provided integral physiological information regarding the ETC in *S. oneidensis* MR-1 that can aid in optimizing inward electron transfer and electrosynthesis.

We first determined the importance of the Nuo and Nqr1 NDHs during aerobic growth in batch cultures. We found that either Nuo or Nqr1 was required for growth to occur under the conditions tested. Knocking out both Nuo and Nqr1 was severely detrimental, resulting in its inability to grow in minimal medium under oxic conditions. Additionally, we found that

knocking out both Nuo and Nqr1 in *S. oneidensis* MR-1 led to suppression of the TCA cycle caused by high NADH concentrations in the cell. TCA cycle suppression led to an inability to completely oxidize substrate, resulting in secretion of high amounts of the metabolites pyruvate and acetate. Overall, tryptone (tryptic digest of casein) supplementation rescued the growth of the strain and allowed us to determine that the growth defect was caused by the lack of TCA cycle function for generating amino acid synthesis precursors.

To further explore how *S. oneidensis* MR-1 utilizes redundancies in its respiratory chain for growth, we investigated how it restructures its ETC under low and high growth rate conditions. We tested this with a growth study conducted in a continuous flow fermenter. In the low growth rate condition, the substrate was fully oxidized and little to no acetate accumulation was observed. Conversely, when shifting to higher growth rates, the cells directed substrate flux away from the TCA cycle via overflow metabolism, resulting in acetate secretion. These findings support recent models suggesting that faster growing bacteria use overflow metabolism to reduce proteome cost or as a result of limited membrane real estate (47, 55–57). If applied to the ETC, these models predict that less energetically efficient configurations would be used at high growth rates, because this could also conserve proteome cost and membrane real estate. However, we found that ETC regulation in *S. oneidensis* MR-1 could not be explained by either of these models and the inefficient NDH, Ndh, was more abundant under the low growth rate condition. Surprisingly, we also found the proton-pumping, Nuo, was more abundant under the high growth rate condition although it was predicted to be more important at the low growth rate. This finding was interesting because it did not fit within the confines of current models that explain the shift to less energetically efficient pathways as growth rate increases (47, 55–57, 126). Further work is necessary to understand why less efficient NADH dehydrogenases may be

beneficial at low growth rates. We hypothesize that substrate limitation at the low growth rate may cause a low NADH:NAD^+, leading to insufficient driving force for the Nuo reaction.

5.2. Future directions

Altogether, we have amassed a large amount of data regarding the function of the highly branched respiratory chain of *S. oneidensis* MR-1. While we now have a better understanding of how the ETC operates during aerobic growth, there is still much to be discovered with respect to their regulation and usage. The projects in this dissertation have laid the foundation for future physiological studies on *S. oneidensis* MR-1. Although our studies were conducted using *S. oneidensis* MR-1, future study of the functionality and versatility of respiratory chains has broader implications for bacterial respiration and biotechnological applications.

5.2.1. Driving *S. oneidensis* MR-1 towards its max growth rate

Our recent work on steady-state growth in a continuous flow fermenter for *S. oneidensis* MR-1 yielded important data regarding its use of overflow metabolism during high growth rates. In this study, we observed overflow metabolism occurring at a growth rate of 0.207 h^{-1}. In comparison, we have observed growth rates up to 0.45 h^{-1} in batch cultures growing in the same minimal medium supplemented with D,L-lactate. Therefore, we did not reach even half of the max growth rate obtained in batch cultures, leaving more room for exploration. Preliminary studies can be conducted to determine *S. oneidensis* MR-1's max growth rate in a continuous flow system. Max growth rate is the highest dilution rate at which cells can maintain a constant density without washing out of the system. Upon determining this rate, one could conduct studies focusing on the differences in substrate metabolism and protein synthesis under low, mid, and max growth rate conditions.

The question then becomes, can we drive more carbon flux through overflow metabolism like *E. coli* (47, 55, 57) and to what extent does it impact the ETC structure of *S. oneidensis* MR-1? The use of ^{13}C-labeled lactate for ^{13}C-metabolic flux analysis (^{13}C-MFA) would be an important addition to this type of work (145). ^{13}C-MFA would allow us to quantify the amount of substrate being directed into overflow metabolism, if there is residual TCA cycle function occurring, and how metabolites are assimilated. We know that TCA cycle function is important for generating amino acid synthesis precursors (137), so a complete shutdown of the TCA cycle would not be likely. Further, we could ascertain the importance of respiratory complexes in *S. oneidensis* MR-1 upon reaching the maximum growth rate. If most of the carbon flux is directed toward acetate production, with residual carbon being assimilated into biomass, then the main mechanism of ATP generation would be substrate-level phosphorylation (47, 55–57). It is also important to note that *S. oneidensis* MR-1 cannot conduct any redox balanced fermentation, so reduced electron carriers generated from lactate metabolism and any residual TCA cycle function would need to be recycled. Therefore, some requirement for ETC function will remain. A repeat of comparative proteome analysis between the low, mid, and max growth rate conditions would allow us to assess the abundance changes of each respiratory complex in the ETC during these conditions.

The addition of a third dilution rate would allow for the comparison of the known ETC structure to the max growth rate condition where a higher extent of respiro-fermentation could be occurring. One potential outcome is a reduction in ETC complex abundance at the max growth rate, which would be expected if the requirement for oxidative phosphorylation decreases.

5.2.2. Investigating the effects of microaerobosis on ETC structure

In a similar study in a continuous flow fermenter, using microoxic conditions could allow us to further investigate the thermodynamic barriers presented with NADH oxidation by the NDHs. Following the experimental design detailed in chapter four of this dissertation, we could initially maintain oxygen concentrations at ~20% saturation at a low dilution rate. Rather than adjusting the dilution rate to increase growth rate, we could gradually increase oxygen concentrations to >80% saturation. We would then repeat this experiment at the high growth rate condition. Cells in microoxic or anoxic conditions maintain higher NADH:NAD^+ levels than those growing under fully oxic conditions. This creates a condition where cells exhibit increased NADH:NAD^+, making the oxidation of NADH more thermodynamically favorable (138). If the expression and synthesis of the more efficient NDHs is constrained by the thermodynamically unfavorable reaction of coupling ion transport with NADH oxidation, then creating a microoxic environment to raise NADH:NAD^+ could help surpass that barrier. Here, we could monitor how the ETC is structured to help regulate the redox state of the cell with comparative proteome analysis.

This study would also allow us to observe how oxygen concentration regulates the terminal oxidases. We would expect increases in the *cbb*$_3$-type cytochrome *c* oxidase (Cco) and the *bd*-type ubiquinol oxidase (Cyd), while the abundance of the *aa*$_3$-type cytochrome *c* oxidase (Cox) would decrease under microoxic conditions. Previously, we did not observe any significant abundance changes in the Cyd terminal oxidase (Ch. 4). Due to their higher oxygen affinity, both Cco and Cyd could become more important during microaerobosis (25, 35, 38, 43). Conversely, the low oxygen affinity of Cox may lead to a reduction in usage (24, 25, 35). In general, the A-type terminal oxidases' optimal function occurs at atmospheric concentrations of

oxygen (35). Altogether, with the additional variable of microoxic conditions, we could observe an additional branch of the ETC being used that we did not previously report.

APPENDIX

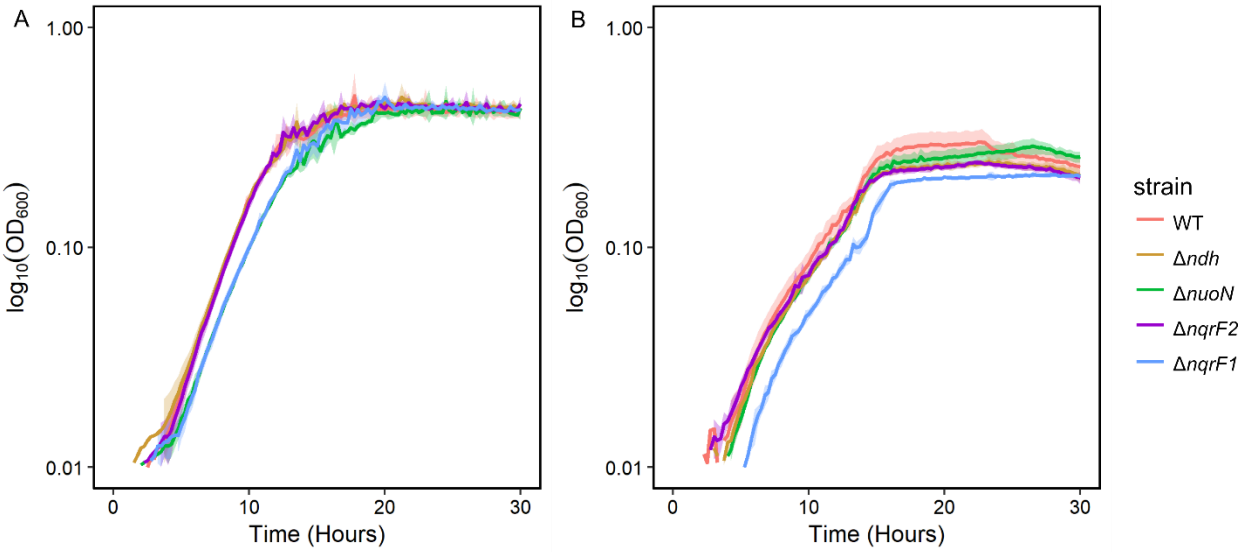

Figure S2.1. Growth of WT and all single NDH knockout strains. Growth of WT, Δ*ndh*, and Δ*nqrF2* in 1 mL minimal medium with (A) 20mM NAG and (B) 20 mM D,L-lactate. Growth was conducted in a 1 mL culture volume and monitored in 15-minute intervals in 24 well plates using the BioTek Synergy HTX plate reader (BioTek Instruments, Winooski, VT) at 30°C.

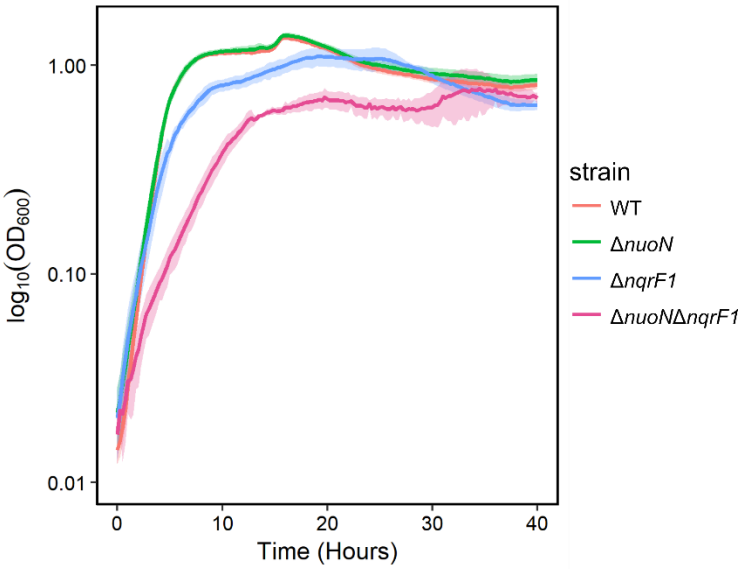

Figure S2.2. The double mutant strain can be cultivated in LB medium. Growth of WT, Δ*nuoN*, Δ*nqrF1*, and Δ*nuoN*Δ*nqrF1* in LB medium. Growth was conducted in a 1 mL culture volume and monitored in 15-minute intervals in 24 well plates using the BioTek Synergy HTX plate reader (BioTek Instruments, Winooski, VT) at 30°C.

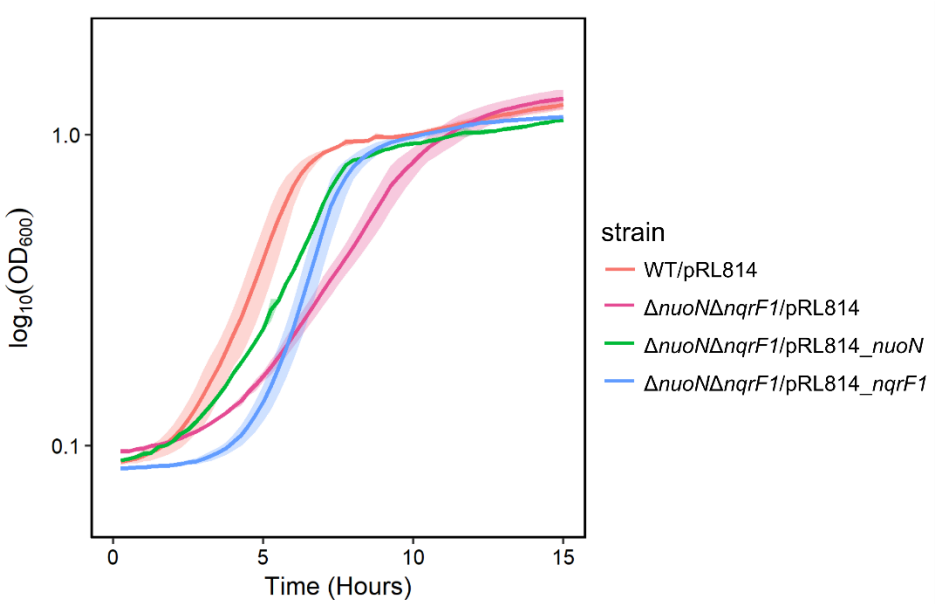

Figure S2.3. Complementation of the double mutant strain. Growth of WT/pRL814 empty vector, Δ*nuoN*Δ*nqrF1*/pRL814 empty vector, Δ*nuoN*Δ*nqrF1* complemented with pRL814_*nuoN*, and Δ*nuoN*Δ*nqrF1* complemented with pRL814_*nqrF1* in 1 mL LB medium. Growth was conducted in a 1 mL culture volume and monitored in 15-minute intervals in 24 well plates using the BioTek Synergy HTX plate reader (BioTek Instruments, Winooski, VT) at 30°C.

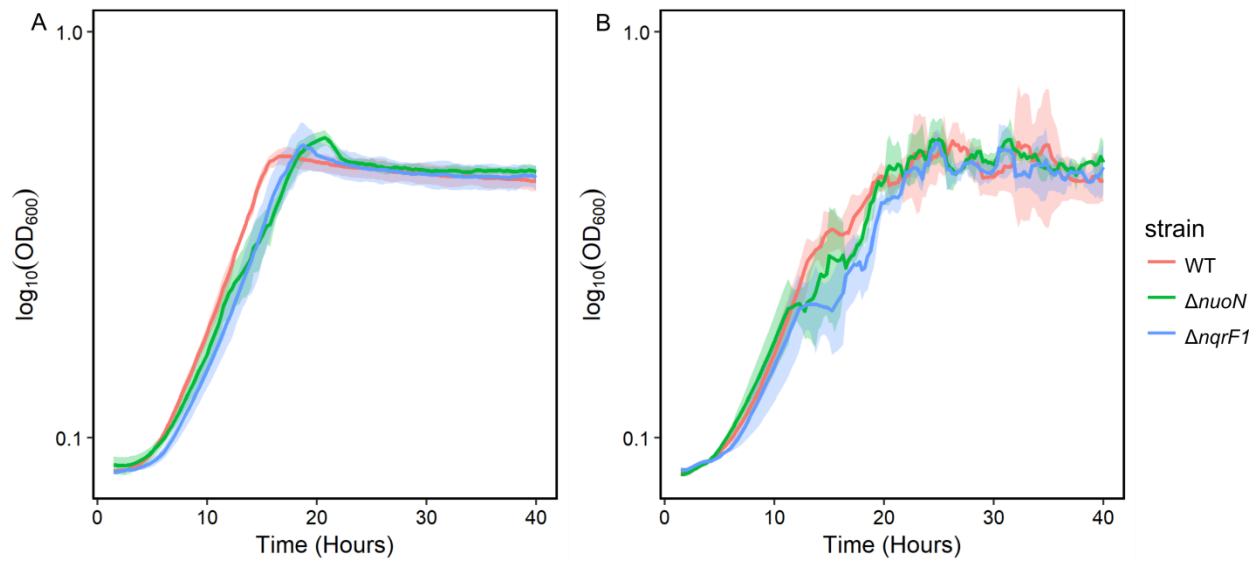

Figure S2.4. Growth of WT and NDH mutants with normalized sodium concentrations. Growth of WT, Δ*nuoN*, and Δ*nqrF1* in 1 mL minimal media supplemented with (A) 10 mM NAG and (B) 10 mM NAG with additional 20 mM NaCl to normalize sodium for 24-well assays conducted with 20 mM sodium D,L-lactate. Growth was conducted in a 1 mL culture volume and monitored in 15-minute intervals in 24 well plates using the BioTek Synergy HTX plate reader (BioTek Instruments, Winooski, VT) at 30°C.

Table 2.1. Growth analysis of WT and NDH mutant strains. Growth rate analysis of *Shewanella oneidensis* NADH dehydrogenase mutants in 50 mL M5 minimal medium with 10 mM NAG, 20mM D,L-lactate in 250 mL flasks and in 1 mL M5 with 10mM acetate in a 24-well plate. Growth rates were calculated using the R package 'growthcurver,' which fits the growth curve data to the best-fit logistic curve (100).

Carbon source	*S. oneidensis*	Growth rate (hr^{-1})	Difference from WT (%)	*p*-values
NAG	WT	0.93 ± 0.05	n/a	n/a
	Δ*nuoN*	0.76 ± 0.06	17.7	0.020
	Δ*nqrF1*	0.81 ± 0.04	12.9	0.027
D,L-lactate	WT	0.45 ± 0.05	n/a	n/a
	Δ*nuoN*	0.41 ± 0.04	9.1	0.33
	Δ*nqrF1*	0.43 ± 0.05	4.8	0.60
Acetate	WT	0.55 ± 0.04	n/a	n/a
	Δ*nuoN*	0.36 ± 0.02	35.0	0.0018
	Δ*nqrF1*	0.32 ± 0.01	42.8	0.0005

Table 2.2. In-frame deletion mutagenesis primers. List of primers used for generation of in-frame deletion mutants.

Gene	Primer	Sequence
nuoN	FO	CTCTCAAATAGAGCACTC
	RO	ACCAGCATCTCCCACATG
	5O	GCTCAATATGATTGCGGGGCT
	5i	GGGATGAACACACCATGTCAGTGTTGCAGTAACGC
	3O	ATCTACTCGGGTAGCGAAGTG
	3i	TGACATGGTGTGTTCATCCCCGGAGAAAGTCATTGCAGGGC
nqrF1	FO	CTGGCCTTCTTCCTCGGTAT
	RO	GCCTTAGCTGCATCAATCTCGG
	5O	AGGGATTGCGGTAGTTGTAGTGT
	5i	CACAGAATCACGCTGTGATTCAGGTCCAATTCAAGAAGCCG
	3O	CGCTTATCAGGTCCAAAACCCCA
	3i	GAATCACAGCGTGATTCTGTGTGTGAATTAGCCCAAGGT
ndh	FO	TACATATCTTCAACATGTTGATTAATA
	RO	CTGAATGAAAATTACATAATTGAAGGG
	5O	ATTTCATCGGTTAGTGTAGTTTG
	5i	ACCCATGACCACTAAAATAGAAATAACAACCTCAACAAACTCAT
	3O	CTTAAAAACCGCCCTACC
	3i	TCTATTTTAGTGGTCATGGGTTCATAAAGAACAAAACAGAGAGCT
nqrF2	FO	CGCTGTCGTTCTTCCTCGGTATGTG
	RO	GTTGCGGCTCAGCTTTTGCG
	5O	GTGCTAATGACCTTAGCCGTGCC
	5i	GGGCTTGAGAGATCCCACTACTTCCATCCGATAACC
	3O	CAACTTGATGCGCTGGTAGAGGTC
	3i	GTAGTGGGATCTCTCAAGCCCGATTAGGTTGTAAGT

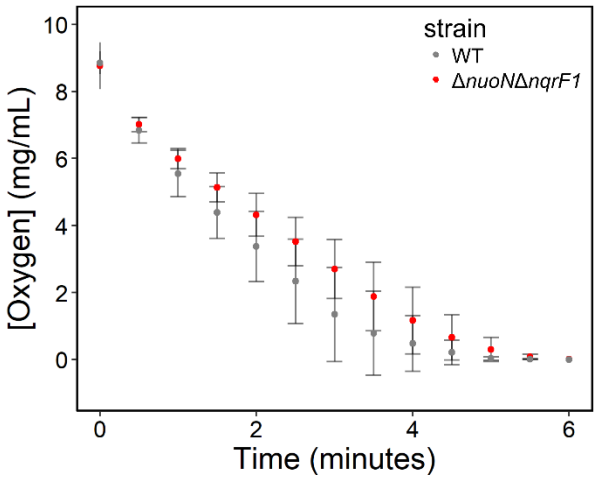

Figure S3.1. Analysis of oxygen consumption in WT and the double mutant strain. Oxygen consumption of WT and Δ*nuoN*Δ*nqrF1* grown in 50 mL culture volumes of M5 supplemented with 0.1% (w/v) tryptone and 20 mM D,L-lactate. 25 mL of oxygen saturated culture were transferred to a 50 mL conical tube and oxygen concentration was measured over time using an optical DO probe.

Table 3.1. Endpoint HPLC analysis of 24-well plate contents. Growth and endpoint HLPC analysis of carbon source utilization from 24-well plate experiments after 48-hour runtime in M5 supplemented with 0.1% tryptone and 20 mM D,L-lactate or 10 mM NAG from Figure 3.2**.**

Strain	Carbon Source	C-source Remaining (mM)	[acetate] (mM)	OD_{MAX}	Growth Rate (h^{-1})
WT	D,L-lactate	0	0	0.747 ± 0.03	0.896 ± 0.036
Δ*nuoN*Δ*nqrF1*	D,L-lactate	5.13 ± 0.24	28.7 ± 0.96	0.252 ± 0.01	0.448 ± 0.021
WT	NAG	0	0	0.765 ± 0.02	0.618 ± 0.033
Δ*nuoN*Δ*nqrF1*	NAG	2.96 ± 0.23	25.1 ± 1.05	0.259 ± 0.01	0.342 ± 0.014

Table 3.2. NAD(H) quantification. Comparison of NAD(H) pools and NADH/NAD^+ ratios of WT and Δ*nuoN*Δ*nqrF1* when grown in 50 mL cultures of M5 supplemented with 0.1% tryptone and either 20 mM D,L-lactate or 10 mM NAG.

Carbon Source	OD_{600}	Strain	NAD(H) pool size (μmol/g protein)	NADH/NAD^+
D,L-lactate	0.1	WT	27.9 ± 3.8	0.28 ± 0.11
		Δ*nuoN*Δ*nqrF1*	48.9 ± 5.5	0.17 ± 0.02
	0.3	WT	51.4 ± 9.5	0.16 ± 0.03
		Δ*nuoN*Δ*nqrF1*	49.5 ± 5.5	0.20 ± 0.04
NAG	0.1	WT	4.84 ± 0.4	0.23 ± 0.08
		Δ*nuoN*Δ*nqrF1*	7.65 ± 2.7	0.37 ± 0.02
	0.2	WT	12.3 ± 0.8	0.20 ± 0.01
		Δ*nuoN*Δ*nqrF1*	26.9 ± 4.5	0.19 ± 0.03

Table 3.3. Analyzing the effect of Rex on growth rate. Comparison of growth rates of WT and Δ*nuoN*Δ*nqrF1* with and without the Rex sensor growing in M5 supplemented with 0.1% tryptone and either 20 mM D,L-lactate or 10 mM NAG from Figure 3.7.

Strain	Growth Rate in D,L-lactate (h^{-1})	Growth Rate in NAG (h^{-1})
WT Rex	0.597 ± 0.024	0.305 ± 0.018
Δ*nuoN*Δ*nqrF1* Rex	0.380 ± 0.012	0.275 ± 0.041
WT	1.00 ± 0.029	0.899 ± 0.024
Δ*nuoN*Δ*nqrF1*	0.416 ± 0.015	0.513 ± 0.020

Table 3.4. HPLC analysis of 24-well plate contents for Rex containing strains. Endpoint HLPC analysis of carbon source utilization from 24-well plate experiments with WT and Δ*nuoN*Δ*nqrF1* containing the Rex redox sensor after 48-hour runtime in M5 supplemented with 0.1% tryptone and 20 mM D,L-lactate or 10 mM NAG**.**

Strain	Carbon Source	C-source Remaining (mM)	[pyruvate] (mM)	[acetate] (mM)
WT	D,L-lactate	0	0	0
Δ*nuoN*Δ*nqrF1*	D,L-lactate	2.15 ± 0.54	0.16 ± 0.03	4.74 ± 1.2
WT	NAG	0	0	0
Δ*nuoN*Δ*nqrF1*	NAG	0.24 ± 0.22	0.63± 0.09	6.99 ± 1.2

Table 4.1. NDH and terminal oxidase combinations. Combinations of NADH dehydrogenases and terminal oxidases with the number of protons translocated/NADH oxidized and theoretical yield of ATP generated per NADH oxidation event.

NADH dehydrogenase	Terminal oxidase	Protons translocated	ATP/NADH generated
Nuo	Cox	12 H^+	4.00
Nuo	Cco	10 H^+	3.33
Nuo	Cyd	6 H^+	2.00
Nqr1/2	Cox	10 H^+	3.33
Nqr1/2	Cco	8 H^+	2.67
Nqr1/2	Cyd	4 H^+	1.33
Ndh	Cox	8 H^+	2.67
Ndh	Cco	6 H^+	2.00
Ndh	Cyd	2 H^+	0.67

Table 4.2. Classification of protein subgroups determined for identified proteins. *Denotes the finding that some identified or unidentified proteins were found in duplicate subgroups.

Protein subgroup	Proteins identified in group	Total proteins in group	Percentage identified (%)	Significant proteins ($p < 0.0001$) (%)
Amino acid biosynthesis	85	91	93.41	44.71
Biosynthesis of cofactors, prosthetic groups, and carriers	95	127	74.80	30.53
Cell envelope	102	170	60.00	36.27
Cellular processes	135	265	50.94	42.22
Central intermediary metabolism	28	54	51.85	60.71
DNA metabolism	58	135	42.96	32.76
Energy metabolism	202	310	65.16	56.44
Fatty acid and phospholipid metabolism	50	66	75.76	48.00
Hypothetical proteins or Unknown function	726	1778	40.83	30.30
Mobile and extrachromosomal element functions	9	74	12.16	33.33
Protein fate	128	193	66.32	38.28
Protein synthesis	118	144	81.94	51.69
Purines, pyrimidines, nucleosides, and nucleotides	54	62	87.10	57.41
Regulatory functions	79	222	35.59	25.32
Signal transduction	20	94	21.28	25.00
Transcription	32	55	58.18	37.50
Transport and binding proteins	133	307	43.32	35.34
Total	2054*	4147*		

Table 4.3. Abundance changes of ETC complexes. Relative abundance changes of NADH dehydrogenases, terminal oxidases, and ATP synthase identified by protein synthesis analysis (Fig. 4.5). Shown are the abundance change values for the high growth rate condition in reference to the low growth rate condition.

Protein	Subunit Name	Log_2 Fold Change	*p*-value
Ndh	Ndh	-0.226	< 0.0001
Nuo	NuoA	0.226	0.33
	NuoB	0.195	< 0.0001
	NuoC	0.188	< 0.0001
	NuoE	0.265	< 0.0001
	NuoF	0.236	< 0.0001
	NuoG	0.172	< 0.0001
	NuoH	0.115	0.097
	NuoI	0.232	0.001
	NuoJ	0.110	0.035
	NuoL	0.011	0.96
	NuoM	0.305	0.014
Nqr1	NqrA1	0.169	< 0.0001
	NqrB1	0.399	0.0002
	NqrC1	0.086	0.0002
	NqrF1	0.203	< 0.0001
Nqr2	NqrA2	-0.270	< 0.0001
	NqrB2	0.177	0.059
	NqrC2	-0.320	< 0.0001
	NqrF2	-0.318	< 0.0001
Cco	CcoN	0.413	< 0.0001
	CcoO	0.516	< 0.0001
	CcoP	0.471	< 0.0001
Cyd	CydA	0.037	0.088
	CydB	-0.095	0.05
Cox	CoxB	-0.584	< 0.0001
ATP Synthase	AtpA	0.412	< 0.0001
	AtpB	0.287	0.017
	AtpC	0.310	0.001
	AtpD	0.455	< 0.0001

Table 4.3. (cont'd)

Protein	Subunit Name	Log_2 Fold Change	*p*-value
ATP Synthase	AtpE	0.448	0.008
	AtpF	0.422	< 0.0001
	AtpG	0.390	< 0.0001
	AtpH	0.155	0.0009

Table S4.1. Abundance changes of RNA polymerase and ribosomal subunits. Relative abundance changes of transcription and translation machinery identified by protein synthesis analysis. Shown are the abundance change values for the high growth rate condition in reference to the low growth rate condition.

Protein	Subunit Name	Log_2 Fold Change	*p*-value
RNA Polymerase	RpoA	0.211	< 0.0001
	RpoB	0.234	< 0.0001
	RpoC	0.293	< 0.0001
	RpoD	0.131	< 0.0001
	RpoE	-0.079	0.073
30S Subunit	RpsA	0.071	< 0.0001
	RpsB	0.131	< 0.0001
	RpsC	0.756	< 0.0001
	RpsD	0.401	< 0.0001
	RpsE	0.623	< 0.0001
	RpsF	0.308	< 0.0001
	RpsG	0.773	< 0.0001
	RpsH	0.541	< 0.0001
	RpsI	1.054	< 0.0001
	RpsJ	0.612	< 0.0001
	RpsK	0.841	< 0.0001
	RpsL	0.626	< 0.0001
	RpsM	0.497	< 0.0001
	RpsN	0.983	< 0.0001
	RpsP	0.380	< 0.0001
	RpsQ	0.450	0.00052
	RpsR	0.401	< 0.0001
	RpsS	0.819	< 0.0001
	RpsT	1.428	0.008
	RpsU	0.456	< 0.0001
50S Subunit	RplA	0.548	< 0.0001
	RplB	0.595	< 0.0001
	RplC	0.629	< 0.0001
	RplD	0.716	< 0.0001
	RplE	0.216	< 0.0001
	RplF	0.195	< 0.0001
	RplI	0.337	< 0.0001
	RplJ	0.429	< 0.0001
	RplK	0.348	< 0.0001

Table S4.1. (cont'd)

Protein	Subunit Name	Log_2 Fold Change	*p*-value
50S Subunit	RplL	0.198	0.004
	RplM	0.560	< 0.0001
	RplN	0.517	< 0.0001
	RplO	0.405	< 0.0001
	RplP	0.441	< 0.0001
	RplQ	0.377	< 0.0001
	RplR	0.229	0.00017
	RplS	0.854	< 0.0001
	RplT	0.562	< 0.0001
	RplU	0.585	< 0.0001
	RplV	0.783	< 0.0001
	RplW	0.536	< 0.0001
	RplX	0.291	< 0.0001
	RplY	-0.065	0.38
	RpmA	0.511	< 0.0001
	RpmB	0.660	< 0.0001
	RpmE	-0.416	0.008
	RpmF	0.546	0.008
	RpmH	0.471	0.001
	RpmI	-0.049	0.72

REFERENCES

REFERENCES

1. Kysela DT, Randich AM, Caccamo PD, Brun Y V. 2016. Diversity takes shape: understanding the mechanistic and adaptive basis of bacterial morphology. PLoS Biol 14:e1002565.

2. Yang DC, Blair KM, Salama NR. 2016. Staying in shape: the impact of cell shape on bacterial survival in diverse environments. Microbiol Mol Biol Rev 80:187–203.

3. Russell JB, Cook GM. 1995. Energetics of bacterial growth: balance of anabolic and catabolic reactions. Microbiol Rev 59:48–62.

4. Steinbüchel A, Valentin HE. 1995. Diversity of bacterial polyhydroxyalkanoic acids. FEMS Microbiol Lett 128:219–228.

5. Haddock BA, Jones CW. 1977. Bacterial respiration. Bacteriol Rev 41:47.
6. Clark DP. 1989. The fermentation pathways of *Escherichia coli*. FEMS Microbiol Rev 5:223–234.

7. Conway T. 1992. The Entner-Doudoroff pathway: history, physiology and molecular biology. FEMS Microbiol Rev 9:1–27.

8. Flamholz A, Noor E, Bar-Even A, Liebermeister W, Milo R. 2013. Glycolytic strategy as a tradeoff between energy yield and protein cost. Proc Natl Acad Sci U S A 110:10039–10044.

9. Bar-Even A, Flamholz A, Noor E, Milo R. 2012. Rethinking glycolysis: on the biochemical logic of metabolic pathways. Nat Chem Biol 8:509–517.

10. Pinchuk GE, Hill EA, Geydebrekht O V, De Ingeniis J, Zhang X, Osterman A, Scott JH, Reed SB, Romine MF, Konopka AE, Beliaev AS, Fredrickson JK, Reed JL. 2010. Constraint-based model of *Shewanella oneidensis* MR-1 metabolism: a tool for data analysis and hypothesis generation. PLoS Comput Biol 6:e1000822.

11. Beliaev AS, Klingeman DM, Klappenbach JA, Wu L, Romine MF, Tiedje JM, Nealson KH, Fredrickson JK, Zhou J. 2005. Global transcriptome analysis of *Shewanella oneidensis* MR-1 exposed to different terminal electron acceptors. J Bacteriol 187:7138–7145.

12. Gralnick JA, Vali H, Lies DP, Newman DK. 2006. Extracellular respiration of dimethyl sulfoxide by *Shewanella oneidensis* strain MR-1. Proc Natl Acad Sci United States Am 103:4669–4674.

13. Gao H, Yang ZK, Barua S, Reed SB, Romine MF, Nealson KH, Fredrickson JK, Tiedje JM, Zhou J. 2009. Reduction of nitrate in *Shewanella oneidensis* depends on atypical NAP and NRF systems with NapB as a preferred electron transport protein from CymA to NapA. ISME J 3:966–976.

14. Shi L, Rosso KM, Clarke TA, Richardson DJ, Zachara JM, Fredrickson JK. 2012. Molecular underpinnings of Fe(III) oxide reduction by *Shewanella oneidensis* MR-1. Front Microbiol 3:50.

15. Hsu L, Masuda SA, Nealson KH, Pirbazari M. 2012. Evaluation of microbial fuel cell *Shewanella* biocathodes for treatment of chromate contamination. RSC Adv 2:5844–5855.

16. Bouhenni RA, Vora GJ, Biffinger JC, Shirodkar S, Brockman K, Ray R, Wu P, Johnson BJ, Biddle EM, Marshall MJ, Fitzgerald LA, Little BJ, Fredrickson JK, Beliaev AS, Ringeisen BR, Saffarini DA. 2010. The role of *Shewanella oneidensis* MR-1 outer surface structures in extracellular electron transfer. Electroanalysis 22:856–864.

17. TerAvest MA, Zajdel TJ, Ajo-Franklin CM. 2014. The Mtr pathway of *Shewanella oneidensis* MR-1 couples substrate utilization to current production in *Escherichia coli*. ChemElectroChem 1:1874–1879.

18. Clarke TA, Edwards MJ, Gates AJ, Hall A, White GF, Bradley J, Reardon CL, Shi L, Beliaev AS, Marshall MJ, Wang Z, Watmough NJ, Fredrickson JK, Zachara JM, Butt JN, Richardson DJ. 2011. Structure of a bacterial cell surface decaheme electron conduit. Proc Natl Acad Sci 108:9384–9389.

19. Coursolle D, Baron DB, Bond DR, Gralnick JA. 2010. The Mtr respiratory pathway is essential for reducing flavins and electrodes in *Shewanella oneidensis*. J Bacteriol 192:467–474.

20. Kracke F, Vassilev I, Krömer JO. 2015. Microbial electron transport and energy conservation – the foundation for optimizing bioelectrochemical systems. Front Microbiol 6:575.

21. Tefft NM, TerAvest MA. 2019. Reversing an extracellular electron transfer pathway for electrode-driven acetoin reduction. ACS Synth Biol 8:1590–1600.

22. Pinchuk GE, Hill EA, Geydebrekht O V., de Ingeniis J, Zhang X, Osterman A, Scott JH, Reed SB, Romine MF, Konopka AE, Beliaev AS, Fredrickson JK, Reed JL. 2010. Constraint-based model of *Shewanella oneidensis* MR-1 metabolism: A tool for data analysis and hypothesis generation. PLoS Comput Biol 6:1–8.

23. 2021. UniProt: the universal protein knowledgebase in 2021. Nucleic Acids Res 49:D480–D489.

24. Le Laz S, Kpebe A, Bauzan M, Lignon S, Rousset M, Brugna M. 2016. Expression of terminal oxidases under nutrient-starved conditions in *Shewanella oneidensis*: detection of the A-type cytochrome *c* oxidase. Sci Rep 6:19726.

25. Kaila VRI, Wikström M. 2021. Architecture of bacterial respiratory chains. Nat Rev Microbiol 19:319–330.

26. Heikal A, Nakatani Y, Dunn E, Weimar MR, Day CL, Baker EN, Lott JS, Sazanov LA, Cook GM. 2014. Structure of the bacterial type II NADH dehydrogenase: a monotopic membrane protein with an essential role in energy generation. Mol Microbiol 91:950–964.

27. Iwata S. 1998. Structure and function of bacterial cytochrome *c* oxidase. J Biochem 123:369–375.

28. Verkhovsky MI, Jasaitis A, Verkhovskaya ML, Morgan JE, Wikström M. 1999. Proton translocation by cytochrome *c* oxidase. Nature 400:480–483.

29. Zhou G, Yin J, Chen H, Hua Y, Sun L, Gao H. 2013. Combined effect of loss of the caa_3 oxidase and Crp regulation drives *Shewanella* to thrive in redox-stratified environments. ISME J 7:1752–1763.

30. Marritt SJ, McMillan DGG, Shi L, Fredrickson JK, Zachara JM, Richardson DJ, Jeuken LJC, Butt JN. 2012. The roles of CymA in support of the respiratory flexibility of *Shewanella oneidensis* MR-1. Portland Press Limited.

31. Poole RK, Cook GM. 2000. Redundancy of aerobic respiratory chains in bacteria? Routes, reasons and regulation.

32. Rojo F. 2010. Carbon catabolite repression in *Pseudomonas*: optimizing metabolic versatility and interactions with the environment. FEMS Microbiol Rev 34:658–684.

33. B. BV, Ranjani M, L. VM, A. BD, Huazhi H, B. GR, I. VM. 2011. Aerobic respiratory chain of *Escherichia coli* is not allowed to work in fully uncoupled mode. Proc Natl Acad Sci 108:17320–17324.

34. Steinsiek S, Stagge S, Bettenbrock K. 2014. Analysis of *Escherichia coli* Mutants with a Linear Respiratory Chain. PLoS One 9:e87307.

35. Morris RL, Schmidt TM. 2013. Shallow breathing: bacterial life at low O2. Nat Rev Microbiol 11:205–212.

36. Pereira MM, Santana M, Teixeira M. 2001. A novel scenario for the evolution of haem–copper oxygen reductases. Biochim Biophys Acta (BBA)-Bioenergetics 1505:185–208.

37. Baker SC, Ferguson SJ, Ludwig B, Page MD, Richter O-MH, van Spanning RJM. 1998. Molecular genetics of the genus *Paracoccus*: metabolically versatile bacteria with bioenergetic flexibility. Microbiol Mol Biol Rev 62:1046–1078.

38. Le Laz S, Kpebe A, Bauzan M, Lignon S, Rousset M, Brugna M. 2014. A biochemical approach to study the role of the terminal oxidases in aerobic respiration in *Shewanella oneidensis* MR-1. PLoS One 9:e86343.

39. D'mello R, Hill S, Poole RK. 1996. The cytochrome *bd* quinol oxidase in *Escherichia coli* has an extremely high oxygen affinity and two oxygen-binding haems: implications for regulation of activity in vivo by oxygen inhibition. Microbiology 142:755–763.

40. Ludwig B. 1987. Cytochrome c oxidase in prokaryotes. FEMS Microbiol Rev 3:41–56.

41. García-Horsman JA, Barquera B, Rumbley J, Ma J, Gennis RB. 1994. The superfamily of heme-copper respiratory oxidases. J Bacteriol 176:5587–5600.

42. Steinsiek S, Frixel S, Stagge S, Bettenbrock K. 2011. Characterization of *E. coli* MG1655 and frdA and sdhC mutants at various aerobiosis levels. J Biotechnol 154:35–45.

43. Bertling K, Banerjee A, Saffarini D. 2021. Aerobic Respiration and Its Regulation in the Metal Reducer *Shewanella oneidensis*. Front Microbiol.

44. Unden G, Bongaerts J. 1997. Alternative respiratory pathways of *Escherichia coli*: energetics and transcriptional regulation in response to electron acceptors. Biochim Biophys Acta (BBA)-Bioenergetics 1320:217–234.

45. Gyan S, Shiohira Y, Sato I, Takeuchi M, Sato T. 2006. Regulatory Loop between Redox Sensing of the NADH/NAD+ Ratio by Rex (YdiH) and Oxidation of NADH by NADH Dehydrogenase Ndh in *Bacillus subtilis*. J Bacteriol 188:7062 LP – 7071.

46. Sokatch JR. 2014. Bacterial physiology and metabolism. Academic Press.

47. Basan M, Hui S, Okano H, Zhang Z, Shen Y, Williamson JR, Hwa T. 2015. Overflow metabolism in *Escherichia coli* results from efficient proteome allocation. Nature 528:99–104.

48. Valgepea K, Adamberg K, Nahku R, Lahtvee P-J, Arike L, Vilu R. 2010. Systems biology approach reveals that overflow metabolism of acetate in *Escherichia coli* is triggered by carbon catabolite repression of acetyl-CoA synthetase. BMC Syst Biol 4:166.

49. Varma A, Palsson BO. 1994. Stoichiometric flux balance models quantitatively predict growth and metabolic by-product secretion in wild-type *Escherichia coli* W3110. Appl Environ Microbiol 60:3724–3731.

50. Majewski RA, Domach MM. 1990. Simple constrained-optimization view of acetate overflow in *E. coli.* Biotechnol Bioeng 35:732–738.

51. Schmidt A, Kochanowski K, Vedelaar S, Ahrné E, Volkmer B, Callipo L, Knoops K, Bauer M, Aebersold R, Heinemann M. 2016. The quantitative and condition-dependent *Escherichia coli* proteome. Nat Biotechnol2015/12/07. 34:104–110.

52. Vazquez A, Oltvai ZN. 2016. Macromolecular crowding explains overflow metabolism in cells. Sci Rep 6:31007.

53. Niebel B, Leupold S, Heinemann M. 2019. An upper limit on Gibbs energy dissipation governs cellular metabolism. Nat Metab 1:125–132.

54. Noor E, Bar-Even A, Flamholz A, Reznik E, Liebermeister W, Milo R. 2014. Pathway Thermodynamics Highlights Kinetic Obstacles in Central Metabolism. PLOS Comput Biol 10:e1003483.

55. Szenk M, Dill KA, de Graff AMR. 2017. Why do fast-growing bacteria enter overflow metabolism? Testing the membrane real estate hypothesis. Cell Syst 5:95–104.

56. Zhuang K, Vemuri GN, Mahadevan R. 2011. Economics of membrane occupancy and respiro-fermentation. Mol Syst Biol 7:500.

57. Vemuri GN, Altman E, Sangurdekar DP, Khodursky AB, Eiteman M. 2006. Overflow metabolism in *Escherichia coli* during steady-state growth: transcriptional regulation and effect of the redox ratio. Appl Environ Microbiol 72:3653–3661.

58. Shi L, Squier TC, Zachara JM, Fredrickson JK. 2007. Respiration of metal (hydr) oxides by *Shewanella* and *Geobacter*: a key role for multihaem *c*-type cytochromes. Mol Microbiol 65:12–20.

59. Kotloski NJ, Gralnick JA. 2013. Flavin electron shuttles dominate extracellular electron transfer by *Shewanella oneidensis*. MBio 4:e00553-12.

60. Marsili E, Baron DB, Shikhare ID, Coursolle D, Gralnick JA, Bond DR. 2008. *Shewanella* secretes flavins that mediate extracellular electron transfer. Proc Natl Acad Sci 105:3968–3973.

61. von Canstein H, Ogawa J, Shimizu S, Lloyd JR. 2008. Secretion of flavins by *Shewanella* species and their role in extracellular electron transfer. Appl Environ Microbiol 74:615–623.

62. Biffinger JC, Pietron J, Ray R, Little B, Ringeisen BR. 2007. A biofilm enhanced miniature microbial fuel cell using *Shewanella oneidensis* DSP10 and oxygen reduction cathodes. Biosens Bioelectron 22:1672–1679.

63. Rosenbaum MA, Bar HY, Beg QK, Segrè D, Booth J, Cotta MA, Angenent LT. 2011. *Shewanella oneidensis* in a lactate-fed pure-culture and a glucose-fed co-culture with *Lactococcus lactis* with an electrode as electron acceptor. Bioresour Technol 102:2623–2628.

64. Carmona-Martínez AA, Harnisch F, Fitzgerald LA, Biffinger JC, Ringeisen BR, Schröder U. 2011. Cyclic voltammetric analysis of the electron transfer of *Shewanella oneidensis* MR-1 and nanofilament and cytochrome knock-out mutants. Bioelectrochemistry 81:74–80.

65. Golitsch F, Bücking C, Gescher J. 2013. Proof of principle for an engineered microbial biosensor based on *Shewanella oneidensis* outer membrane protein complexes. Biosens Bioelectron 47:285–291.

66. Webster DP, TerAvest MA, Doud DFR, Chakravorty A, Holmes EC, Radens CM, Sureka S, Gralnick JA, Angenent LT. 2014. An arsenic-specific biosensor with genetically engineered *Shewanella oneidensis* in a bioelectrochemical system. Biosens Bioelectron 62:320–324.

67. Flynn JM, Ross DE, Hunt KA, Bond DR, Gralnick JA. 2010. Enabling unbalanced fermentations by using engineered electrode-interfaced bacteria. MBio 1:e00190-10.

68. Anraku Y. 1988. Bacterial electron transport chains. Annu Rev Biochem 57:101–132.

69. Pinchuk GE, Geydebrekht O V., Hill EA, Reed JL, Konopka AE, Beliaev AS, Fredrickson JK. 2011. Pyruvate and lactate metabolism by *Shewanella oneidensis* MR-1 under fermentation, oxygen limitation, and fumarate respiration conditions. Appl Environ Microbiol 77:8234–8240.

70. Brutinel ED, Gralnick JA. 2012. Preferential utilization of D-lactate by *Shewanella oneidensis*. Appl Environ Microbiol 78:8474–6.

71. Meshulam-Simon G, Behrens S, Choo AD, Spormann AM. 2007. Hydrogen metabolism in *Shewanella oneidensis* MR-1. Appl Environ Microbiol 73:1153–1165.

72. Kreuzer HW, Hill EA, Moran JJ, Bartholomew RA, Yang H, Hegg EL. 2014. Contributions of the [NiFe]- and [FeFe]-hydrogenase to H_2 production in *Shewanella oneidensis* MR-1 as revealed by isotope ratio analysis of evolved H_2. FEMS Microbiol Lett 352:18–24.

73. Kane AL, Brutinel ED, Joo H, Maysonet R, VanDrisse CM, Kotloski NJ, Gralnick JA. 2016. Formate metabolism in *Shewanella oneidensis* generates proton motive force and prevents growth without an electron acceptor. J Bacteriol 198:1337–46.

74. Paulick A, Koerdt A, Lassak J, Huntley S, Wilms I, Narberhaus F, Thormann KM. 2009. Two different stator systems drive a single polar flagellum in *Shewanella oneidensis* MR-1. Mol Microbiol 71:836–50.

75. Saville RM, Rakshe S, Haagensen JAJ, Shukla S, Spormann AM. 2011. Energy-Dependent stability of *Shewanella oneidensis* MR-1 biofilms. J Bacteriol 193:3257–3264.

76. Johnson ET, Baron DB, Naranjo B, Bond DR, Schmidt-Dannert C, Gralnick JA. 2010. Enhancement of survival and electricity production in an engineered bacterium by light-driven proton pumping. Appl Environ Microbiol 76:4123–4129.

77. Madden T. 2013. The BLAST sequence analysis tool.

78. Schulz S, Iglesias-Cans M, Krah A, Yildiz Ö, Leone V, Matthies D, Cook GM, Faraldo-Gómez JD, Meier T. 2013. A new type of Na^+-driven ATP synthase membrane rotor with a two-carboxylate ion-coupling motif. PLoS Biol 11:e1001596.

79. Thomas PD, Campbell MJ, Kejariwal A, Mi H, Karlak B, Daverman R, Diemer K, Muruganujan A, Narechania A. 2003. PANTHER: a library of protein families and subfamilies indexed by function. Genome Res 13:2129–2141.

80. Mulkidjanian AY, Dibrov P, Galperin MY. 2008. The past and present of sodium energetics: may the sodium-motive force be with you. Biochim Biophys Acta (BBA)-Bioenergetics 1777:985–992.

81. Rosenbaum MA, Bar HY, Beg QK, Segrè D, Booth J, Cotta MA, Angenent LT. 2012. Transcriptional analysis of *Shewanella oneidensis* MR-1 with an electrode compared to Fe(III)citrate or oxygen as terminal electron acceptor. PLoS One 7:e30827.

82. Leyn SA, Li X, Zheng Q, Novichkov PS, Reed S, Romine MF, Fredrickson JK, Yang C, Osterman AL, Rodionov DA. 2011. Control of proteobacterial central carbon metabolism by the HexR transcriptional regulator: A case study in *Shewanella oneidensis*. J Biol Chem 286:35782–35794.

83. Novichkov PS, Kazakov AE, Ravcheev DA, Leyn SA, Kovaleva GY, Sutormin RA, Kazanov MD, Riehl W, Arkin AP, Dubchak I, Rodionov DA. 2013. RegPrecise 3.0 – A resource for genome-scale exploration of transcriptional regulation in bacteria. BMC Genomics 14:745.

84. Cruz-García C, Murray AE, Rodrigues JLM, Gralnick J a, McCue LA, Romine MF, Löffler FE, Tiedje JM. 2011. Fnr (EtrA) acts as a fine-tuning regulator of anaerobic metabolism in *Shewanella oneidensis* MR-1. BMC Microbiol 11:64.

85. Deutschbauer A, Price MN, Wetmore KM, Shao W, Baumohl JK, Xu Z, Nguyen M, Tamse R, Davis RW, Arkin AP. 2011. Evidence-based annotation of gene function in *Shewanella oneidensis* MR-1 using genome-wide fitness profiling across 121 conditions. PLoS Genet 7:e1002385.

86. Brutinel ED, Gralnick JA. 2012. Anomalies of the anaerobic tricarboxylic acid cycle in *Shewanella oneidensis* revealed by Tn-seq. Mol Microbiol 86:273–283.

87. Myers CR, Nealson KH. 1988. Bacterial manganese reduction and growth with manganese oxide as the sole electron acceptor. Science (80-) 240:1319–1321.

88. Dehal PS, Joachimiak MP, Price MN, Bates JT, Baumohl JK, Chivian D, Friedland GD, Huang KH, Keller K, Novichkov PS. 2009. MicrobesOnline: an integrated portal for comparative and functional genomics. Nucleic Acids Res 38:D396–D400.

89. Paulick A, Delalez NJ, Brenzinger S, Steel BC, Berry RM, Armitage JP, Thormann KM. 2015. Dual stator dynamics in the *Shewanella oneidensis* MR-1 flagellar motor. Mol Microbiol 96:993–1001.

90. Padan E, Venturi M, Gerchman Y, Dover N. 2001. Na^+/H^+ antiporters. Biochim Biophys acta (BBA)-bioenergetics 1505:144–157.

91. Desloover J, Arends JBA, Hennebel T, Rabaey K. 2012. Operational and technical considerations for microbial electrosynthesis. Portland Press Limited.

92. 2011. The past and present of the sodium energetics: May the sodiummotive force be with you 72:181–204.

93. Cao Y, Li X, Li F, Song H. 2017. CRISPRi–sRNA: Transcriptional–Translational regulation of extracellular electron transfer in *Shewanella oneidensis*. ACS Synth Biol.

94. Gibson DG, Young L, Chuang R-Y, Venter JC, Hutchison III CA, Smith HO. 2009. Enzymatic assembly of DNA molecules up to several hundred kilobases. Nat Methods 6:343.

95. R Core team. 2015. R Core Team. R A Lang Environ Stat Comput R Found Stat Comput , Vienna, Austria ISBN 3-900051-07-0, URL http//wwwR-project.org/.

96. Wickham H. 2009. ggplot2 Elegant Graphics for Data AnalysisMedia.

97. Wickham H. 2007. Reshaping data with the reshape package. J Stat Softw 21:1–20.

98. Wickham H, Francois R. 2015. dplyr: A Grammar of Data Manipulation. R Packag version 042 3.

99. Ulrich J. 2017. TTR: Technical Trading Rules. R Packag version 023-2.

100. Sprouffske K, Wagner A. 2016. Growthcurver: An R package for obtaining interpretable metrics from microbial growth curves. BMC Bioinformatics 17.

101. Duhl KL, Tefft NM, TerAvest MA. 2018. *Shewanella oneidensis* MR-1 utilizes both sodium-and proton-pumping NADH dehydrogenases during aerobic growth. Appl Environ Microbiol AEM-00415.

102. Meshulam-Simon G, Behrens S, Choo AD, Spormann AM. 2007. Hydrogen metabolism in *Shewanella oneidensis* MR-1. Appl Environ Microbiol 73:1153–1165.

103. Coursolle D, Gralnick JA. 2012. Reconstruction of extracellular respiratory pathways for iron(III) reduction in *Shewanella oneidensis* strain MR-1. Front Microbiol 3:56.

104. TerAvest MA, Angenent LT. 2014. Oxidizing Electrode Potentials Decrease Current Production and Coulombic Efficiency through Cytochrome *c* Inactivation in *Shewanella oneidensis* MR-1. ChemElectroChem 1:2000–2006.

105. Heidelberg JF, Paulsen IT, Nelson KE, Gaidos EJ, Nelson WC, Read TD, Eisen JA, Seshadri R, Ward N, Methe B, Clayton RA, Meyer T, Tsapin A, Scott J, Beanan M, Brinkac L, Daugherty S, DeBoy RT, Dodson RJ, Durkin AS, Haft DH, Kolonay JF, Madupu R, Peterson JD, Umayam LA, White O, Wolf AM, Vamathevan J, Weidman J, Impraim M, Lee K, Berry K, Lee C, Mueller J, Khouri H, Gill J, Utterback TR, McDonald LA, Feldblyum T V, Smith HO, Venter JC, Nealson KH, Fraser CM. 2002. Genome sequence of the dissimilatory metal ion-reducing bacterium *Shewanella oneidensis*. Nat Biotech 20:1118–1123.

106. Senior AE. 1988. ATP synthesis by oxidative phosphorylation. Physiol Rev 68:177–231.

107. Matsushita K, Ohnishi T, Kaback HR. 1987. NADH-ubiquinone oxidoreductases of the *Escherichia coli* aerobic respiratory chain. Biochemistry 26:7732–7737.

108. Yagi T. 1991. Bacterial NADH-quinone oxidoreductases. J Bioenerg Biomembr 23:211–225.

109. Tran QH, Bongaerts J, Vlad D, Unden G. 1997. Requirement for the proton-pumping NADH dehydrogenase I of *Escherichia coli* in respiration of NADH to fumarate and its bioenergetic implications. Eur J Biochem 244:155–160.

110. Hunt KA, Flynn JM, Naranjo B, Shikhare ID, Gralnick JA. 2010. Substrate-level phosphorylation is the primary source of energy conservation during anaerobic respiration of *Shewanella oneidensis* strain MR-1. J Bacteriol 192:3345–3351.

111. Liu Y, Landick R, Raman S, Landick B, Raman S. 2019. A regulatory NADH/NAD+ redox biosensor for bacteria. ACS Synth Biol 8:264–273.

112. Serres MH, Riley M. 2006. Genomic analysis of carbon source metabolism of *Shewanella oneidensis* MR-1: predictions versus experiments. J Bacteriol 188:4601–4609.

113. de Graef MR, Alexeeva S, Snoep JL, Teixeira de Mattos MJ. 1999. The steady-state internal redox state (NADH/NAD^+) reflects the external redox state and is correlated with catabolic adaptation in *Escherichia coli*. J Bacteriol 181:2351–7.

114. Kanehisa M, Goto S. 2000. KEGG: kyoto encyclopedia of genes and genomes. Nucleic Acids Res 28:27–30.

115. BD Biosciences. 2006. BD Bionutrients Technical Manual Advanced Bioprocessing.

116. Rodionov DA, De Ingeniis J, Mancini C, Cimadamore F, Zhang H, Osterman AL, Raffaelli N. 2008. Transcriptional regulation of NAD metabolism in bacteria: NrtR family of Nudix-related regulators. Nucleic Acids Res 36:2047–2059.

117. Stokell DJ, Donald LJ, Maurus R, Nguyen NT, Sadler G, Choudhary K, Hultin PG, Brayer GD, Duckworth HW. 2003. Probing the roles of key residues in the unique regulatory NADH binding site of type II citrate synthase of *Escherichia coli*. J Biol Chem 278:35435–35443.

118. Weitzman PDJ, JONES D. 1968. Regulation of citrate synthase and microbial taxonomy. Nature 219:270.

119. Shen LC, Atkinson DE. 1970. Regulation of pyruvate dehydrogenase from *Escherichia coli* interactions of adenylate energy charge and other regulatory parameters. J Biol Chem 245:5974–5978.

120. Kern SE, Price-Whelan A, Newman DK. 2014. Extraction and measurement of $NAD(P)^+$ and NAD(P)H. Methods Mol Biol 1149:311–23.

121. Berríos-Rivera SJ, Bennett GN, San K-Y. 2002. Metabolic engineering of *Escherichia coli*: increase of NADH availability by overexpressing an NAD+-dependent formate dehydrogenase. Metab Eng 4:217–229.

122. Balzer GJ, Thakker C, Bennett GN, San K-Y. 2013. Metabolic engineering of *Escherichia coli* to minimize byproduct formate and improving succinate productivity through increasing NADH availability by heterologous expression of NAD^+-dependent formate dehydrogenase. Metab Eng 20:1–8.

123. Atsumi S, Cann AF, Connor MR, Shen CR, Smith KM, Brynildsen MP, Chou KJY, Hanai T, Liao JC. 2008. Metabolic engineering of *Escherichia coli* for 1-butanol production. Metab Eng 10:305–311.

124. Li F, Li Y, Sun L, Chen X, An X, Yin C, Cao Y, Wu H, Song H. 2018. Modular engineering intracellular NADH regeneration boosts extracellular electron transfer of *Shewanella oneidensis* MR-1. ACS Synth Biol 7:885–895.

125. Myers CR, Myers JM. 1997. Replication of plasmids with the p15A origin in *Shewanella putrefaciens* MR-1. Lett Appl Microbiol 24:221–225.

126. Peebo K, Valgepea K, Maser A, Nahku R, Adamberg K, Vilu R. 2015. Proteome reallocation in *Escherichia coli* with increasing specific growth rate. Mol Biosyst 11:1184–1193.

127. Molenaar D, Van Berlo R, De Ridder D, Teusink B. 2009. Shifts in growth strategies reflect tradeoffs in cellular economics. Mol Syst Biol 5:323.

128. Michael D, Tazio S, Uwe S. 2001. Bacillus subtilis Metabolism and Energetics in Carbon-Limited and Excess-Carbon Chemostat Culture. J Bacteriol 183:7308–7317.

129. Tang YJ, Martin HG, Deutschbauer A, Feng X, Huang R, Llora X, Arkin A, Keasling JD. 2009. Invariability of central metabolic flux distribution in *Shewanella oneidensis* MR-1 under environmental or genetic perturbations. Biotechnol Prog 25:1254–1259.

130. Valgepea K, Adamberg K, Vilu R. 2011. Decrease of energy spilling in *Escherichia coli* continuous cultures with rising specific growth rate and carbon wasting. BMC Syst Biol 5:1–11.

131. Wolfe AJ. 2005. The acetate switch. Microbiol Mol Biol Rev 69:12–50.

132. Carlson RP, Beck AE, Phalak P, Fields MW, Gedeon T, Hanley L, Harcombe WR, Henson MA, Heys JJ. 2018. Competitive resource allocation to metabolic pathways contributes to overflow metabolisms and emergent properties in cross-feeding microbial consortia. Biochem Soc Trans 46:269–284.

133. Bosdriesz E, Molenaar D, Teusink B, Bruggeman FJ. 2015. How fast-growing bacteria robustly tune their ribosome concentration to approximate growth-rate maximization. FEBS J2015/03/26. 282:2029–2044.

134. Klumpp S, Hwa T. 2008. Growth-rate-dependent partitioning of RNA polymerases in bacteria. Proc Natl Acad Sci 105:20245 LP – 20250.

135. Renilla S, Bernal V, Fuhrer T, Castaño-Cerezo S, Pastor JM, Iborra JL, Sauer U, Cánovas M. 2012. Acetate scavenging activity in *Escherichia coli*: interplay of acetyl–CoA synthetase and the PEP–glyoxylate cycle in chemostat cultures. Appl Microbiol Biotechnol 93:2109–2124.

136. Tang YJ, Meadows AL, Keasling JD. 2007. A kinetic model describing *Shewanella oneidensis* MR-1 growth, substrate consumption, and product secretion. Biotechnol Bioeng 96:125–133.

137. Duhl KL, TerAvest M. 2019. *Shewanella oneidensis* NADH dehydrogenase mutants exhibit an amino acid synthesis defect. Front Energy Res 7:116.

138. Milo R, Phillips R. 2015. Cell biology by the numbers. CRC Press, Boca Raton, Fl.

139. Karp PD, Billington R, Caspi R, Fulcher CA, Latendresse M, Kothari A, Keseler IM, Krummenacker M, Midford PE, Ong Q. 2019. The BioCyc collection of microbial genomes and metabolic pathways. Brief Bioinform 20:1085–1093.

140. Erdjument-Bromage H, Huang F-K, Neubert TA. 2018. Sample Preparation for Relative Quantitation of Proteins Using Tandem Mass Tags (TMT) and Mass Spectrometry (MS). Methods Mol Biol 1741:135–149.

141. Cox J, Mann M. 2008. MaxQuant enables high peptide identification rates, individualized p.p.b.-range mass accuracies and proteome-wide protein quantification. Nat Biotechnol 26:1367–1372.

142. Cox J, Neuhauser N, Michalski A, Scheltema RA, Olsen J V, Mann M. 2011. Andromeda: A Peptide Search Engine Integrated into the MaxQuant Environment. J Proteome Res 10:1794–1805.

143. RStudio Team. 2019. RStudio: Integrated Development for R. RStudio, Inc., Boston, MA.

144. Karp PD, Riley M, Paley SM, Pellegrini-Toole A. 2002. The metacyc database. Nucleic Acids Res 30:59–61.

145. Long CP, Antoniewicz MR. 2014. Metabolic flux analysis of *Escherichia coli* knockouts: lessons from the Keio collection and future outlook. Curr Opin Biotechnol 28:127–133.